A decorative horizontal line with a small green circle at its right end. Above the line, a green line graph shows a peak with a small secondary peak. To the right of the line, there are two solid green circles of different sizes.

# Thermodynamics of nerves

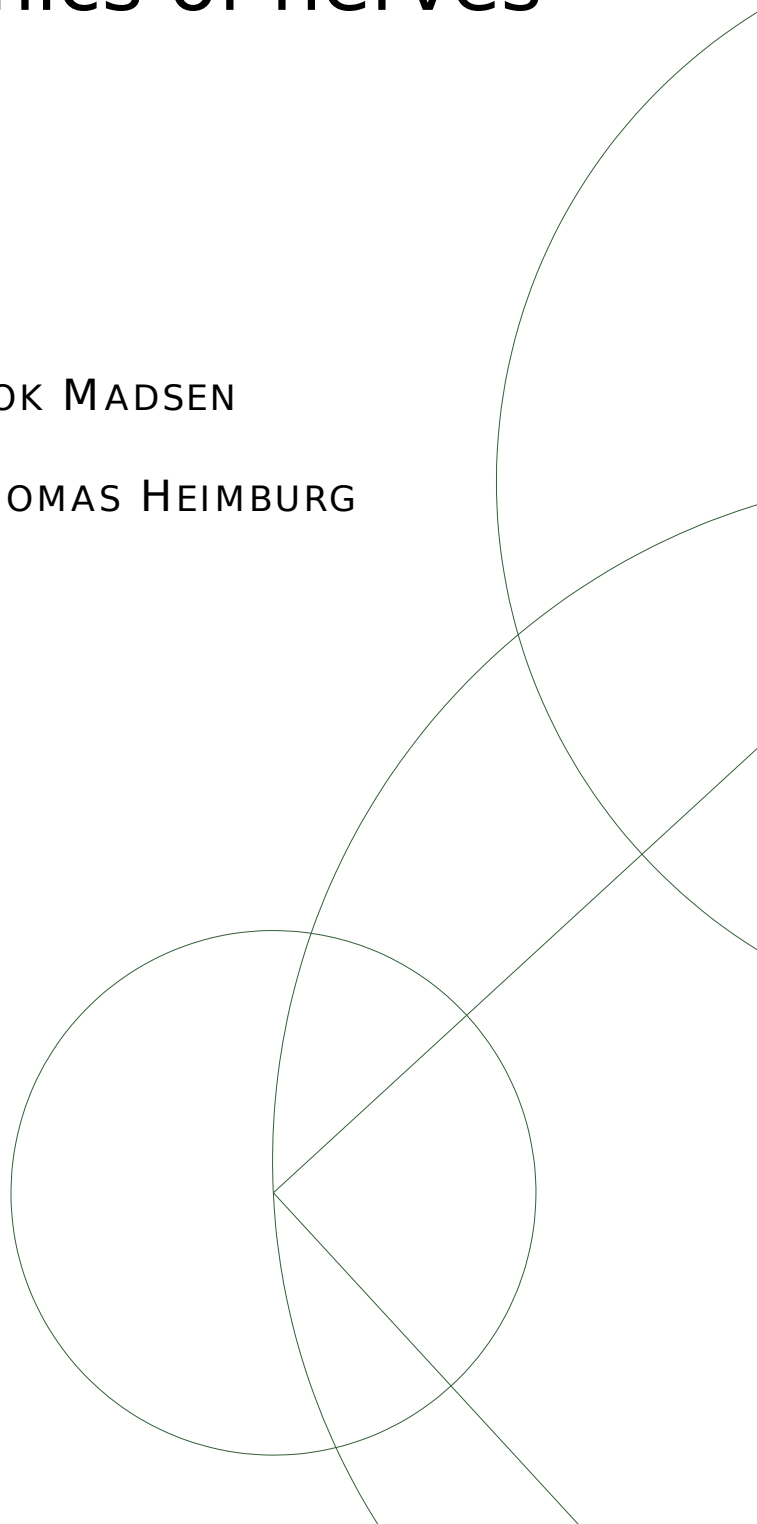
SØREN BLOK MADSEN

SUPERVISOR: THOMAS HEIMBURG

A Thesis Presented for the Degree of  
Cand. Scient. in Physics

Niels Bohr Institute  
University of Copenhagen  
Denmark

November 14, 2011





# Abstract

Phospholipid membranes increase their permeability in the gel-fluid phase transition, therefore it is relevant to investigate the phase transition of different membranes under the influence of different chemicals. Further, the soliton model is based on the presence of a phase transition.

Therefore this master thesis investigates the heat capacity profile of different membranes relevant for biology. This being the synthetic membranes DMPC and DPPC. Also biological membranes collected from a rat brain were investigated. The membranes were investigated with a VP-DSC (MicroCal, Northhampton/MA, USA). It was found that the melting point of the synthetic membranes were changed by menthol and allyl isothiocyanate and not by tetrodotoxin.

Furthermore, it was found that the melting profile of the biological membrane was changed if heated above  $85^{\circ}\text{C}$  - indicating that the state of the proteins in the biological membrane, influence the melting profile of the rest of the membrane.

## Dansk resume

Phosphorlipid membraner øger deres permeabilitet når de er i faseovergangen mellem gel-fluid. Det er derfor relevant at undersøge hvad der sker med faseovergangen når forskellige kemikalier tilsættes. Endvidere er soliton modellen baseret på tilstedeværelsen af en faseovergang.

Derfor blev varmekapacitet profiler af forskellige biologisk relevante membraner blev undersøgt gennem dette speciale. De kunstige membraner DPPC og DMPC blev undersøgt. Der ud over blev membranen fra en rottehjerne undersøgt. Smelteprofilerne blev optaget med et VP-DSC kalorimeter fra (MicroCal, Northhampton/MA, USA). Det vistest sig at de kunstige membrane ændrede deres smeltepunkt med tilstedeværelsen af menthol eller allyl isothiocyanate hvorimod tetrodotoxin ikke ændre smelte punktet.

Yderlig blev det fundet at smelteprofilen fra den biologiske membran ædre sig efter at være varmet op over  $85^{\circ}\text{C}$ . Dette indikere af tilstanden af proteinerne har indflydelse på hvordan resten af smelteprofilen ser ud.

## Acknowledgment

I would like to thanks:

- Thomas Heimburg fore providing the project and many crazy ideas.
- Lars Dalskov Mosgaard for always being ready to discuss and answer questions - and for being as big a coffee snop as me.
- Niels Vidiendal Olsen for providing the rat brains.
- C, B and A floor hang arounds for distraction and moral support.
- Lotte for reading the thesis as a non-physicist.
- Astrid for being awesome and for Astrifyreing the thesis.

The thesis is submitted to fulfill the requirements for M.Sc. in Biophysics at the Niels Bohr Institute, Faculty of Sceince, University of Copenhagen, Denmark. The experimental work was conducted at the Niels Bohr Institute, University of Copenhagen.

Figures are unless otherwise specified made by my self in Inkscape, paint or Igor Pro.

**Abbreviation**

AITC	Allyl isothiocyanate
DASM	Differential Adiabatic Scanning Microcalorimeter
DMPC	1,2-Dimyristoyl-sn-glycero-3-phosphocholine
DPPC	1,2-Dipalmitoyl-sn-glycero-3-phosphocholine
DSC	Differential Scanning Calorimeter
EDTA	Ethylenediaminetetraacetic acid
HEPES	4-(2-hydroxy-ethyl)-1-piperazine- ethane-sulfonic acid
HH	Hodgkin and Huxley
HHM	Hodgkin-Huxley Model
HJ	Heimburg-Jackson
HJM	Heimburg-Jackson model also known as the Soliton model
LD	Liquid-Disordered
LUV	Large unilamellar vesicles
MLV	Multilamellar vesicles
nplab	Department of Neuroscience and Pharmacology Faculty of Health Sciences University of Copenhagen
PT	Phase Transition
Ratbuffer	150 mM KCl, 3 mM EDTA, 3 mM Hepes, pH 7.2-7.4
SM	Soliton Model
SUV	Small unilamellar vesicles
TRP	Transient Receptor Potential
TTX	Tetrodotoxin
UPB	Upper phase boundary

*Before the dawn of civilization, the primitive man believed, as does primitive man today, in animism, magic, and supernatural forces to account for events in the world he experienced.*

*Frazer, 1922 [1]*

*Imagination is more important than knowledge. For knowledge is limited to all we now know and understand, while imagination embraces the entire world, and all there ever will be to know and understand.*

*Albert Einstein*

*Everything should be made as simple as possible, but not simpler.*

*Albert Einstein*

# Contents

<b>1</b>	<b>Introduction</b>	<b>1</b>
1.1	Introduction . . . . .	1
1.2	The cell . . . . .	2
1.2.1	The membrane . . . . .	3
1.2.2	Lipids . . . . .	4
1.3	Thermodynamich . . . . .	5
1.3.1	The tails of the lipid . . . . .	6
1.3.2	Structure of the membrane in different phases . . . . .	6
1.4	Phase transition . . . . .	7
1.4.1	Location of the phase trantion . . . . .	7
1.5	Heat capacity . . . . .	8
1.6	Pressure . . . . .	10
1.7	Melting point depression . . . . .	11
<b>2</b>	<b>Nerves</b>	<b>15</b>
2.1	Nerves . . . . .	15
2.2	The nerve signal . . . . .	16
2.2.1	The Hodgkin-Huxley model . . . . .	16
2.2.2	<i>The Physics</i> . . . . .	17
2.3	The soliton model . . . . .	19
<b>3</b>	<b>A little about channels</b>	<b>23</b>
3.1	Introduction to channels . . . . .	23
3.2	Membrane transport proteins . . . . .	23
3.3	Patch clamp . . . . .	24
3.4	Sensory . . . . .	25
3.5	Lipid ion channels . . . . .	27
3.5.1	The relaxation time of the membrane . . . . .	27
<b>4</b>	<b>The Calorimeter</b>	<b>29</b>
4.1	Historical background . . . . .	29
4.2	Different types of calorimeters . . . . .	29
4.3	The DSC . . . . .	30

4.3.1	A brief history of the Differential Scanning Calorimeter	30
4.3.2	The VP-DSC	30
4.3.3	Pressure	31
<b>5</b>	<b>Sample preparation</b>	<b>33</b>
5.1	Lipid samples	33
5.2	Ion channel blocking molecules	34
5.2.1	Chemicals	34
5.3	Rat brain	35
<b>6</b>	<b>Experimental procedure</b>	<b>37</b>
6.1	Filling the calorimeter	37
6.2	Running the calorimeter	38
6.3	Cleaning the calorimeter	38
<b>7</b>	<b>Results and discussion</b>	<b>41</b>
7.1	Pure lipid samples	42
7.1.1	Scanrate	42
7.1.2	Up- and down-scans	42
7.1.3	DMPC vs. DPPC	43
7.1.4	Sonication	44
7.1.5	Pressure	44
7.1.6	Discussion in regard to pure lipid samples	45
7.2	Lipid with tetrodotoxin	46
7.3	TRP-channel activation molecules.	47
7.3.1	Lipids with Allyl isothiocyanate.	47
7.3.2	Lipids with menthol	48
7.3.3	Discussion in regard to the TRP-activation molecules.	49
7.4	Ratbrain.	50
7.4.1	Rat brain under pressure.	53
7.4.2	Rat brain with menthol.	53
7.4.3	Discussion of the rat brain results	55
<b>8</b>	<b>Conclusion</b>	<b>57</b>
<b>9</b>	<b>Future work</b>	<b>59</b>
<b>A</b>	<b>Protocol for dissection of the Rat brain</b>	<b>61</b>
<b>B</b>	<b>Lipid Sample preparation</b>	<b>63</b>
B.1	Lipid samples	63
B.2	Extrusion procedure	63
B.3	Sonication (SUV and LUV)	64
B.4	Menthol samples	64
B.5	AITC	64

<i>CONTENTS</i>	ix
<b>C relaxtion time</b>	<b>65</b>
<b>D Derivations</b>	<b>67</b>
<b>E Publication</b>	<b>69</b>
<b>Bibliography</b>	<b>83</b>



# Chapter 1

## Introduction

### 1.1 Introduction

Throughout history there have been many explanations on how we move our limbs. Since the Greek physician Aelius Galenus (AD 129-199) suggested that the brain controls the voluntary motion of the body through the motor nerve [2], it has been the common understanding that the brain controls our motions.

In 1786 Luigi Galvani (1737-1798) discovered, that the leg of a dead frog twitched when he dissected the frog when tempting to prove that the testicles of a frog were placed in its legs. With further studies of the phenomena Galvani showed that when the a nerve in the spinal cord was exposed to a charged piece of metal the legs of the frog kicked Fig. 1.1. He called this the *animal electricity* which he equated to the animal spirit whose source was the brain. He hypothesized that the animal electricity ran from the brain through the spinal cord into hollow nerves and then activating the muscles. He compared the muscles with a Leyden jar [3]. This approach was later proven to be wrong by Alessandro Volta (1745-1827). How the brain communicate with the muscles is still today a big mystery to many.

In this thesis there will be given a introduction to the basic components of the cell and how to study them with calorimetric. Further there will be given an introduction to two models on how nerves signals propagate. One of them being the textbook model through more than 50 years and the other being the soliton model from 2005. The latter is build on thermodynamic considerations and thereby related to properties such as entropy, enthalpy and heat capacity. Further it relies on the membrane going through a phase transition. Since a phase transition is easily measured with calorimetric experiments this is a natural approach to use.

Therefore, the aim of this thesis is to try and map different effects on the melting profile of different membranes under influence off chemicals that

are known to have an effect on the nerve signal. This being chemicals as Tetrodotoxin that is thought to block sodium ion channels. Also menthol that is known to stimulate the sensation of cold, through the activation of the TRPM8 receptor, will be investigated. Further, real biological membranes will be investigated to test if the effect of the chemicals are the same on complicated biological systems as on the one component lipid systems. Further, it should be noted that the aim of this thesis isn't to give a quantitative description of the system, but rather serve as an indicator of what happens to a system under the influence of different chemicals.

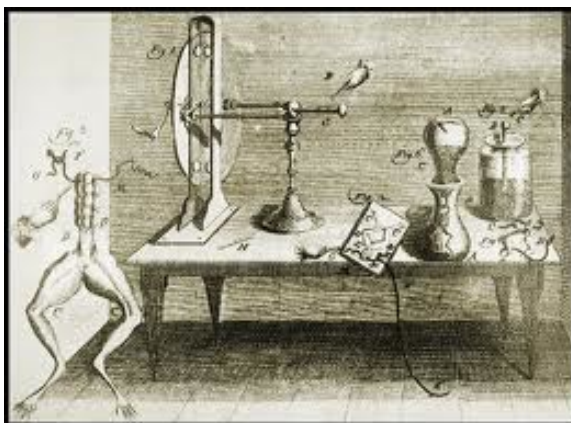


Figure 1.1: A drawing showing Galvani's basic observation. A static charged knife blade touching a nerve of the spinal cord of a frog. Hereby making the muscles contract in the frog's leg. [3]

## 1.2 The cell

In 1665 Robert Hooke noted that the structure of cork seen under the magnifying glass had the same structure as a honeycomb. He called the structure *cellula* and later on he also saw these structures in living tissue. Later, in the 1830s, Matthias Schleiden and Theodor Schwann introduced *the cell theory* according to which cells are the basic units of life [4] with life being plants, animals and humans - in fact a human consists on average of  $10^{14}$  cells.

*But what is a cell?*

In Latin *cella* means *small room* and in fact the name captures the essence quite good. A cell is an enclosed space that is surrounded by a membrane, where the membrane defines the boundary between the inside and outside of the cell. The membrane can to some extent be compared to the walls in a house, it ensures that the "house" doesn't collapse and it keeps ions

and nutrients from diffusing away from where they are needed. Further, the membrane can also separate vital components within the cell (the bathroom, the kitchen... ), such as the Golgi complex, the endoplasmic reticulum, the mitochondria etc, as seen in Fig. 1.2.

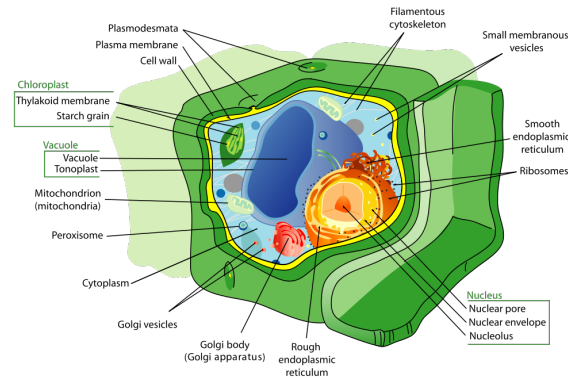


Figure 1.2: Illustration of an idealised plant cell [5].

### 1.2.1 The membrane

In 1748 *Abbá Nollet* was the first to perform an osmosis experiment. He separated alcohol and water using an animal bladder membrane and observed that water slowly passed over to the alcohol side but not the other way around. In the late 19<sup>th</sup> century, *Charles E. Overton* performed many experiments on the permeability of living plant and animal cells. He found that the permeability of a given substance depended upon how well it mixed with oil (lipophilicity). This let Overton to proclaim that the cell was surrounded by a thin layer, that had the same properties as oil and he called it lipid, referring to lipophilicity which is the ability of a chemical compound to dissolve in fats. Although Overton's theory didn't answer all question, it was accepted as a valid theory. [4,6]

In 1925, Gorter and Grendel made an experiment where they extracted lipids from red blood cells, spread them on a water surface and found that the area corresponded to two times the area of the blood cell. Gorter and Gredel concluded that the lipids surrounding the cell must lay in a bilayer, and it turned out to be a correct assumption. Later came additions to the bilayer model, one being that protein could be embedded into the bilayer first introduced by Singer and Nicolson [7] and later refined by Mouritsen and Bloom. Mouritsen and Bloom proposed the mattress model [8], which suggested that lipid-protein interaction could change the thickness of the bilayer Fig. 1.3(b). [6]

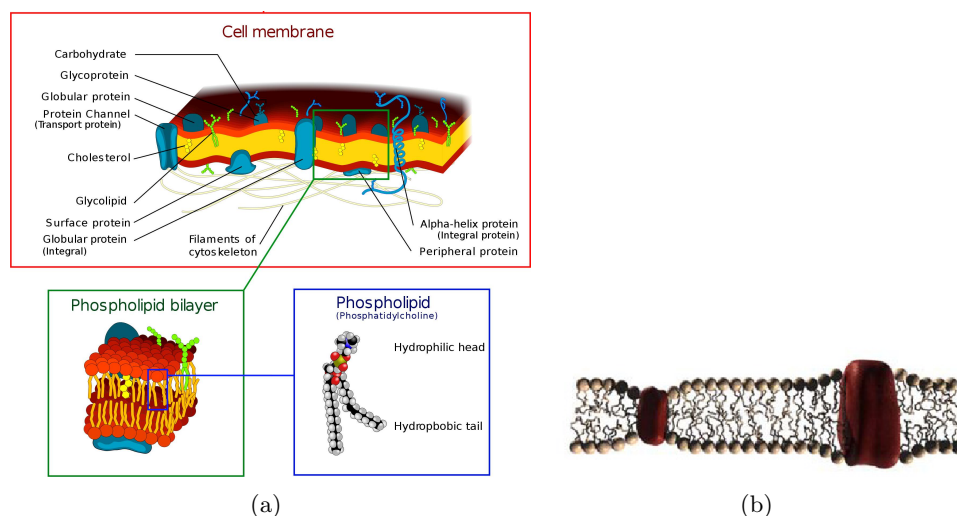


Figure 1.3: (a) Figure of a cell membrane [9] (b) Illustrates Mouritsen and Blooms mattress model, from [10]

## 1.2.2 Lipids

*So what is a lipid?*

The composition of lipids differs a lot even within the same organism and in some cases also within the same cell. But there are some commonalities. The most common lipids in a biological cell membranes are the glycerol-based phospholipids [11], an example can be seen in Fig. 1.4. A phospholipid can be divided into two subgroups: the head group and the tail as seen in Fig. 1.4. The link between the tail and the headgroup is called the backbone, that consists of a glycerol group to which two fatty acids and a phosphate group can be attached through ester bonds. Different organic compounds can be attached to the phosphate group, this could be choline as in Dipalmitoylphosphatidylcholine (DPPC) Fig. 1.4. Other examples are ethanolamine (-PE), serine (-PS) or glycerol (-PG), PC and PE are zwitterionic while PG and PS are negatively charged.

On the other two spots of the backbone two fatty acids are added these fatty acids can vary in length and degree of unsaturation. The most common in nature is a chain length between 16-18 carbon atoms but up to 24 can appear with up to 4 double bonds [6]. As seen in Fig. 1.4 the head group is usually polar and the tail is apolar making the lipid an amphiphilic molecule. If lipids are put into a polar solvent they will form different structures as seen in Fig. 1.5(a), since it is energetically favourable that the hydrophobic tails point away from the polar solvent.

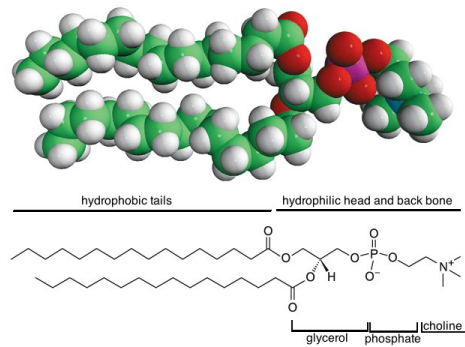


Figure 1.4: Structure of DPPC. Modified figure from [12]

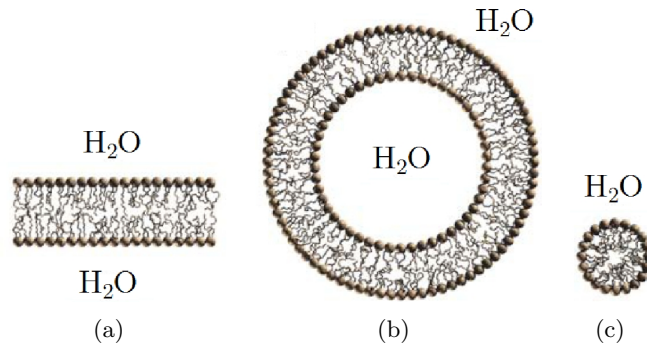


Figure 1.5: Examples of how lipids can selfassemble in different formations when dissolved in water. In (a) a bilayer, (b) a unilamellar vesicle and in (c) a micell. The form will off course depend on the concentration and the conformation of the lipids. Modified Figures from [10].

### 1.3 Thermodynamics of the membrane

In summary - we know that biological membranes primarily consist of proteins and lipids and that they can form a bilayer if dissolved in water.

If we now imagine a pure lipid membrane, it has some quite interesting properties. The membrane can exist in different phases like we know from metal and water. Since the membrane can exist in different phases it will necessarily go through phase transitions. In the transition, some of the thermodynamical properties such as relaxation time, heat capacity, area compressibility etc., change. Some of them can be experimentally determined and we thereby learn a lot about the system.

### 1.3.1 The tails of the lipid

The tails of the lipids consist of long fatty acids, hence a long chain of carbon-carbon bonds. All the c-c bonds can twist, which give rise to three energy minima, the lowest being the trans conformation<sup>1</sup>, and the two others being a rotation of  $\pm 120^\circ$  called gauche, as plotted in Fig. 1.6(b). The energy difference between trans and gauche state is  $2.5\text{kJ}$ , with trans being the lowest. If all c-c bonds are in the trans position, the tail has the lowest energy possible corresponding to a low temperature. If the system is heated the gauche conformation becomes accessible. When the c-c bond is twisted away from trans the chain necessarily has to bend. So if one heats the lipid the C-C bonds can go into the gauche position. Hence the carbon chain will bend and thereby taking up more space as seen in Fig. 1.6(a). [6]

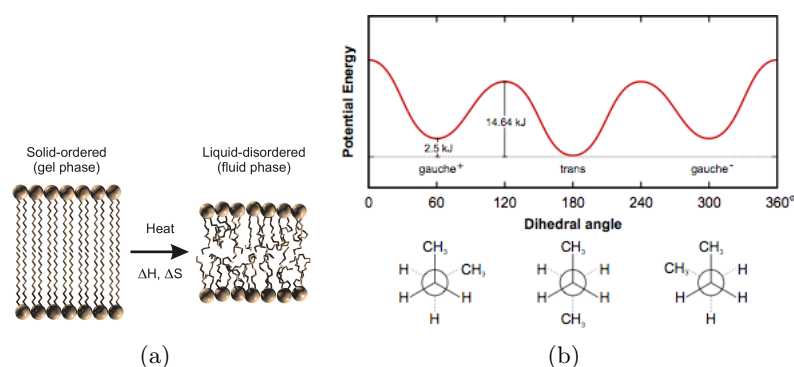


Figure 1.6: (a) Example of the melting of a lipid membrane. (b) Illustrates the energy difference for being in different states. The lowest energy state is the alltrans conformation that can be illustrated as the gel phase (a sawtooth pattern) [10].

### 1.3.2 Structure of the membrane in different phases

Four phases of the lipid membrane can be defined Fig. 1.7:

- $S_o$  - Solid ordered. State where the head groups are arranged in a hexagonal structure and the tails are all in the trans conformation (low temperature).
- $L_o$  - Liquid ordered. The chains are all-trans (ordered) and tilted. This phase is sometimes called the solid-ordered phase, or also the gel phase.
- $L_d$  - Liquid disordered. State where the lipids are randomly distributed (free to move around) and the tails are disordered. This state is often called the fluid state (high temperature)

<sup>1</sup>trans meaning that the  $\text{CH}_2$ , on the c's, are rotated  $180^\circ$  in relation to each other

- $P'_\beta$  - Ripple phase. State in between  $S_o$  and  $L_o$ . The system is partly fluid and partly solid and display periodic order it has periodic ordering.

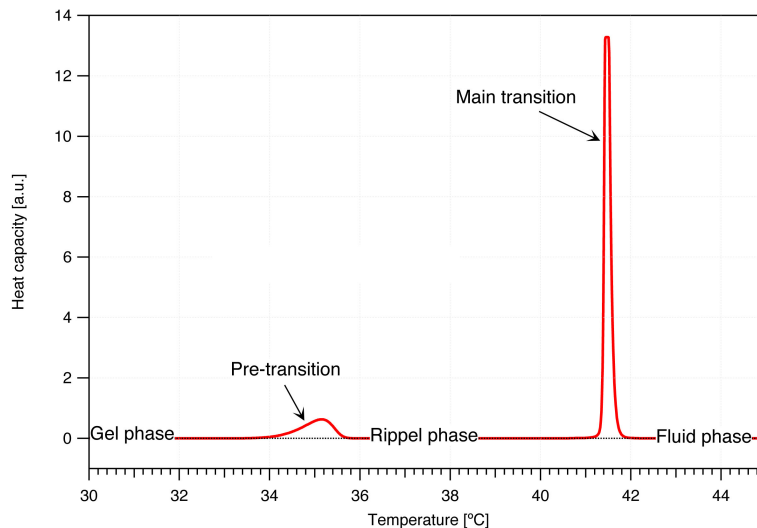


Figure 1.7: The three phases  $L_o$ ,  $P'_\beta$  and  $L_d$  and the phase transitions in between them are seen in the heat capacity profile of a DPPC sample.

Throughout this thesis I will only focus on the main transition ( $S_o \leftrightarrow L_d$ ), since this transition is close to living conditions in most biological systems [6, 13] and because it is the one with the biggest energy absorption/release. Hence, everything below the main transition will be referred to as the gel phase and all above the fluid phase.

## 1.4 Phase transition

As mentioned above I will only focus on the main transition, but what is a transition? Phase transition occurs when the system absorbs energy without increasing its temperature. The energy has to be stored in a reorganization of the system and it will therefore show in a heat capacity scan as in Fig. 1.7. However, a phase transition does not happen at one temperature but rather over a few degrees in vivo and down to 0.1 degree in vitro.

### 1.4.1 Location of the phase transition

If we assume that the lipid can only be in two states, this being either the all trans (ground) state or the disordered state (excited state), with the

enthalpies  $H_l$  or  $H_g$ , and degeneracies  $\Omega_0$  and  $\Omega_1$ . The probability of finding the system in the excited state is given by:

$$P_1 = \frac{\Omega_1 \exp\left(-\frac{H_1}{kT}\right)}{\Omega_0 \exp\left(-\frac{H_0}{kT}\right) + \Omega_1 \exp\left(-\frac{H_1}{kT}\right)} = \frac{\frac{\Omega_1}{\Omega_0} \exp\left(-\frac{\Delta H}{kT}\right)}{1 + \frac{\Omega_1}{\Omega_0} \exp\left(-\frac{\Delta H}{kT}\right)} \equiv \frac{K}{1 + K} \quad (1.1)$$

and

$$P_0 = \frac{1}{1 + K} \quad (1.2)$$

Further we define the melting point as being the temperature where the two states are equally likely.

$$\frac{P_{disordered}(T_m)}{P_{all-trans}(T_m)} = K(T_m) = \exp\left(\frac{-\Delta G}{kT_m}\right) = 1 \quad (1.3)$$

$$\rightarrow \Delta G = \Delta H - T_m \Delta S = 0 \rightarrow T_m = \frac{\Delta H}{\Delta S} \quad (1.4)$$

However, I will in most cases throughout this thesis refer to the melting point as being the top of the peak and not the point where half of the sample has melted.

For most biological lipids the melting point is between  $-20^\circ C$  to  $+60^\circ C$  depending on the properties of the lipid (the head group, chain length and saturation). The environment, such as pH, pressure and other intensive thermodynamic variables, can also change the melting point. So nature has many different ways of altering the transition phase and nature has done it so that biological membranes usually melt about  $15^\circ C$  below living conditions [6, 13], as seen in Fig. 1.8.

## 1.5 Heat capacity

*What is the heat capacity?*

The heat capacity is defined as the amount of heat required to change a system's temperature a given amount. Written mathematically:

$$c = \frac{dQ}{dT} \quad (1.5)$$

If we assume that we have a perfect isolated system, the internal energy of a system only changes if work is being done on or by the system or by adding/ removing heat from the system. Since  $dH = dQ + Vdp$  and  $dQ = TdS$ , the heat capacity under constant pressure is given by

$$c_p = \left(\frac{dH}{dT}\right)_p \quad (1.6)$$

$$c_p = T \left(\frac{dS}{dT}\right)_p \quad (1.7)$$

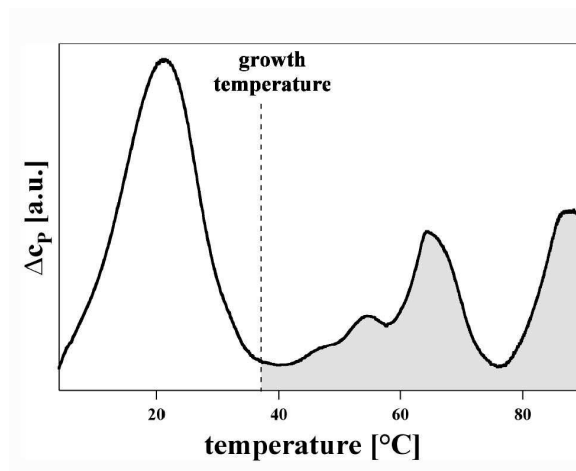


Figure 1.8: Heat capacity profile of E.coli grown at  $37^{\circ}\text{C}$ . The growth temperature is indicated by the dashed line. The peak below growth temperature can be attributed to the melting of lipids in membrane, the peaks above are attributed the unfolding of membranes. [14].

It is thereby easy find the enthalpy and entropy of the of the system by integrating the heat capacity.

$$\Delta H = \int_{T_1}^{T_2} c_p dT \quad (1.8)$$

$$\Delta S = \int_{T_1}^{T_2} \frac{c_p}{T} dT \quad (1.9)$$

## Cooperativity

In biophysical experiments one can usually not measure the enthalpies on the individual molecules, since they are very small. But rather measures the average over many of lipids. Nevertheless us assume that lipids melt independently of each other. Then the free energy by going from gel to fluid state is,  $\Delta G$ . Hence the equilibrium constant  $K = \exp(-\Delta G/RT)$  is a function of  $\Delta H$  and T.

$$\ln K(T) = -\frac{\Delta H}{RT} \rightarrow RT^2 \frac{d \ln K}{dT} = \Delta H \quad (1.10)$$

this is Van't Hoff law. As written in section 1.4 the probability of finding a lipid in the gel state is given by  $1/(1 + K)$ . The mean enthalpy is then given by

$$\langle \Delta H(T) \rangle = \Delta H \frac{K(T)}{1 + K(T)} \quad (1.11)$$

We know from Eq. 1.6 that

$$c_p = \left( \frac{\langle \Delta H \rangle}{dT} \right)_p = \frac{K(T)}{(1 + K(T))^2} \frac{\Delta H^2}{RT^2} \quad (1.12)$$

This gives an expression for heat capacity that depends of temperature and enthalpy. If this is plotted one get a rather broad transition compared with experimental result. However this can be explained by the fact that lipids melt in big groups so  $\Delta H \rightarrow n\Delta H$ . This phenomenon is called cooperativity. [6]

## 1.6 Pressure

In section 1.3 it is established what a phase transition is. Pressure interestingly shifts the phase transition to a higher temperature. In Fig. 1.9 pressure is applied to a 10 mM DMPC MLV sample and that has a high cooperativity hence a very narrow half width ( $0.1K$ ) and the heat capacity profile clearly shows that the transition has shifted.

$T_m$  is under constant pressure given by Eq. 1.4.

$$T_m = \frac{\Delta H_0}{\Delta S_0} \quad (1.13)$$

given that the enthalpy of each state at pressure  $p_0$  is given by

$$\Delta H^0 = \Delta E_0 + p_0 \Delta V \quad (1.14)$$

and, at a different pressure  $p_0 + \Delta p$ , the enthalpy is given by

$$\Delta H_0^{\Delta p} = \Delta E_0 + (p_0 + \Delta p) \Delta V \quad (1.15)$$

If Eq. 1.15 is substituted into Eq. 1.13

$$T_m = \frac{\Delta E_0 + (p_0 + \Delta p) \Delta V}{\Delta S} \quad (1.16)$$

if the pressure is changed  $\Delta p \neq 0$  the melting enthalpy is change

$$\Delta(\Delta H) = \Delta p \Delta V \quad (1.17)$$

Let us assume that the entropy change  $\Delta S_{\Delta p} = \text{constant}$ , meaning that the lipids are in the same states at low and high temperature, as they are with out pressure. The melting temperature is then given by [6]:

$$\Delta T_m = \frac{\Delta(\Delta H)}{\Delta S} = \frac{\Delta p \Delta V}{\Delta S} = \Delta p T_m \frac{\Delta V}{\Delta H_0} \quad (1.18)$$

This can be rewritten

$$\Delta T_m = \gamma_V \Delta p T_m \quad (1.19)$$

Where  $\gamma_V$  is a constant that can be found experimentally. For DMPC-MLV it was found to be  $\gamma_V = 7.841 \cdot 10^{-10} \frac{m^2}{N}$  [14–16]

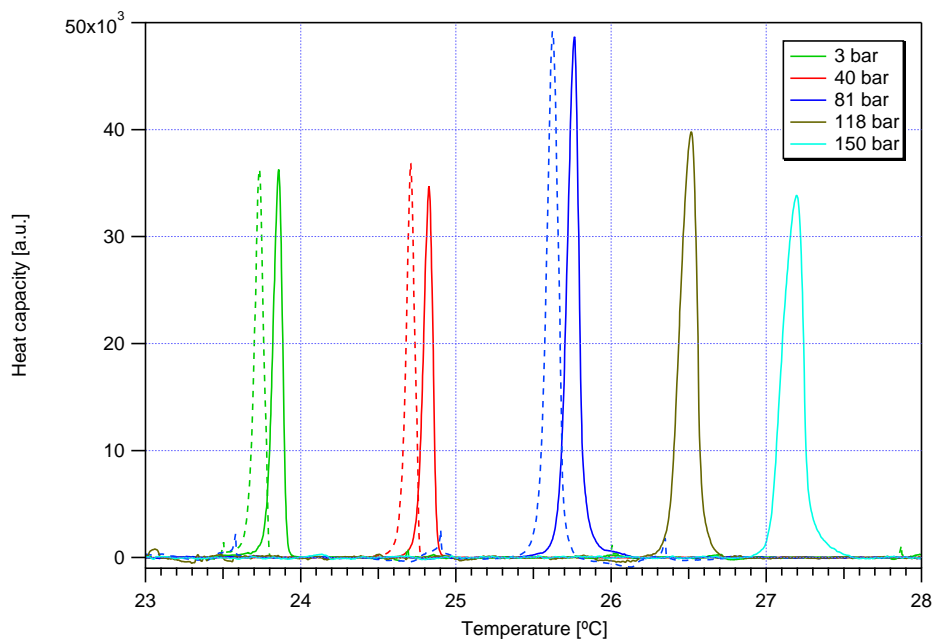


Figure 1.9: Heat capacity profile off  $\sim 10$ mM DMPC MLV under pressure. This graph will be explained in section 7.1. The solid lines are up-scans and the dotted lines are down-scans. Scans were done during this thesis.

## 1.7 Melting point depression

Every child in Denmark knows that salt is spread upon the roads in winter to melt the ice. So it will not come as a surprise that one can change the melting point of a system by adding another compound. In our case we have a membrane consisting of lipids and we assume that a small molecule is mixed in the fluid phase and not with the gel phase, further the small molecule shall not have a phase transition around the transition of the lipid of interest. By further assuming that the melting of the lipid is like a chemical reaction and using the "mass action law" one obtains:

$$\mu_M^g = \mu_{M,0}^g \quad (1.20)$$

$$\mu_M^f = \mu_{M,0}^f + RT \ln(x_M^f) \quad (1.21)$$

$f$  refers to the fluid state,  $g$  to the gel state,  $x_M^f$  is the fraction of lipid in the fluid phase and  $1 - x_M^f$  is the amount of solvent. The chemical potential

of the gel and fluid state must be equal in the equilibrium state so

$$\ln(x_M^f) = -\frac{\mu_{M,o}^f - \mu_{M,0}^g}{RT} = -\frac{\Delta H_{M,0}}{R} \left( \frac{1}{T} - \frac{1}{T_{m,M}} \right) \quad (1.22)$$

and we know that all the solvent  $x_s$  is in the fluid phase

$$x_M^f = 1 - x_s^f = 1 - x_s \quad (\text{for } T \geq T_{m,M}) \quad (1.23)$$

$$\Rightarrow \ln(1 - x_s) = -\frac{\Delta H_{M,0}}{R} \left( \frac{T_{m,M} - T}{T_{m,M}T} \right) \quad (1.24)$$

If the amount of solvent is small, we can write  $\ln(1 - x_s) \approx -x_s$  and  $T_{m,M} \cdot T \approx T_{m,M}^2$ , then equation Eq. 1.24 can be rewritten to

$$x_s = \frac{\Delta H_{M,0}}{R} \left( \frac{T_{m,M} - T}{T_{m,M}^2} \right) \Rightarrow \quad (1.25)$$

$$\Delta T_m = T_{m,M} - T = \left( \frac{RT_{m,M}^2}{\Delta H_{M,0}} \right) x_s \quad (1.26)$$

From equation Eq. 1.26, we see that the melting point depression is linearly dependent on the amount of solvent put into the membrane. [6]

*So far so good...*

It is naive to think that all the solvent goes into the membrane, therefore one has to know how well the solvent mixes with the membrane/water. This is known as the partition coefficient,  $\beta$ .

$$\beta = \frac{c_{mem}}{c_{buffer}} \Rightarrow \quad (1.27)$$

$$c_{mem} = \frac{\beta n_{solvent}}{\beta V_{mem} + V_{buffer}} \quad (1.28)$$

where  $\beta$  is the partition coefficient,  $c_{mem}$  is the concentration of the solvent in the membrane,  $c_{buffer}$  the concentration of the solvent in the buffer,  $V_{buffer}$  the volume of the buffer,  $V_{mem}$  the volume of the membrane and  $n_{solvent}$  is the amount of added solvent. If we assume that ( $\beta V_{mem} \ll V_{buffer}$ ) then:

$$c_{mem} \simeq \beta \frac{n_{solvent}}{V_{buffer}} \propto x_s \quad (1.29)$$

which is also intuitively what one would expect.

One could compare the temperature shift due to a pressure section 1.6 and

due to solvent dissolved in the membrane. They should be able to cancel each other out. [13] So if equation 1.19 and 1.26 are set equal to each other it results in the following

$$\Delta T_m = \gamma_V \Delta p T_m \quad (1.30)$$

$$\Delta T_m = - \left( \frac{RT_m^2}{\Delta H} \right) x_s \Rightarrow \quad (1.31)$$

$$\Delta p \approx \frac{1}{\gamma_V} \frac{RT_m}{\Delta H} x_s \quad (1.32)$$

To sum up we have seen that pressure can change the melting point and by dissolving small molecules in the membrane we can also change the melting point.

Since there are so many ways of changing the melting point of a membrane, combined with the fact that many native membranes melt around  $10 - 15^\circ$  below living conditions, one might conclude that it is vital for cells to have a melting point a bit below living conditions. [6, 13]



## Chapter 2

# Nerves

### 2.1 Nerves

*So what is a nerve?*

A nerve is a cell much like other cells. But what makes a nerve cell different from a normal cell is its ability to communicate with other cells very fast via synapses. In Fig. 2.1 a schematic illustration shows the basic structure of a nerve. Typically, one divide the nerve cell into tree parts, this being the soma (cell body), dendrites and axon.

- The Soma (Greek translation for body) contains the nucleus of the cell and resembles a normal cell. It receives the nerve signal from the dendrites and send it along the axon.
- The dendrites/ incoming signal: The dendrites are attached to the Soma (not only at one place), and have a tree like structure. In the part away from the Soma (the outer end of the tree) the dendrites have many synapse, where the signals are received.
- The axon/ outgoing signal. The axon has a cable-like structure, that carries the signal from the soma to the endpoint (axon terminal). The Axon can differ in length from a few micrometers to 1 meter (in humans). Most axon is covered by a myelin layer that is produced by the Schwann cells. The myelin layer is primarily a layer of lipids and proteins.

The synapse is the end point or starting point of the nerve. It is a membrane to membrane junction and textbooks state that chemicals are released from the endpoint (as a result of a signal). These chemicals induce a signal at the starting point of the next nerve. Whether or not this is realistic model is another story but nevertheless this is the common understanding of the synapse.

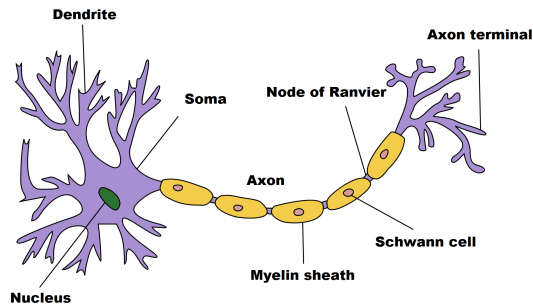
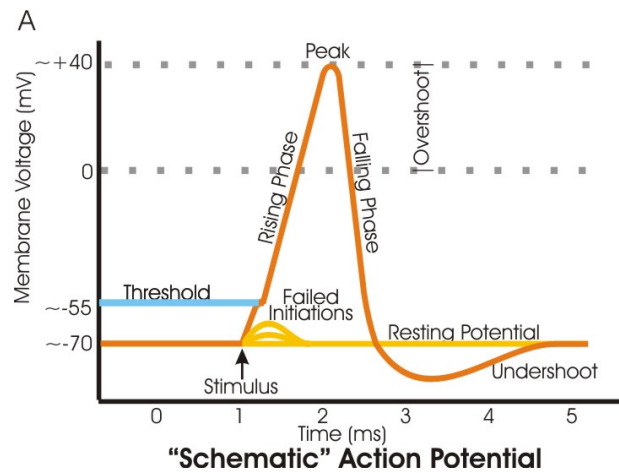


Figure 2.1: A schematic illustration of a nerve. [17]

## 2.2 The nerve signal

As described in section 1.1 Galvani discovered in 1786 that the movement of muscles could be associated with electricity. Since many associate the nerve signal with an electric signal, it is referred to as the ‘Action Potential’ Fig. 2.2. The action potential was first measured by Hermann von Helmholtz in 1850. It was however not known until 1952, when Alan Lloyd Hodgkin and Andrew Huxley came up with a mathematical solution, to what gave rise to the action potential. Hodgkin and Huxley proposed that the action potential was due to ions passing over the membrane via ion channel proteins. [3, 18]

Figure 2.2: An idealized action potential at a point on a cell membrane when the nerve signal passes (with a potential difference of  $\sim 100$  mV). [19]

### 2.2.1 The Hodgkin-Huxley model

The model (HHM) that Hodgkin and Huxley proposed was based on experiments performed on giant squid axons. The model was further based on

high concentration of sodium outside and high concentration of potassium inside the nerve. In fact, the concentration for the squid axon is  $400mMK^+$  inside and  $20mMK^+$  outside and the opposite for  $Na^+$ . The concentration difference gives rise to a voltage difference that can be calculated via the Goldman-Katz equation

$$V_m = \Psi_{in} - \Psi_{out} \frac{RT}{F} \ln \left( \frac{P_{Na}[Na^+]_o + P_K[K^+]_u}{P_{Na}[Na^+]_i + P_K[K^+]_i} \right) \quad (2.1)$$

By further introducing specific ion channels, that are sensitive to voltage, they postulated an ion channel that would open if the membrane potential was changed, hence ions would flow towards the low concentration. This leads to a bigger change in the potential, hence more channels opens and hereby making a wavelike signal down though the membrane where sodium is flowing in to the cell and potassium flowing out.

### 2.2.2 The Physics

Hodgkin and Huxley treated the system as an electric circuit as seen in Fig. 2.3, where  $I$  is the current,  $R$  the resistance,  $C_m$  the capacity,  $E$  the membrane potential and  $E_x$  the equilibrium potential.

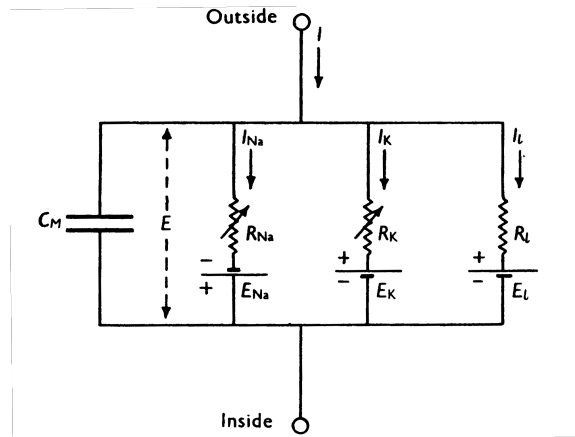


Figure 2.3: The nerve circuit as Hodgkin and Huxley saw it. The subscript Na, K, L stands for Sodium, Potassium and leak. The figure was taken from [18]

The current through the membrane can be described by equation 2.3 where  $g_x = \frac{1}{R_x}$ , under the assumption that the membrane act as a capacitor. We know that the charge on the capacitor,  $Q$ , is  $Q = C_m \cdot U$  and that the capacitor current is given by the derivative of  $Q$ . Further assuming that the capacitance of the membrane is constant

$$I_C = \frac{dQ}{dt} = C_m \frac{dU}{dt} + U \underbrace{\frac{dC_m}{dt}}_{=0} \quad (2.2)$$

HH derived the current over the membrane

$$I_m = \underbrace{C_m \frac{dU}{dt}}_{I_C} + g_K(t, U)(U - E_K) + g_{Na}(t, U)(U - E_{Na}) \quad (2.3)$$

So the Hodgkin-Huxley quite decently described the shape of action potential in a squid axon, by letting the specific ions flow over the membrane according to Eq. 2.3 and thereby changing the concentrations difference of ions hence the potential Eq. 2.1. Nevertheless Hodgkin and Huxley wrote in the original article:

*The agreement must not be taken as evidence that our equations are anything more than an empirical description of the time-course of the changes in permeability to sodium and potassium. An equally satisfactory description of the voltage clamp data could no doubt have been achieved with equations of very different form, which would probably have been equally successful in predicting the electrical behaviour of the membrane. [...] the success of the equations is no evidence in favour of the mechanism of permeability change that we tentatively had in mind when formulating them. [18]*

This quote will necessarily give rise to speculations about alternative explanations to the action potential, which will be given in section 2.4. [6, 18]

### ***pros and cons...***

Pro the HHM is that it is very simple and easy to understand the concept of the model, even for a non-academic. Further the HHM opened up for the concept of specific channels, that ever since has been a big field of interest in biochemistry.

But there is also a lot of disadvantages in the model, one being that it only describes the specific squid axon system and not a nerve in general. Another is, that if the nerves/ ion channels are acting as an electric circuit, one would expect heat to be generated when ions flow back and forth through the ion-channels/ resistors. This is however not the case and according to Tasaki [20] and Keynes [21] heat is released, but it is fully reabsorbed during the action potential indicating that this is a reversible adiabatic process. Further Tasaki showed in 1980 [22] that the action potential of a squid giant axon is accompanied by a small swelling, hence a change in the membrane capacity, which is not explained by the HHM. In fact the HHM assumes that the capacity is constant (Eq. 2.3)

## 2.3 The soliton model

*From experiments it is obvious that thickness and density changes occur in nerve membrane, accompanied by changes in lipid state. Reversible processes clearly play a role that are not included in the HH model.*

*However, there is another phenomenon in physics that shares a lot of similarities[...] This is the propagation of sound. [6]*

As written above there are many unresolved issues with the Hodgkin-Huxley model, one being the reversible heat signal. This led Heimburg and Jackson to propose a new model for the action potential in 2005 [23], that not only explained the action potential but also dealt with the mystery of anesthetics. According to Ritchie and Keynes [21] the signal is adiabatic, further we know from Tasaki [22] that the action potential is accompanied by a density pulse and a shortening of the nerve [24]. Heimburg and Jackson proposed a soliton as the solution to the problem, since it met the criteria of Keynes and Tasaki.

### The requirements of a soliton

A soliton is a wave that travels with the same shape without attenuation at constant speed. It requires a medium with nonlinear elastic constants upon density change. Further it requires that the speed of the wave depends on the frequency of the wave (dispersion). It turns out that a biological membrane is such a medium.

If we now consider a density pulse traveling along the x-axis in a cylindrical membrane, one can describe this by the following equation

$$\frac{\partial^2}{\partial t^2} \Delta \rho^A = \frac{\partial}{\partial x} \left[ c^2 \frac{\partial}{\partial x} \Delta \rho^A \right] - \underbrace{h \frac{\partial^4}{\partial x^4} \Delta \rho^A}_{\text{dispersion}} \quad (2.4)$$

where  $c^2 = (1/\kappa_S^A \rho^A)$ ,  $\kappa_S^A$  being the adiabatic area compressibility, that depends on the density ( $\rho^A$ ).  $\kappa_S^A$  displays non-linear properties close to the melting transition and can be calculated from the heat capacity in the low frequency regime [25].

The speed of the sound in the membrane is approximated to

$$c^2 = \frac{1}{\kappa_S^A \rho^A} = c_0^2 + p \Delta \rho^A + q (\Delta \rho^A)^2 + \dots \quad (2.5)$$

where  $c_0$  is the velocity in the fluid state (away from the phase transition),  $p < 0$  and  $q > 0$  are Taylor expansion coefficients which can be experimentally determined. If we introduce the propagation velocity,  $v$  so that ( $z = x - v \cdot t$ ) and substituted Eq. 2.5 into Eq. 2.4 we arrive at:

$$v^2 \frac{\partial^2}{\partial z^2} \Delta \rho^A = \frac{\partial}{\partial z} \left[ (c_0^2 + p \Delta \rho^A + q (\Delta \rho^A)^2) \frac{\partial \Delta \rho^A}{\partial z} \right] - h \frac{\partial^4}{\partial z^4} \Delta \rho^A \quad (2.6)$$

It has been shown by Lautrup et al. [26] that there is an exact solution for a given value of the velocity.

$$\Delta \rho^A = \frac{p}{q} \frac{1 - \left( \frac{v^2 - v_{min}^2}{c_0^2 - v_{min}^2} \right)}{1 + \left( 1 + 2 \sqrt{\frac{v^2 - v_{min}^2}{c_0^2 - v_{min}^2}} \right) \cosh \left( \frac{c_0}{\sqrt{h}} z \sqrt{1 - \frac{v^2}{c_0^2}} \right)} \quad (2.7)$$

The minimum velocity allowed by Eq. 2.7 is

$$v_{min}^2 = c_0^2 - \frac{p^2}{6q} \quad (2.8)$$

We can now calculate the minimum velocity of the soliton. We just need the values  $p, q$  and  $c_0$ . We can obtain  $p, q$  and  $c_0$  for a pure DPPC system at  $45^\circ C$  by fitting Eq. 2.5 to the right of Fig. 2.4 ( $\omega = 0$ ),  $p = -16.6c_0^2/\rho_0^A$ ,  $q = 79.5c_0^2/(\rho_0^A)^2$  and  $c_0 = 176.6m/s$ . This gives a velocity of  $v_{min} = 0.650c_0 \approx 115m/s$ , which is very close to the velocity of the signal in a myelinated nerve. As a consequence of the equations, a slower velocity of a soliton gives a bigger amplitude. Hence

$$\Delta \rho_{max,limit}^A = \frac{|p|}{q} \quad (2.9)$$

The biggest density change due to a soliton is  $\rho_{max}^A/\rho_0^A = 0.21$ . This corresponds to  $\approx 85\%$  of the density change when a DPPC lipid goes through the transition. Hence the soliton forces  $85\%$  of the DPPC membrane through a transition. This will necessarily change the thickness of the membrane as observed in nerve membranes by Tasaki in 1980 [22]. [6, 14, 23, 25]

### pros and cons

Pro the soliton model is its ability to explain the reversible heat and the thickness and length change of the nerve. Hence it explains the change in different variables such as temperature, voltage and why a nerve can be mechanically stimulated. Further it can predict what will happen if an arbitrary variable is introduced to the system, since it will follow the laws of thermodynamics.

Con the model is that it only describes myelinated nerves. Since the velocity of the nerve signal in non-myelinated nerves are much slower (about 100 times slower) this would correspond to a much higher compressibility ( $10^4$  higher) which is clearly not the case. So one would have to find another explanation for the non myelinated nerves.

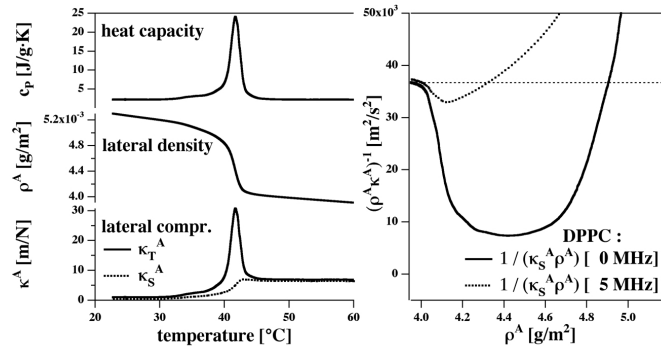


Figure 2.4: To the left: heat capacity of DPPC LUV (top), the lateral density,  $\rho^A$ , and the corresponding isothermal area compressibility (bottom, solid curve, corresponding to a low frequency case) and adiabatic area compressibility (dotted line corresponding to a 5 MHz experiment), calculated from the heat capacity. To the right: The lateral sound velocity as a function of membrane area density at 45°C. From this figure  $p$  and  $q$  can be found by fitting a second order function to the "dip". [6]



## Chapter 3

# A little about channels

### 3.1 Introduction to channels

We know from section 1.2 that the membrane seals the inside from the outside of the cell, but we also know that cells often have waste products that it needs to get rid of and that it need new nutrients such as ions and molecules to survive. It means that the membrane needs to be permeable. The textbook solution to this is that different proteins form tunnel-like structures across the membrane and that these tunnels / ion channels are to some extent selective. This implies that it is only possible to cross the membrane through the channels. Off course, this is not the case since there is always a finite probability for a substance to spontaneously cross the membrane. For example it has been shown experientially that water can cross a pure lipid membrane [27]

The concept of ion channels spanning the membrane was not fully accepted by the biophysical community until the 1970s, when the patch clamp technique was developed. Nevertheless the pore hypothesis for biological membranes can be dated back to Ernst Brücke, who in 1843 described pores in membranes in the attempt to describe osmotic phenomenon from experiments done on pig bladder membranes.

### 3.2 Membrane transport proteins

Proteins are long chains of amino acids that fold into a yarn like structure. The sequence of the amino acid is determined by the DNA. Hence, the DNA sequence has a big influence on structure of the folded protein. Further the shape and therefore the function of the protein is highly correlated with the surroundings. Hence a protein embedded in a membrane will look different than a protein dissolved in water.

Protein channels play a major role in the function of the cell. As indicated

above the protein channels are thought to be responsible for the transport of ions and other molecules across the membrane. It is assumed that there exists a specific protein channel for all molecules, which should make it possible to design specific blocking molecules that block the effect of a given channel.

Since many diseases are associated with defects in protein channels, channelopathies, the pharmaceutical industry has a big interest in developing molecules that act on specific channels, hence there is a lot of specific channel blocking molecule available. TTX<sup>1</sup> is one of them. TTX is thought to block the sodium channel, hence the action potential, and is therefore often used in nerve-associated experiments.

Actually, the common way to study the effect of a given protein channel is to block the channel with a specific blocking molecule and study the membrane with the patch clamp technique. If there is a reduced channel activity, this is taken as a proof for the function of both the protein channel and the blocking molecule. Another way is to use patch clamp combined with molecular biology that enables one to knock out or express a certain gene and see if it still reacts to the specific binding molecule [28–31].

### 3.3 Patch clamp

Throughout this section I will give a brief introduction to the patch clamp technique, since it is used by many to verify specific channels as described above. Further, the use of AITC and menthol was motivated by the work done by a group from Institute of Physiology, Medical Faculty, RWTH Aachen University. By using patch clamp techniques, they have explored the effect of these chemicals on various TRP-receptors.

The Nobel Prize in Physiology or Medicine was in 1991 rewarded Erwin Neher and Bert Sakmann for their development of the patch clamp technique. Neher and Sakmann introduced the patch clamp technique in a Nature article in 1976 [32], and the basic principle is quite simple.

A glass pipette with a very small opening ( $\sim \mu m$ ), is put in contact with a small area, a patch, of the membrane (by slight suction on the pipette). The inside of the pipette is filled with the same solution as the surrounding environment and a electrode is also fitted inside the pipette making it possible to measure the current flowing over the membrane in the clamp region. [33] A schematic representation can be seen in Fig. 3.1

The drawing in Fig. 3.1 is the so called *on-cell* mode. The on-cell mode allows one to measure on a single channel without destroying the cell. An-

---

<sup>1</sup>TTX was not developed by the pharmaceutical industry, but it occurs naturally in pufferfish and other animals

other mode is the *whole-cell* mode, where suction is applied to rupture the membrane in the patch area making it possible to measure the current flowing over the rest of the membrane ( $\sim$  the whole cell).

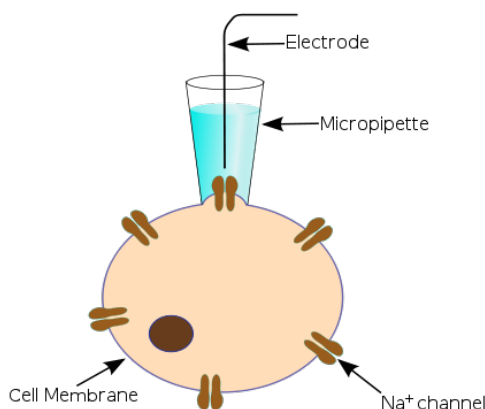


Figure 3.1: Schematic drawing of the patch-clamp technique [34].

### 3.4 Sensory

How we sense things is conceptually complicated, perhaps it is more suited for philosophy than physiology. Nevertheless, scientists have tried to describe how we sense. Almost all sensors act as a modulator of ionic flux and thereby stimulate an electrical signal. The common understanding of sensing is illustrated through the chain of events:

$$\text{stimulus} \rightarrow \begin{matrix} \text{receptor} \\ \text{molecule} \end{matrix} \rightarrow \begin{matrix} \text{transduction} \\ \text{channel} \end{matrix} \rightarrow \begin{matrix} \text{receptor} \\ \text{potential} \end{matrix} \rightarrow \text{signal}$$

The transduction channel is a specific protein channel, as described above, that can be activated by a specific stimuli and hereby allowing ions to flow over the membrane. [28–30].

#### TRP receptors

Transient receptor potential (TRP) channels are a large family of ion channel proteins. They are characterized by having a sequence homology rather than a particular ligand that activates them. TRP channels can be stimulated by many different mechanisms (pH, pressure, heat, cold or ligand). It is assumed that the TRP protein has 6 trans membrane (TM) spanning domains called S1-S6 and between S5 and S6 a pore is created. The S1-S4 domain is together with the amino (N) and carboxyl (C) terminals most

likely involved in channel activation. The N and C terminals are, as seen in Fig. 3.2 located intra cellularly and they can vary in length.

The TRP family can be grouped into six subfamilies based on the amino acid sequence homology (TRPC, TRPV, TRPM, TRPA, TRPP, and TRPML). Fig. 3.2. [35, 36]

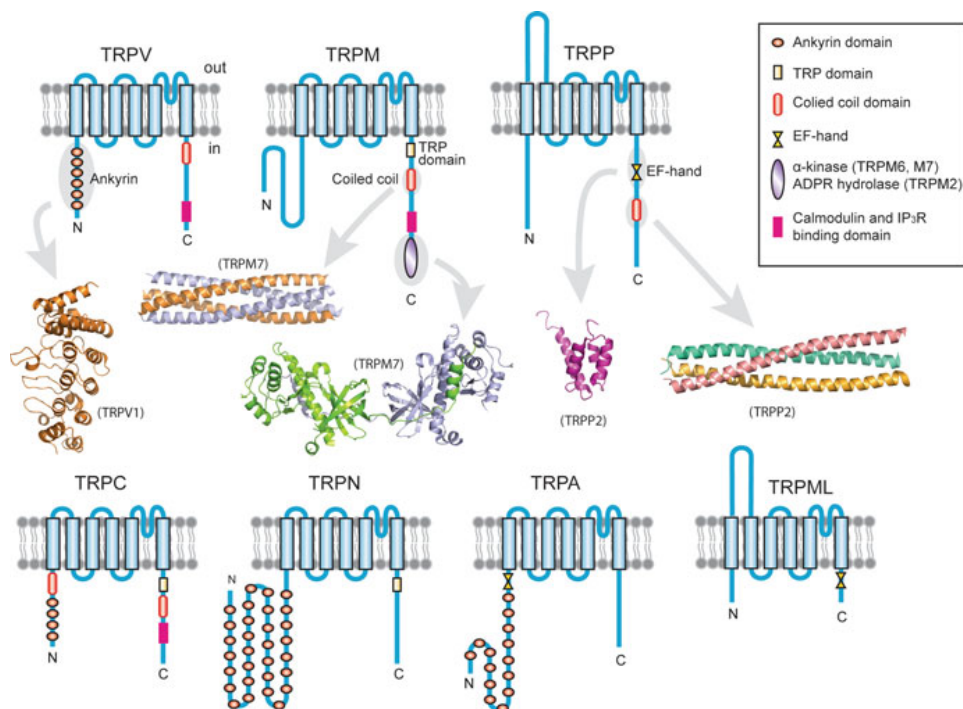


Figure 3.2: A schematic drawing of the 6 families of the TRP receptor. A 7<sup>th</sup> protein (TRPN) is also in the drawing, it is however not expressed in mice and humans [35].

### TRPM8 receptors

The subfamily TRPM (melastatin) is presumed to have 8 members (TRPM1-8) and they are categorized as having a long amino acid chain at the N-terminal (around 700 amino acid).

The TRPM8 receptor is known as the *cold sensing receptor* since it is activated by cold (8 – 28°C). Further it can be activated by the cooling agents menthol and icilin. Studies have shown that mice with TRPM(-/-) has deficiencies to a range of cold stimuli. This implies that the TRPM8 protein is believed to be the dominant detector of cold in vivo but how it works in vivo is still unknown [31].

## 3.5 Lipid ion channels

As implied in section 3.1, proteins are not necessary for ions to pass the membrane. In fact, due to thermal fluctuations pores can form in protein free membranes. Already two years before Neher and Sakmann published their famous article about patch clamp [32], Yafuso et al. [37] reported spontaneous multi-level conductance states in pure black lipid membranes<sup>2</sup>. In principle this experiment provided evidence for a quantized conduction through a membrane in the absence of proteins. Despite the clear evidence, many patch clamp studies tend to ignore the fact that the membrane itself is permeable.

In 1989 Kaufmann proposed that by changing the intensive thermodynamic variables, such as surface pressure, voltage or temperature one could generate ion channels. Hence, membrane proteins can alter the lipid state and therefore control the probability of the appearance of ion channels in the lipid bilayer lattice [38].

Furthermore, it has been shown for the KcsA-channel that the channel activity peaks in the membranes transition and that the typical time scale of opening and closing in lipid pores are similar to the relaxation time of the membrane [39].

There is a strong correlation between the phase transition of the lipid and the protein activity, but whether it is the lipids that control the activity of the channel proteins or it is the proteins that control the permeability of the lipid membrane is an open question.

### 3.5.1 The relaxation time of the membrane

It has been shown by Grabitz in 2002 [40] that the relaxation time of a lipid membrane can be calculated from the heat capacity and that they are proportional ( $\tau \propto c_p$ ). This means that the higher the heat capacity is the slower is the reaction time for the lipid membrane. This phenomena is known as critical-slowness. The derivations are shown in appendix C. If it is assumed that the relationship between heat capacity and relaxation time is the same for biological membranes as for pure lipid membranes, it is possible to calculate the relaxation time for the biological membrane as well. As seen in Fig. 1.8 the heat capacity profile of a biomembrane is much broader, hence the maximum is lower and thereby the a relaxation time is much shorter. In order to calculate the relaxation time it is also required that the proportionality factor is the same for biomembranes as for the pure lipid membranes. For lung surfactant the maximum heat capacity is approximately  $1.6 J/mol K$  giving a relaxation time of about  $50 - 130ms$  [40]. As previously mentioned the normal living temperature in biology is

---

<sup>2</sup>A black lipid membrane is basically a bilayer that separates two electrodes, hence it is possible to measure a current over the membrane.

10 – 15°C above the melting peak, hence the heat capacity is lower at this temperature and thereby also the relaxation time. In fact one would expect relaxation times of  $\approx 10ms$  [6], which is interestingly the time scale of the opening and closing of a ion channel [6, 15, 40]

## Chapter 4

# The Calorimeter

### 4.1 Historical background

*First a little history about temperature, heat and calorimetry.*

That the science of heat took much longer to develop than many other disciplines in science cannot come as a surprise to many, since the concept of heat still today is difficult to understand. The concept *heat* came with the invention of the thermometer. Galileo is by many given the credit for the invention of the thermometer, but the first written record of the invention was made by physiologist Santorio Santorii (1561-1636) in 1612. The next big step was made by Daniel Gabriel Fahrenheit (1686-1734) with the invention of a reliable liquid thermometer devised a scale for temperature, the Fahrenheit scale. Later came the Scottish chemist Joseph Black (1728-1799) who by many is called the grandfather of calorimetry. He was the first to distinguish the concepts heat and temperature. He also defined the concept '*capacity for heat*' which is nowadays called '*specific heat*' or '*heat capacity*'. [41]

### 4.2 Different types of calorimeters

In latin calor means heat and a calorimeter is a device used for measuring heat in chemical reactions, physical changes or heat capacity and there are different types of calorimeters for each purpose. For example, when measuring the energy released in a chemical reaction one uses a reaction calorimeter. This is basically a closed box wherein a chemical reaction is started and the heat is measured over time, so that one can calculate the total energy release or uptake from a given reaction. Within this category there are different types of calorimeters such as the heat flow calorimeter, the heat balance calorimeter, the power compensation. Other types of calorimeters

are the constant pressure calorimeter, the isothermal titration calorimeter (ITC) and the differential scanning calorimeter (DSC). Within life science *ITC* and *DSC* are the most used and throughout this thesis a VP-DSC from MicroCal was used Fig. 4.1.



Figure 4.1: VP-DSC Calorimeter from MicroCal

## 4.3 The DSC

### 4.3.1 A brief history of the Differential Scanning Calorimeter

Until 1963 it was almost impossible to measure what happened with a dissolved biopolymer when heated. But in 1963 an article by Privalov et al. [42] described an effective thermoanalytical tool that could measure these effects, they called it the Differential Adiabatic Scanning Microcalorimeter (DASM). A nice feature of the *DASM* was, that it continuously measured the difference in heat capacity between two samples loaded in identical cells, one loaded with a sample dissolved in buffer the other loaded only with buffer. The difference in the feedbacks could hereby be assigned to the heat capacity of the sample. Additionally it monitored the *heating power* needed in one cell to keep the same temperature in both cells. Making it possible to have the same temperature in both cells at all time through a feed back loop [43]. The Differential Scanning Calorimeter was further developed and the VP-DSC from MicroCal, that has been used throughout this thesis, is a third generation DSC.

### 4.3.2 The VP-DSC

The VP-DSC Fig. 4.1 is a calorimeter working at constant pressure ( $\approx 50\text{psi}$ ). A schematic representation can be seen in Fig. 4.2. As with the DASM the VP-DSC has two cells, the cells are in an adiabatic box isolating them from the outside Fig. 4.1. As in the case with the DASM one cell is filled with sample and the other with the solution the sample is dispersed in. The DSC continuously changes the temperature and ensures through the feedback loop that the temperature difference of the cells is close to zero

by adding different amounts of power to the cells ( $P_r, P_s$ ). In other words if an exothermic or endothermic process takes place and  $\Delta T \equiv 0$  then

$$\Delta P = P_r - P_s \neq 0 \quad (4.1)$$

meaning that one cell receives more heat than the other to maintain the same temperature. The excess heat,  $\Delta Q$  is calculated by integration of the excess power with respect to  $t$ .

$$\Delta Q = \int_t^{t+\Delta t} \Delta P(t') dt' \simeq \Delta P \cdot \Delta t \quad (4.2)$$

The heat capacity is, at constant pressure and volume, given by Eq. 4.3

$$C_p = \left( \frac{\partial Q}{\partial T} \right)_p \simeq \left( \frac{\Delta Q}{\Delta T} \right)_p = \frac{\Delta Q}{\frac{\Delta T}{\Delta t}} \quad (4.3)$$

Where  $\frac{\Delta T}{\Delta t}$  is the scan rate. By monitoring the power given to each cell one can easily calculate the heat capacity. If one cell requires more energy to heat by  $1^\circ$  it means that the two samples have different heat capacity at that temperature, which could be attributed to a transition of something in one of the cells (e.g. a lipid melting or a protein melting).

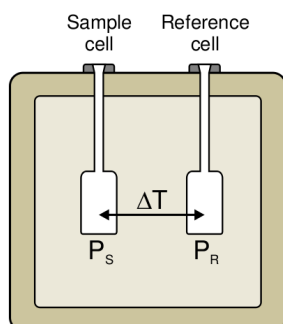


Figure 4.2: A schematic representation of the DSC. The two cells are encapsulated in a box. The cells are adiabatically shielded from the surrounding, both can be heated or cooled at a constant rate so that they have the same temperature at all time. The system is under constant pressure (50 psi) hence the heat capacity can easily be found.

### 4.3.3 Pressure

The pressure cell Fig. 7.5 is a home made addition to the DSC made by the mechanical workshop of the Max-Planck Institute for biophysical chemistry at the University of Göttingen. It is a single capillary with a head welded upon. The head can be connected to a gas bottle, and the system can withstand pressure up to at least 200 bar.

The capillary is filled with the sample and inserted into the sample cell of the DSC. To improve the thermal contact between the sample cell and the pressure cell the sample cell has beforehand been filled with water. Now one can add pressure to the system.

Several valves have been mounted between the gas bottle and the pressure cell to make sure that the pressure cell doesn't explode inside the sample cell. The pressure was recorded with a sensor (EBM 6045) by Nova Swiss (Effretikon, Switzerland).

When inserting a large steel capillary into the sample cell it will naturally affect the measurement, but since the metal does not go through a phase transition in the temperature range where the DSC works, it only contributes to the baseline. For several reasons the measured enthalpy differs from the normal DSC experiment. One reason is that it is not known how much of the working volume of the capillary is in the sample cell and how much is in the capillary leading down to the cell. The exact enthalpy of the system is not of known, however it is the phase transition shift that is interesting in this setup.



Figure 4.3: The pressure cell, to the left side is the head of the pressure cell that is mounted to a nitrogen gas bottle, to the right side the capillary that contains the sample.

## Chapter 5

# Sample preparation

Throughout this thesis DMPC, DPPC and rat brain were investigated in various ways. DMPC and DPPC was bought from Avanti Lipids and stored minus at  $30^{\circ}\text{C}$ . The rat brain was provided by Niels Vidiendal Olsen from Department of Neuroscience and Pharmacology Faculty of Health Sciences at the University of Copenhagen (*nplab*) and was stored at minus  $30^{\circ}\text{C}$ . The Rats were primarily male Wistar rats.

### 5.1 Lipid samples

The lipid samples were produced the following way:

1. The container with frozen lipids was warmed to room temperature before opening. ( $\sim 10 - 15$  min at roomtemperature)
2. The lipids were dissolved in rat buffer (150 mM KCl, 3mM Hepes, 3 mM EDTA, pH 7.2-7.4) and stirred at a temperature above the phase transition (depending of the lipid used), until no visible clumps remained ( $>30$  min).

By warming the lipids to room temperature before opening the container, one prevents the lipids from absorbing water from the surroundings and thereby changing their molecular weight. The buffer contains HEPES which acts as a pH buffer, EDTA acts as a  $\text{Ca}^{2+}$  buffer inhibiting bacteria growth and the  $\text{KCl}^{-}$  resembles the salt concentrations around a nerve and thereby the native conditions of a nerve. By following the recipe above one produces multilamellar vesicles (MLV). MLV's have an onion like structure, where you have membrane layer on a membrane layer on... with a size of  $1 - 10\mu\text{m}$ . A property of MLV's is that they have a high cooperativity meaning that all the lipids tend to be in the same phase, which give rise to a sharp transition peak in the heat capacity profile. In some cases it is more appropriate to look at large unilamellar vesicles

(LUV) instead of MLV's. The LUV's are one lipid bilayer vesicles. They are not as cooperative as the MLV's and the heat capacity profile peak is therefore broader.

The LUV's can be produced in two ways. The first method was an extrusion of MLV's where the sample was pushed through a filter with small pore size (typically  $100nm$ ). This method was not successful since there were a leak from the syringe. Instead the LUV's were produced by ultrasonication of the MLV's. The LUV's then assemble as small unilamellar vesicles (SUV  $\approx 25nm$ ). The SUV's are unstable below the phase transition and will therefore fuse together into LUV's ( $\approx 140nm$ ) if stored below phase transition [44].

## 5.2 Ion channel blocking molecules

Throughout this thesis, different types of chemicals have been used, which are known to influence the membrane conductivity. The chemicals were added to the sample in different ways depending on how well it mixed with water.

Some chemicals were soluble in water and they were just added to the buffer and then mixed with the lipids or they were put directly into a preprepared lipid sample.

Chemicals that were sparingly soluble in water were handled in the following way.

1. The chemical were dissolved in a 50:50 di-chloro-methane/methanol mixture together with the lipids.
2. The sample was dried under an inert gas.
3. The sample is put in the vacuum dessicator over night to extract all the methanol and di-chloro-methane.
4. Buffer was added to the wanted concentration.
5. The mixture was stirred at a temperature above the phase transition for at least half an hour.

A more schematic description can be seen in appendix [B](#)

### 5.2.1 Chemicals

Chemicals that were used were the following.

#### **Tetrodotoxin (TTX)**

TTX is known as the poison from the pufferfish (a very expensive sushi

fish that can kill you if not prepared properly). TTX is a known nerve poison and it is believed that it binds near the sodium channel and thereby preventing sodium to pass over the membrane. TTX is a very effective poison it blocks the action potential at concentrations of  $10^{-7} - 10^{-9} g/mL$  [45].

#### Allyl isothiocyanate (AITC)

AITC is known as oil of mustard and as the name indicates AITC is associated with the taste and smell of mustard. AITC is thought to be acting on the TRPA1 and the TRPV1 receptors. [46, 47]

#### Menthol

Menthol is originally obtained from peppermint and is by many associated with freshness. It is thought to activate the TRPM8 receptor and thereby create the sensation of cold. [31, 48, 49]

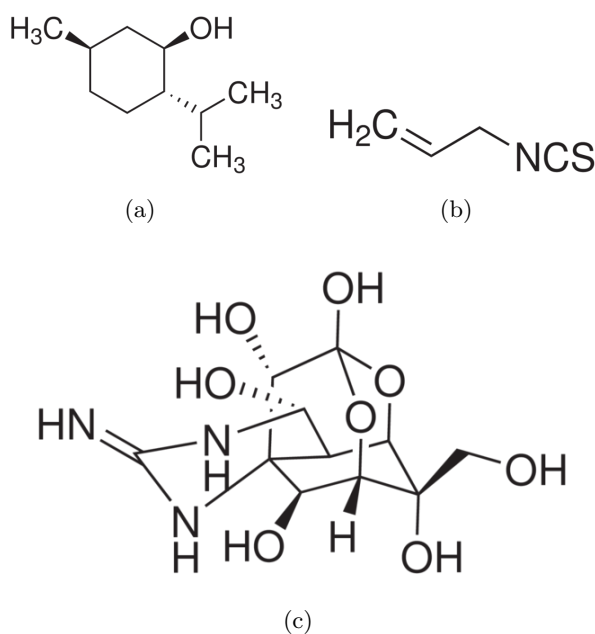


Figure 5.1: The molecule structure of the chemicals described above. (a) (1R,2S,5R)-(-)-Menthol, (b) Allyl isothiocyanate and (c) Tetrodotoxin.

### 5.3 Rat brain

It was not possible to find a suitable method in the literature describing how to prepare brain tissue for calorimetric examination. A few pilot studies were done to determine a suitable method. It was kept in mind that the sample needed to be in liquid form to get into the calorimeter, hence the

sample needed to be grinded in some way. The samples in the pilot studies were prepared the following way:

The first approach was to grind the brain tissue with a mortar and pestle, and then dilute the brain juice with buffer. Afterwards it was sonicated with ultrasound to homogenize even more, assuming that the lipid and proteins would self assemble again. Finally the blood was washed away from the sample by centrifuging and pipetting the non solid parts away.

This first approach worked quite well. However several considerations were made on how to optimize the procedure. One consideration was to prevent oxidation of the sample while doing the grinding and therefore a glove compartment/ gas chamber was build Fig. 5.2(a). It turned out to make no difference. Another consideration was whether or not the proteins could denature if the sample was cooled [50]. But since cold denatured proteins renature to some extent and the brain tissue was received frozen, it didn't make sense to optimize here. A last consideration was, that different parts of the brain could contain different ratios of lipid/protein and thereby give different signals. For this reason the brain was dissected into different parts a medulla, a cerebellum and the rest Fig. 5.2(b). The medulla part gave the best lipid/protein signal and therefore the medulla part was the preferred sample to work with. For a detailed description on how the rat brain samples were prepared look in appendix A.

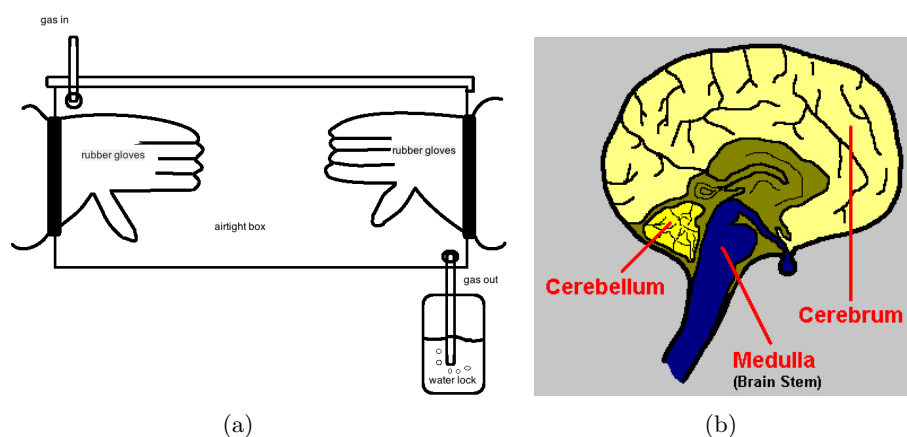


Figure 5.2: (a) A schematic drawing of the home build gas chamber/ box. (b) A simplified schematic drawing of the rat brain

## Chapter 6

# Experimental procedure

*How to master the calorimeter!!!*

The procedure given in the manual from MicroCal (Northhampton, USA) was followed to some extent throughout all the experiments. There are two vital steps in the procedure; the filling of the calorimeter and the cleaning of the cells. Furthermore, the setup of the scan rates, feedback loops etc. was also essential.

### 6.1 Filling the calorimeter

All the samples were prepared as described in chapter 5. Before filling the sample into the cells it was degassed to prevent air bubbles. Air bubbles can appear in the sample when heating it - especially if it has been air-saturated at low temperature. It is therefore important to be aware of air bubbles because they give wrong results. According to the manual 5 min of degassing in vacuum while stirring the sample should do the job. In my setup it was not possible to stir the sample while degassing, but still 5-10 min of degassing was sufficient to prevent air bubbles. Of course not all samples needed to be degassed, the rat brain samples were usually freshly prepared at room temperature and therefore didn't need degassing.<sup>1</sup> Perhaps the most crucial and simplest step in the experiment is filling the cell.

The filling syringe was filled with ( $> 5mL$ ) of sample and position it at  $1 - 2mm$  from the bottom of the calorimeter cell. Slowly, the syringe was

---

<sup>1</sup>Solutions or solvents that have been previously stored in the refrigerator for a long time must be degassed before they are entered into the cells. Solutions that have been air-saturated at low temperature and not degassed prior to loading will tend to form air bubbles as they are heated in the cells, and this will produce large aberrations in the baseline. Solutions equilibrated for long times at room temperature will normally not require degassing. [51]

depressed until the sample raises up into the access tube. The syringe was removed slowly and any excess sample from the overflow reservoir was removed.

## 6.2 Running the calorimeter

After the cells were filled, the lid was screwed on and the pressure raised to 50 psi. Different setups can be chosen on the computer software to optimize the scan. The most imported is the scanrate (the rate of which the temperature is changed). If the sample is expected to have a very narrow phase transition it is important to scan with a low scan rate, to avoid shifting of the transition point due to hysteresis effects. In the opposite case, when you have a broad phase transition, you can benefit from a fast scan rate.

## 6.3 Cleaning the calorimeter

Depending on the experiment the cleaning procedure differs. Independently of the experiment the cells were washed manually with water and then mechanically with ethanol and water. The manual procedure is filling and emptying the cell with a syringe three times. A schematic representation of mechanical cleaning can be seen in Fig. 6.1(b). When using the mechanical setup 100 – 200 mL of water and 50 – 100 mL of ethanol was used. The cleaning procedure was as followed:

- A long needle (cleaning needle) was inserted into the sample cell until the o-ring sealed the opening of the cell.
- The upper end of the "cleaning needle" was connected to the cleaning agent while the lower end was connected to a vacuum flask.
- The pump was started.  
When the determined amount of cleaning agent (water, ethanol...) had run through the system, the upper tube was removed from the cleaning agent and the pump ran a few minutes to dry out the cell.
- Rinse with water at last. Or rinse with ethanol and heat the calorimeter to above  $78^{\circ}C$  to evaporate the ethanol.

If a sample with protein has been run in the calorimeter, as the rat brain sample, 14% phosphoric acid was used in the manual procedure as a cleaning agent. The reason is that protein tend to become "sticky" when denatured or as it comes into contact with ethanol. Therefore it can be difficult to wash away all the protein with water and ethanol.

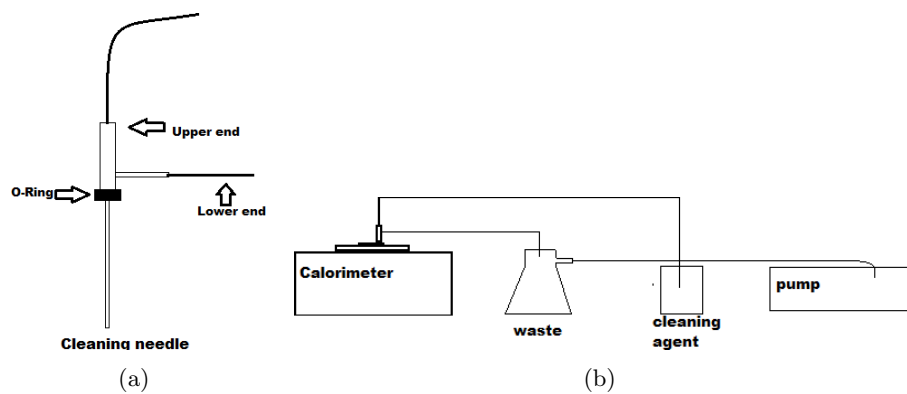


Figure 6.1: (a) The cleaning needle, (b) the cleaning setup, where the needle has been inserted into the calorimeter. The figures were made in paint.



## Chapter 7

# Results and discussion

In this chapter I will present the results obtained during the experiments. The results have been divided into sections with the associated discussions following.

The presented heat capacity profiles are not raw data, if not indicated otherwise. The data have been modified in Igor pro. The calorimeter can either start at low temperature and end at a high temperature, this is called an up-scan. Starting at a high temperature and then cooling the sample is called a down-scan. Since there are hysteresis effects it is important to distinguish between up- and down-scans. All the data presented are up-scans if otherwise is not indicated. The hysteresis effects can be neglected if one scans very slowly. For this reason the lipid samples were usually scanned at  $5^{\circ}\text{C}/\text{h}$ . On the other hand the biological samples were scanned at  $20^{\circ}\text{C}/\text{h}$ . Since the biological sample has a very broad transition the hysteresis effect is negligible and one can benefit from a fast scan rate.

The data is presented without error bars. Since the error of the calorimeter are very small. However there will necessarily be systematic errors. It is assumed that the biggest systematic errors in the lipid samples were in the weighing of the different compounds, which were weighed on a balance with a precision of  $0.1\text{mg}$ . In the biological samples there are many steps where errors could occur. One, perhaps the biggest, is that all the samples are from different rats. Another is in the process of removing the brain from the rest of the rat. Hence where exactly the decapitation is made. A third cause of error is in the dissection of the brain.

## 7.1 Pure lipid samples

### 7.1.1 Scanrate

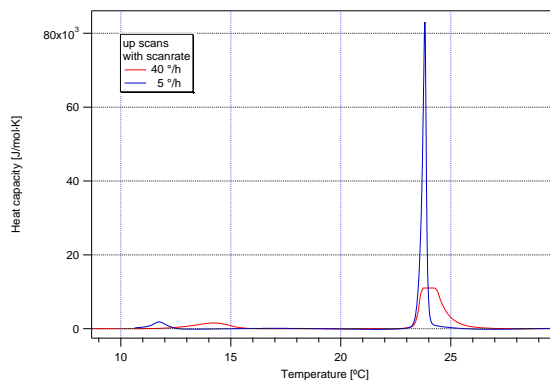


Figure 7.1: Excess specific heat capacity of the phase transition in DMPC-MLV. Heat capacity profiles varies, even for scans of the same sample, because of long relaxation times and hysteresis. Presented are two scans of the same sample at two difference scans.

As seen in Fig. 7.1 the scan rate makes a big difference, not only does the peak move toward higher temperature with the scan rate, but it also broadens the phase transition and lower the peak.

### 7.1.2 Up- and down-scans

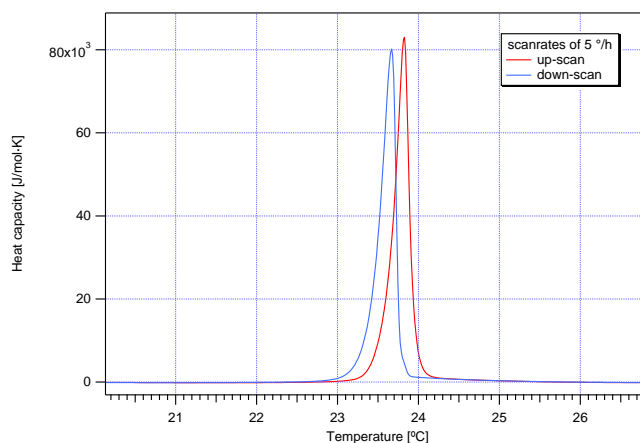


Figure 7.2: Heat capacity of the phase transition in DMPC-MLV. Here the hysteresis effects can be seen, there is clearly a difference in the up- and down-scan

In Fig. 7.2 it is seen that the phase transition shift in response to the scan direction. This is due to the response time of the membrane. It can

be avoided by lowering the scan rate. The enthalpy differs less than 0.5% in this measurement.

### 7.1.3 DMPC vs. DPPC

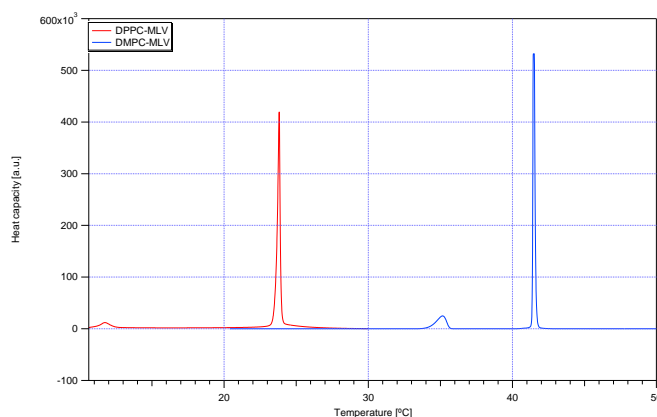


Figure 7.3: Heat capacity profile of the two different lipid types used in the thesis, this being DMPC-MLV and DPPC-MLV.

In Fig. 7.3 the heat capacity profile for a pure DMPC-MLV and DPPC-MLV membranes are plotted. These two different lipids have different advantages. Since it is easiest to mix the buffer and lipids when the lipids are in the fluid phase, it is quite easy to work with DMPC, since, as seen in Fig. 7.3, DMPC has a melting point around room temperature, whereas DPPC has a melting point above  $40^\circ\text{C}$  and it is therefore necessary to heat the sample when preparing it. The reason to work with DPPC is that it has a very sharp transition and a clear pretransition.

### 7.1.4 Sonication

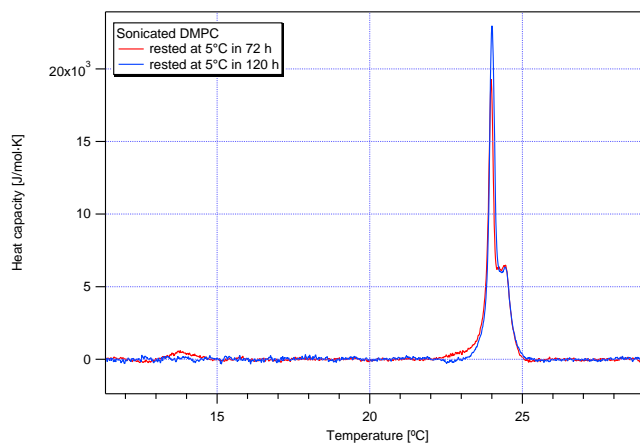


Figure 7.4: Heat capacity profile of DMPC-MLV that has been sonicated.

In Fig. 7.4 one can see that the profile broadens. When a MLV sample is sonicated the MLV's are destroyed, and the lipids self assembled into SUV with a size of about ( $\propto 30nm$ ), that will fuse into LUV with a size of about ( $\propto 100nm$ ).

### 7.1.5 Pressure

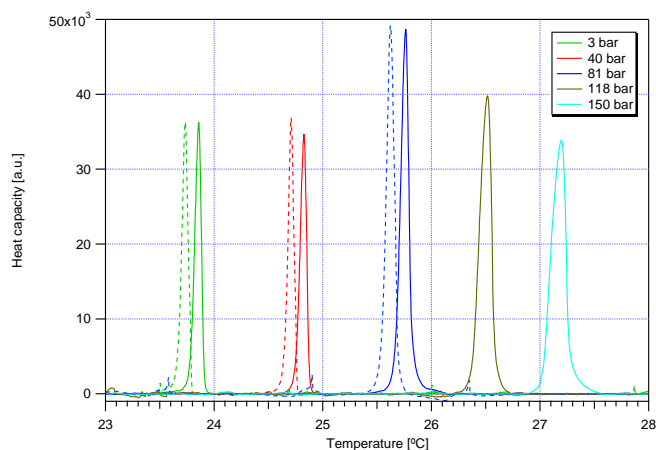


Figure 7.5: Heat capacity profile of DMPC-MLV, recorded in the pressure setup under different pressure. The solid lines are up-scans and the dotted lines are down scans.

### 7.1.6 Discussion in regard to pure lipid samples

In section 7.1, several scans of pure lipid samples have been shown. It is seen that the heat capacity profile depends a lot on the way the scan is performed. In Fig. 7.1, it is clearly seen how the scan rate effects the result. Further in Fig. 7.2 and 7.4 it is seen that the direction of the scan and even how the sample is prepared effects the results. In the standard setup for the VP-DSC, the sample is in a cell with  $50 \text{ psi} \approx 3 \text{ bar}$ . In Fig. 7.5 a pure DMPC-MLV was scanned under different pressure with the pressure setup described in section 4.3.3. Since it is the exact same sample that have been scanned in all 5 scans, one would have expected that the enthalpy of each scan to be the same. This is not the case, the most likely case is do to some of the capillary being placed outside the sample cell, hence some of the sample is placed outside the sample cell. Since the scans where don over 6 days, it is likely that some of the sample has sedimentated hence a higher concentration within the sample cell, giving a higher signal.

Nevertheless, it is clear that the melting point is shifted upwards as the pressure is increased, as predicted in section 1.6. By using Eq. 1.6 the expected change in the peak temperature due to pressure can be calculated. From Fig. 7.5 the melting peak for 3 and 150 bar are found to be  $23.858^\circ\text{C}$  and  $27.196^\circ\text{C}$

$$\Delta T_m = \gamma_V \Delta p T_m \Rightarrow \quad (7.1)$$

$$\Delta T_m = 7.8 \cdot 10^{-10} \cdot \frac{\text{m}^2}{\text{N}} \cdot 147 \cdot 10^5 \cdot \frac{\text{N}}{\text{m}^2} \cdot (273.15 + 23.858)^\circ\text{K} \Rightarrow (7.2)$$

$$\Delta T_m = 3.41^\circ\text{K} \Rightarrow \quad (7.3)$$

$$T_{m, 150 \text{ bar}} = 27.26^\circ\text{C} \quad (7.4)$$

The constant  $\gamma_V$  was taken from [15]

To sum up there is a lot of ways to change the melting profile of a very simple system such as the pure lipid system.

## 7.2 Lipid with tetrodotoxin

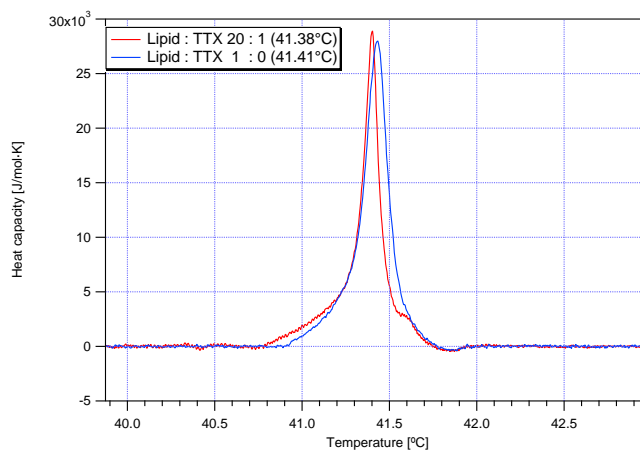


Figure 7.6: Heat capacity profile of sonicated DPPC, recorded with a scan rate of  $0.8^{\circ}\text{C}/h$ , with and without TTX. Another buffer was used in these scans (75 mM KCl, 3 mM EDTA and HEPES)

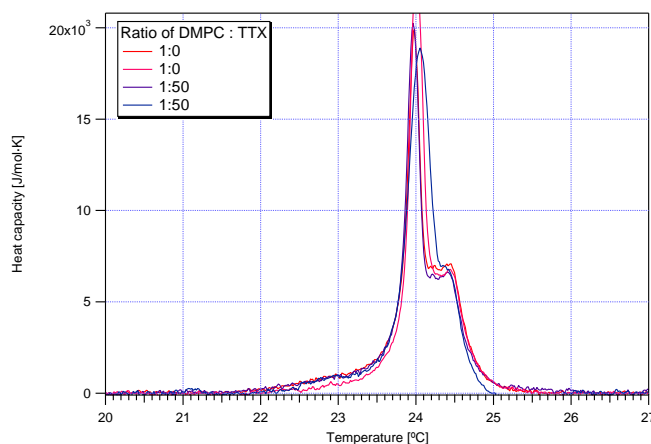


Figure 7.7: Heat capacity profile of sonicated 1 mM DMPC, recorded with a scan rate of  $5^{\circ}\text{C}/h$ , with and without TTX.

In Fig. 7.6 and Fig. 7.7 we see DMPC and DPPC heat capacity profiles where TTX (Tetrodotoxin) has been added. It should be noted that the samples have been sonicated before and after TTX was added, to make sure that every lipid, in principle, have seen a TTX molecule. As described in section 5.2.1, TTX is a known ion channel blocking molecule. So one would expect that there was a big interaction between the membrane and TTX, hence a big change in the melting profile. However, it seems that TTX does not change the melting profile. Since TTX is easily soluble in water and

since the samples are at low concentrations one could imagine that TTX is not dissolved in the membrane. One way to test this would be to use higher concentrations, however TTX is a rather costly chemical.

## 7.3 TRP-channel activation molecules.

### 7.3.1 Lipids with Allyl isothiocyanate.

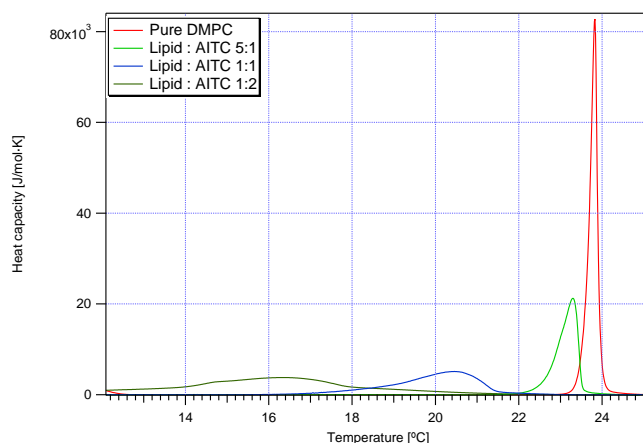


Figure 7.8: Heat capacity profile of 10 mM DMPC-MLV added AITC in different concentrations.

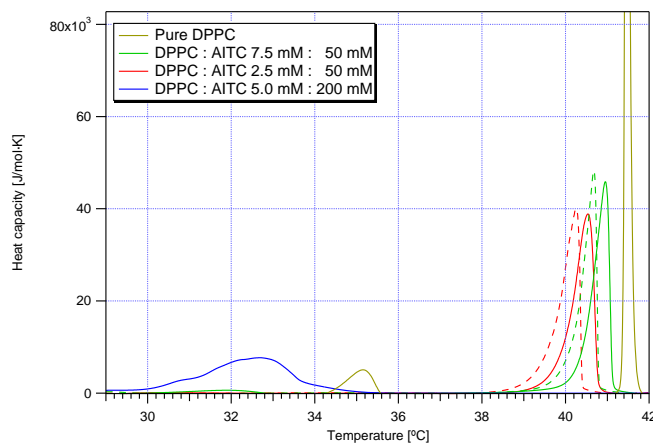


Figure 7.9: Heat capacity profile of DPPC-MLV added AITC in different concentrations. The dotted lines are down-scans and the solid lines are up-scans

In Fig. 7.8 and Fig. 7.9 different concentrations of AITC were added to different lipids. It is clearly seen that adding AITC lowers and broadens the melting profile. It seems that DMPC is much more effected by AITC

than DPPC. Since DMPC in the 1 : 1 ratio drops ( $\sim 3^\circ$ ), whereas DPPC only drops ( $\sim 1^\circ$ ) when there is 25 times more AITC molecules than lipids. However it should be noted that the samples were prepared in different ways. In the case of the DMPC, the concentration of AITC was varied and the concentration of DMPC was kept constant at  $10mM$ , whereas the DPPC samples the concentration of DPPC was varied. Since AITC is fat-soluble it was assumed that most of the AITC would go into the membrane. Therefore it is the ratios between lipid and AITC that are interesting. However, to conclude that AITC has a bigger effect on DMPC than on DPPC one would have to repeat the same experiments. Having the same concentration and the same ratios of lipid AITC in both the DPPC and the DMPC parts of the experiments. Furthermore it should be noted that the concentration of AITC is the concentration in the buffer before lipid was added.

### 7.3.2 Lipids with menthol

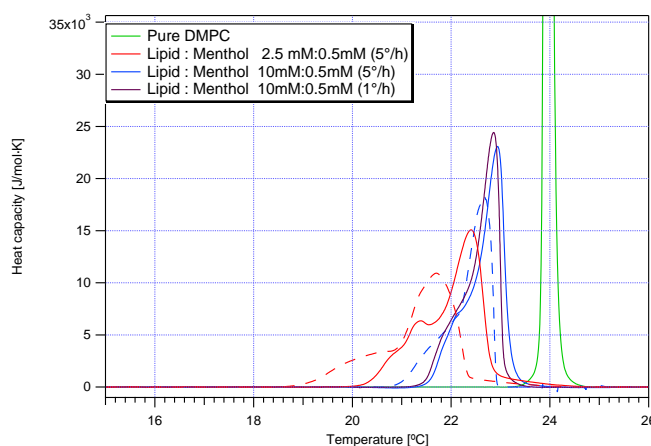


Figure 7.10: Heat capacity profile of DMPC-MLV added menthol in different concentrations. The solid lines are up-scans and the dotted lines are down-scans

In Fig. 7.10 and Fig. 7.11 the heat capacity profile of DMPC and DPPC with and without menthol is shown. It is clearly seen that by adding menthol to the sample the profile is broadened and the melting point is lowered. As with AITC it seems that menthol has a bigger effect on DMPC than on DPPC. In the case where a lipid to menthol ratio of 20 to 1 the half-melt point has been lowered by  $0.63^\circ$  for DPPC and  $1.23^\circ$  for DMPC. Whereas with the ratio of 5 to 1 is  $1.70^\circ$  for DPPC and  $1.85^\circ$  for DMPC. So it seems that DMPC is easier to effect. However when we go to higher concentrations the effect on DPPC and DMPC is very similar. Another thing to notice is that the hysteresis effect is bigger in the DPPC samples than in the DMPC samples. As with the AITC samples the menthol concentrations are the

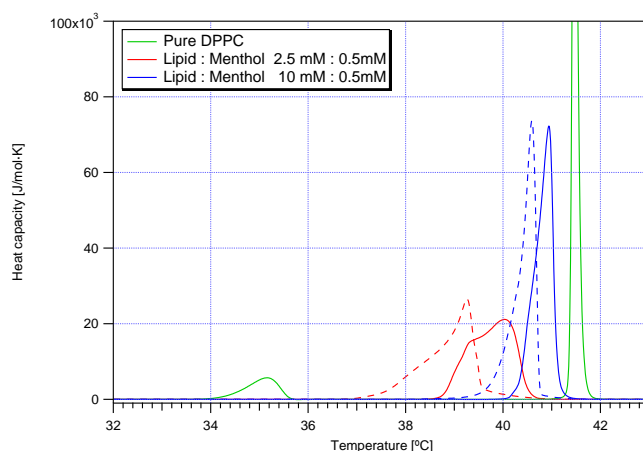


Figure 7.11: Heat capacity profile of DPPC-MLV added menthol in different concentrations. The solid lines are up-scans and the dotted lines are down-scans

concentrations in the buffer before lipids were added.

### 7.3.3 Discussion in regard to the TRP-activation molecules.

It is clear that menthol and AITC have an effect on the melting of pure lipid membranes. As written in section 3.5 the permeability of the membrane peaks in the phase transition [39]. If we further assume that menthol and AITC have different effects on different lipids, as the result indicate. It would be possible that different membranes react different to different molecules. Hence, the whole membrane could act as specific receptor. However, this is highly speculative and one would have to do many experiments on pure lipid systems with different compositions of different lipids types added with different activation molecules, to see how different systems react to different activation molecules. If there is a difference in the reaction of different lipid systems it would be interesting to try with real biological tissue. This could be brain tissue from rats. Further it would be interesting to compare the melting profile from normal rats with the melting profile from rats where a TRP gene has been knock out, both with and without the respective activation molecule.

## 7.4 Ratbrain.

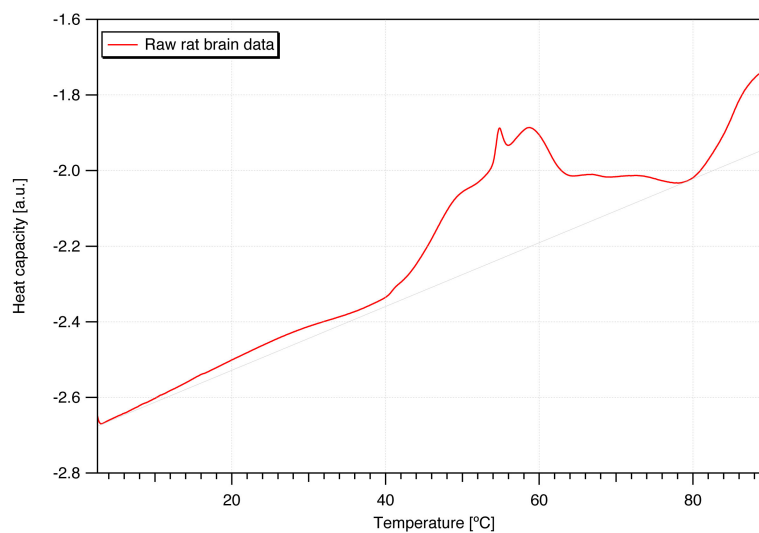


Figure 7.12: The raw heat capacity data from the melting of a rat brain.

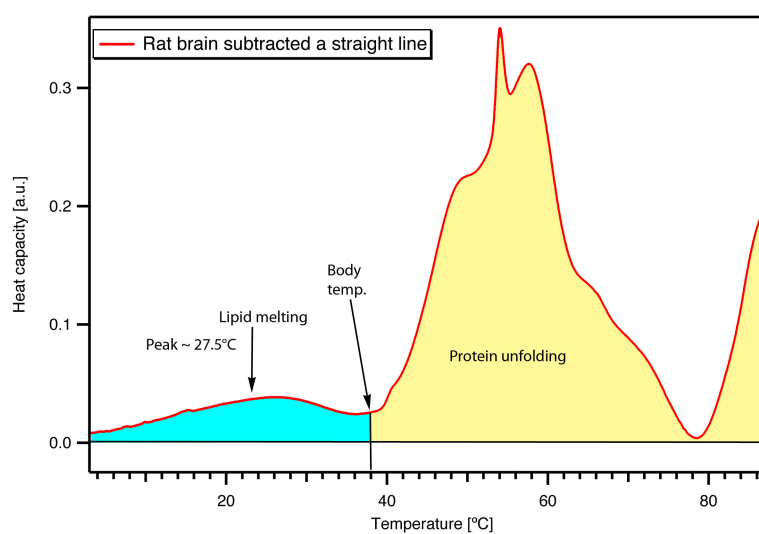


Figure 7.13: The heat capacity data from the melting of a rat brain, where a straight line has been subtracted. (The same data as in Fig. 7.12).

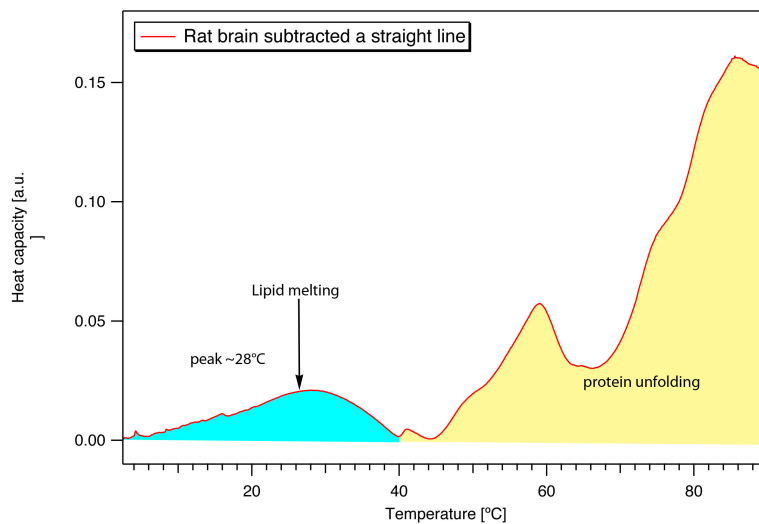


Figure 7.14: Medulla from a rat brain has been scanned and a straight line has been subtracted. If compared with Fig. 7.13 it is seen that the signal due to melting of lipids is bigger and that the peak has shifted a bit upwards.

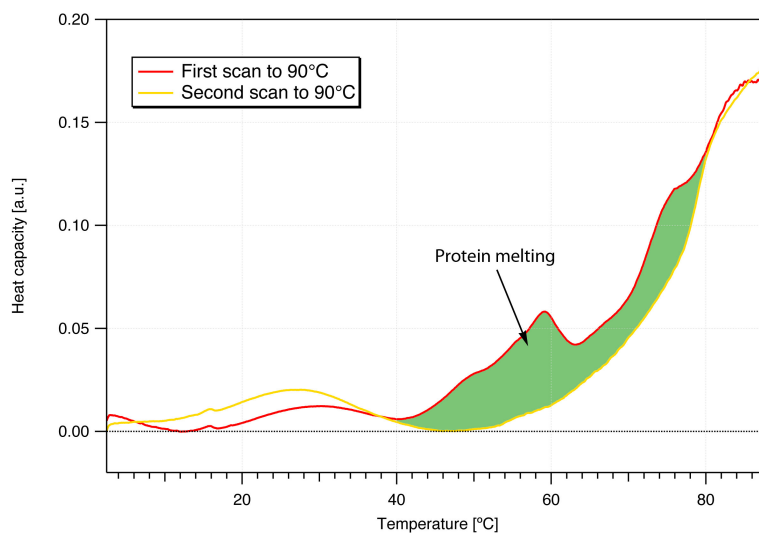


Figure 7.15: Medulla from a rat brain where scanned two times. The green area is a irreversible protein denaturation. Further it is seen that the lipid part of the signal is changed after the protein has melted.

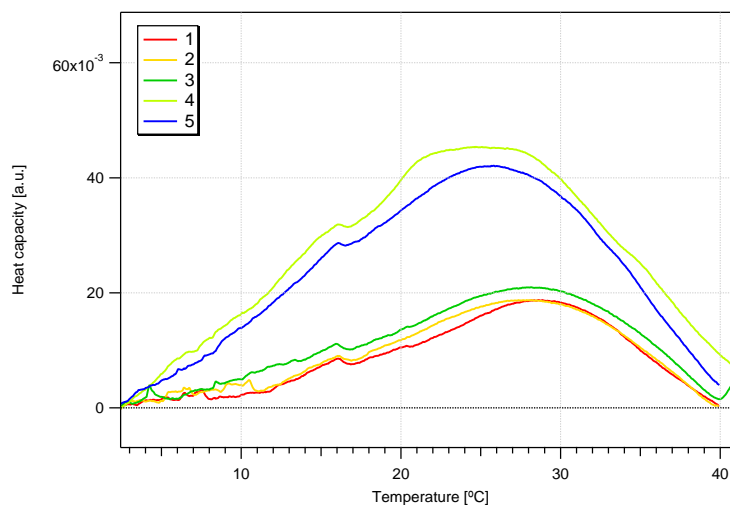


Figure 7.16: Zoom in on a medulla rat brain sample scan. The same sample has been scanned five times. Scan number 1, 2 and 5 are scans to  $40^{\circ}\text{C}$  and scan 3 and 4 to  $90^{\circ}\text{C}$ . It is seen that scan 1, 2 and 3 are almost identical where as scan 4 and 5 have shifted their maximum to a lower temperature and their signals have become bigger. This is most likely do to the denaturation of the protein referred to in Fig. 7.15

In Fig. 7.12 the raw data of the first calorimetric scan with rat brain is shown, and it is clear that something melts. Further it is seen that there is drift in the data, which is probably due to different volume in the sample and the reference cells. It is assumed that the signal difference due to volume difference (of water) is linear, hence a straight line can be subtracted (baseline). This is done in Fig. 7.13.

In Fig. 7.13 the signal has been divided into two parts. A part from  $(0 - 38^{\circ}\text{C})$  and a part from  $(38 - 90^{\circ}\text{C})$ . The lower part is attributed to the melting of the lipids whereas the higher part is attributed to the melting of proteins. To get a better ratio between protein and lipid, the brain was dissected into different parts as written in section 5.3. It was expected that the medulla part would have a better ratio. It turned out to be a correct assumption. The cerebellum and cerebrum samples had a weaker lipid signal, therefore only the medulla part of the rat brain were used. In Fig. 7.14 the heat capacity for the medulla sample from a rat brain is shown and the lipid part of the signal is now clear.

In Fig. 7.15 it is seen that some part of the melting is reversible and others are not. The green area is the irreversible part and it is interpreted to be melting of proteins. In Fig. 7.16 where the exact same sample has been scan 5 times, it is seen that the signal between  $0 - 40^{\circ}\text{C}$  has changed after the temperature of the sample has been above  $85^{\circ}\text{C}$ .

### 7.4.1 Rat brain under pressure.

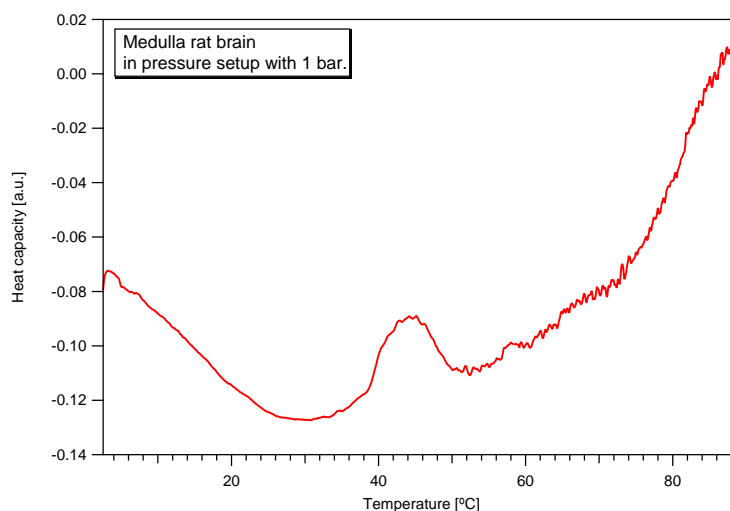


Figure 7.17: Pure medulla rat brain sample scanned in the pressure setup at 1 bar.

In Fig. 7.17 a rat brain sample has been scanned in the pressure setup, where no pressure has been applied. Therefore one would expect the data to look like the data presented in Fig. 7.14. This is clearly not the case, further the rat brain scans done with the pressure setup was not reproducible, most likely do to the high level of noise compared to the signal (very little sample volume).

### 7.4.2 Rat brain with menthol.

As written in section 7.3.3, it would be interesting to have a look on the heat capacity profile of a biological sample where an activation molecule has been added. Therefore a rat brain sample with menthol was prepared. The preparations were done as described in appendix A were the rat buffer was added 0.5 mM menthol. The preliminary result is seen in Fig. 7.18 and a comparison with the standard rat brain sample is seen in Fig. 7.19. It is clear from Fig. 7.19 that something has changed in the sample. But since only one sample has been prepared so fare, it is to soon to conclude anything other than it look interesting.

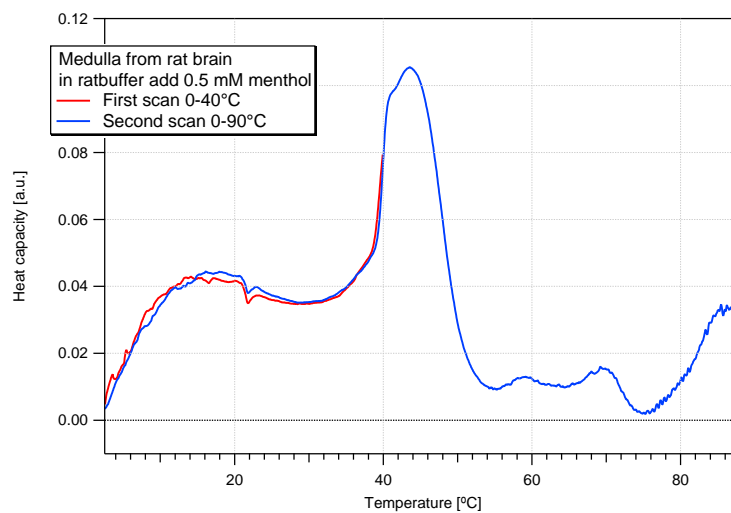


Figure 7.18: Scan of medulla rat brain sample, where  $0.5mM$  menthol has been added to the rat buffer.

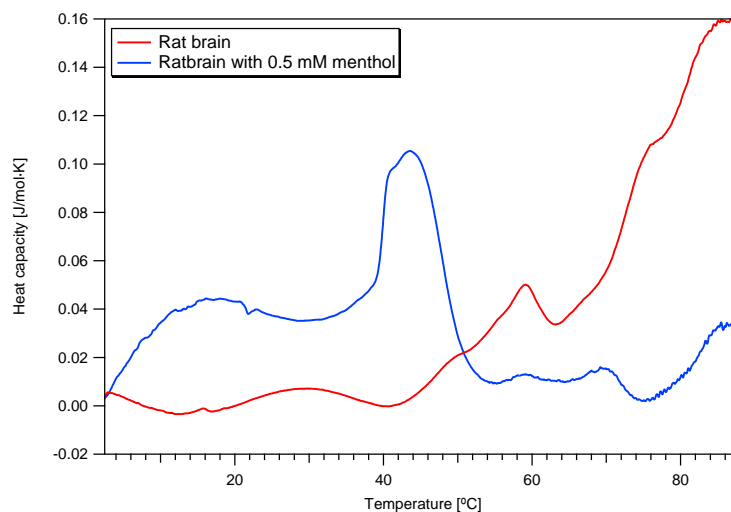


Figure 7.19: Comparison of the standard rat brain signal and rat brain where  $0.5mM$  menthol has been added to the buffer.

### 7.4.3 Discussion of the rat brain results

Throughout this section the melting profiles of rat brain have been shown, and it is also shown that the signal can be altered by dissecting the brain into different part. Due to the properties of the the medulla part of the rat brain, this part was chosen.

First of all the signal from the medulla samples, had the stronger signal in the lower temperature regime compared to the other samples as see when comparing Fig. 7.13 and Fig. 7.14.

Second the medulla is the lower half of the brainstem. Thereby a nerve and therefore the most interesting part of the brain in respect to the work don in this thesis. In Fig. 7.13 and Fig. 7.14 the graph has been cut in half, where the higher part is attributed to being the melting of a proteins, and the lower part is attributed to the melting of lipids. Since most proteins above body temperature denature this part of the signal is irreversible. While the signal below  $40^{\circ}\text{C}$  can be measured again and again. Indicating that this part of the signal might be due to the melting of lipids. Since proteins and lipids react differently to pressure [52] the sample was scanned in the pressure setup. As seen in Fig. 7.5 lipid melts at a higher temperature when pressure is applied. Whereas protein tend to lower their melting point when pressure is applied. Further proteins melting point are not as easily shifted with pressure - several *kbar* are needed [53]. But as seen in Fig. 7.17 and written in section 7.4.1 the pressure setup available at the time was not successful in measuring the rat brain sample, most likely due to the little volume in the capillary. However a Pressure Perturbation Calorimetry (PPC) Accessory from microcal [54] have been purchased and with this it should be possible to make pressure measurements on the rat brain sample, since it uses the entire working volume of the DSC.

The perhaps most interesting discovery is seen in Fig. 7.16. In this figure it is clear that the first three scans are almost identical up to  $40^{\circ}\text{C}$ . Whereas scans 4 and 5 differ from the first scans. It should be noted that scans 1, 2 and 5 are scans from  $0 - 40^{\circ}\text{C}$  whereas scan 3 and 4 are scans to  $\approx 90^{\circ}\text{C}$ . As described above the lipid part of the signal shift after the sample has been heated to above  $85^{\circ}\text{C}$ . Indicating that the lipid signal depend on the state of the proteins. An explanation could be that the lipids rearranges, do to hydrophobic matching with the changed proteins, in according to the Mattress model [8] and there by change their melting point. Nevertheless it is clear that the state of the protein change the melting point of the membrane.

As written above, a medulla rat brain sample where menthol had been added were prepared and scanned. Since only one menthol rat brain sample has been prepared to date, it is hard to state anything with certainty. Nevertheless if it is assumed that the data presented in Fig. 7.18 is reproducible, it would seem that the lipid melt at lower temperature, which would also be

consistent with the result presented in section 7.3.2. Further it seems that all the proteins melt between  $40 - 50^{\circ}C$ . But as written above since the experiment hasn't been reproduced it is pure speculations.

## Chapter 8

# Conclusion

The main aim of this thesis was to get a better understanding of how different chemicals alter the melting profile of membranes. The chemical of most interest was Tetrodotoxin (TTX), since it is directly correlated to the nerve signal by the blocking of the sodium channel. However as presented in chapter 7 the experiments conducted in this thesis with TTX didn't show any significant change of the melting profile of the lipid membranes. There can be multiple reasons for this. One being that TTX only acts on the sodium channel as are believed and thereby doesn't interact with a pure lipid membrane. Another reason is, that the concentrations of lipids used in the experiments were too small meaning that there is too much free water for the TTX to be dissolved in. Hence TTX is not dissolved in the membrane but floats freely around in the water of the sample, I find this plausible since TTX is easily dissolved in water.

Further experiments with rat brain dissolved in buffer with TTX were conducted during this thesis, however without any success.

Another aim was to test the effect of chemicals that were known to activate certain TRP receptors. Menthol was chosen since it is both cheap and harmless to work with and also because its effect the TRPM8 receptors, which is one of the most studied TRP receptors. Menthol samples were made with both DMPC and DPPC. The results show that both lipid species were affected by menthol. They melt at a lower temperature and over a broader temperature span. Further the results indicate that at a relative low concentration of menthol has a bigger effect on DMPC than on DPPC, whereas at higher concentrations of menthol the effect is approximately the same. Also allyl isothiocyanate (AITC), which is known to activate the TRPV1 receptor, was examined. These experiments gave similar results as with menthol however not identical. With these results in mind and that the permeability of the KcsA-channel peaks in the phase transition, one could speculate that it is not the TRP protein that acts as a receptor but instead the whole membrane. As further described in section 7.4.2 preliminary ex-

periments with rat brain diluted in buffer with menthol have been started, to investigate the effects on a system with many components.

Most of the experiments in this thesis serve as pilot studies, that tested whether or not different chemicals had an effect on the melting profile of simple lipid systems. It was expected that TTX would have a huge effect, which it did not have. In the contrary to this are the effects of menthol and AITC.

In the case with the rat brain experiments, it was expected to be easy just to grind the brain, scan it and then add different chemicals. It turned out to be rather difficult. Much of the time spend during this thesis was therefore spend on developing a procedure on how to prepare the brain samples. During this process it was discovered that the signal look different if scanned several times. This did not come as a surprise since it was expected that the samples contained proteins that would denature at high temperatures. However it was not expected that the denaturation of the protein would change the lipid signal significantly. But as presented in Fig. 7.16 it is clear that the signal between  $0 - 40^{\circ}C$  has changed after the proteins have denatured. The fact that the state of the proteins can change the melting profile of a complicated system and the fact that the ion flux of the KcsA-channel peaks in the transition phase indicate that a reason for some proteins to be in the membrane are to give the membrane a specific melting profile.

## Chapter 9

### Future work

As mentioned above most of the experiments in this thesis serve as indicators for future work. Since it is known that TTX plays a vital role in the ability to conduct nerve signals, it would be very interesting to see if TTX has an effect on a pure lipid system if much higher lipid concentrations were used. Another approach could be to increase the amount of TTX, however these experiments would become rather expensive due to the price of TTX. Further calorimetric scans of biological tissue mixed with TTX should be possible, although the attempts during this thesis failed. These experiments are of huge relevance.

The results indicates that menthol and AITC have different effects on different lipid species and it would be relevant to investigate this further. This could perhaps explain how membranes can distinguish between different molecules. Further it would be relevant to compare ws12 and icilin with menthol since they all are thought to activate the TRPM8 receptor in different degrees. For example ws12 is thought to activate the TRPM8 receptor 200 times better than menthol.

Other studies have shown [31, 55, 56], that mice where the TRPM8 receptors have been knocked out, don't react to cold stimuli. It would be interesting to test whether or not there is a difference in the melting profile of samples from the TRPM8(-/-) mice and the normal mice.



## Appendix A

# Protocol for dissection of the Rat brain

### Protocol for dissection of the Rat brain

First find all the lab equipment that is needed for the dissection of the rat brain

- tweezers, 3 or more marked container (determine the mass of the containers), scalpel, loop, rat brain, pipetes, mortar and pestel.

Fore later use it might be useful to know:

- determine the mass of the containers with the sample an there by the sample mass.

How to dissect

- The slightly frozen rat brain, is cut in half, by turning it up side down and cutting it at the central nerve.
- Separate the central nerve from the rest of the two brain half's. By letting the brain defrost, then put the tweezers in between the different parts of the brain and slowly open the tweezers again
- The same is done for the other parts of the brain that are to be examine.
- Measure the mass of the containers and sample.

How to handle the dissected brain.

- First grind the samples individual with a mortar and pestel.
- Then put it into a sample tube and add 3 ml of buffer is added.

## Appendix A. Protocol for dissection of the Rat brain

---

- Sonicate the sample with a ultrasound source to burst all cells, to avoid heating of the sample, set the sonicator to sonicate in short pulses and sonicate until the sample looks as a homogeneous liquid.
- Centrifuge the samples in 5 min at 3000 rpm... (make sure that you have a balance weight)
- Pipettes the liquid away, and save for later use.
- Add 3 mL of buffer, and centrifuge for 5 min, and pipetted the liquid away, this is don 3 times or more until the solid part of the sample looks clean.
- Add 1 mL buffer and shake the sample until the solid part has dissolved. If there are any impurities, remove them.

### How to use the calorimeter

- Make sure that the calorimeter and the syringe is clean.
- Degass the sample and the buffer.

### Filling the calorimeter:

- Cells are always to be filled from the bottom up. The end of the syringe should be positioned about 1-2 mm from the cell bottom during the filling.
- First fill the reference cell with the buffer (the cell to the right, marked with and R)
- Second fill the cell to the left with the sample.
- Ready to scan

### Cleaning of the Calorimeter

- First rinse the sample cell with 100 mL of millipore water
- Using the filling syringe rinse the sample cell with acid (only if one has used protien that have denatured)
- then rinse first with water (50-100mL) then with ethanol (100 mL) and then either dry out cell by heating it ore rinse with water again (100-200mL) (after each rinse agent "rinse with air to dry out cell)
- Fill the cells with the buffer that are to be used in the next experiment

## Appendix B

# Lipid Sample preparation

This part is included so other people may reproduce the work of this thesis. It should not be necessary to read it to understand the thesis itself, but is simply here as documentation.

### B.1 Lipid samples

1. Let the container with the lipids heat to room temperature before opening (to avoid them absorbing water from the surroundings)
2. Measure out an appropriate amount of lipids. Since the vesicles only consist of one type of lipid (e.g. DMPC or DPPC), then simply dissolve it in the wanted buffer solution. If a mix of lipids is necessary (e.g. DPPC and DPPG) dissolve the lipids in a 2:1 mix of dichloromethane:methanol, and then let the solvent evaporate in a desiccator (vacuum chamber) before dissolving it in the buffer solution.
3. Heat it to above the phase transition temperature while stirring it for at least half an hour. (the sample should appear milky.)
4. Once done, transfer the sample to a small vial and store it in the fridge.

### B.2 Extrusion procedure

1. Proceed as in the lipid samples point 1 – 3.
2. Meanwhile, turn on the heat bath for the extruder, setting it to above the phase transition.
3. Fill the sample in the extruder syringe and put the filled syringe in the extruder for 15 minutes, thus allowing the syringe and the sample to get heated to the same temperature as the extruder itself. (when

### B.3. Sonication (SUV and LUV) Appendix B. Lipid Sample preparation

mounting the filter in the extruder setup, add a drop of water, it makes the filter easier to handle).

4. Extrude slowly (about one cycle per two minutes), and make sure that it's done an odd number of times, thus ending up with the sample in the opposite syringe. This should reduce the amount of dust and aggregates in the sample (as this will be left in the first syringe) and it will ensure that all of the vesicles have been through the filter at least once.
5. Once done, transfer the extruded sample to a small vial and store it in the fridge.

[10]

### B.3 Sonication (SUV and LUV)

1. Proceed as in the lipid samples point 1 – 3.
2. Mount the ultrasonication source in the sample and turn up the sound...Keep the power so low that gas bubbles are not created in the sample, since this could destroy the ultrasonic source. Stop when the sample turns transparent.
3. Once done, transfer the extruded sample to a small vial and store it in the fridge for a few days to get LUV. If SUV's are wanted then use the sample just after sonication

### B.4 Menthol samples

The menthol samples are made as written above, however the buffer has been added 0.5mM menthol.

### B.5 AITC

The samples are prepared as written above, however the AITC buffer has been prepared as follow.

1. dissolve the wanted amount of AITC in a 1:1 mix of dichloromethane:methanol, and then let the solvent evaporate in a desiccator (vacuum chamber) before dissolving the wanted buffer
2. Continue as written

## Appendix C

### relaxation time

$$c_p = \frac{d\langle H \rangle}{dT} = \dots = \frac{\langle H^2 \rangle - \langle H \rangle^2}{kT^2} \equiv \frac{\sigma^2}{kT^2} \quad (\text{C.1})$$

Shows that the heat capacity is related to the mean square deviation from the enthalpy. Meaning that the fluctuations are high when the heat capacity is high. This has fully be deduced in appendix D. Further we assume that the fluctuations of the enthalpy is Gaussian distributed.

$$P(H) = \frac{\exp\left(-\frac{(H - H_0)^2}{2\sigma^2}\right)}{\sigma\sqrt{2\pi}} = \frac{\exp(-G(H)/kT)}{Q} \quad (\text{C.2})$$

It is further assumed that the volume, enthalpy and areal do not flucturate independently, but they are dependent of each other. So the free energy function of enthalpy is given by

$$G(H) = -kT\ln(H) + \text{const.} \quad (\text{C.3})$$

and the entropy function of enthalpy is given by

$$S(H) = \frac{-G(H) + H}{T} \Rightarrow \quad (\text{C.4})$$

$$S(H) = \frac{kT \ln(p(H)) - \text{const.} + H}{T} \quad (\text{C.5})$$

$$= \frac{kT \ln\left(\exp\left(\frac{-(H-H_0)^2}{2\sigma^2}\right)\right) - \text{const.} + (H - H_0)}{T} \quad (\text{C.6})$$

$$= \frac{kT \left(\frac{-(H-H_0)^2}{2\sigma^2}\right) - \text{const.} + (H - H_0)}{T} \quad (\text{C.7})$$

$$= -\frac{k(H - H_0)^2}{2\sigma^2} - \frac{\text{const.} + H - H_0}{T} \quad (\text{C.8})$$

$$\approx \frac{k(H - H_0)^2}{\sigma^2}, \text{ for small } \sigma \quad (\text{C.9})$$

since enthalpy, volume and area all are proportional, it is the same as there only being one force driving the system back to equilibrium

$$X_H = \frac{\partial S}{\partial H} = -\frac{k}{\sigma^2}(H - H_0) \quad (\text{C.10})$$

now we can write Onsagers phenomenological equation, where  $J_H$  is the flux

$$J_H = \frac{d(H - H_0)}{dt} = LX_H = -\frac{L \cdot k}{\sigma^2}(H - H_0) \quad (\text{C.11})$$

from from Eq. C.1 and Eq. C.11 we know that

$$c_p = \frac{\sigma^2}{kT^2} \Leftrightarrow \sigma^2 = c_p k T^2 \Rightarrow \quad (\text{C.12})$$

$$J_H = \frac{d(H - H_0)}{dt} = Lk(H - H_0) \frac{1}{kT^2 c_p} \Rightarrow \quad (\text{C.13})$$

$$= -\frac{L(H - H_0)}{T^2 c_p} \quad (\text{C.14})$$

This we can solve and get

$$H - H_0 = (H - H_0)_0 \exp\left(-\frac{t}{\tau}\right) \text{ where } \tau = \frac{T^2 c_p}{L} \quad (\text{C.15})$$

so the relaxation time is then given by

$$\tau = \frac{T^2 c_p}{L} \Rightarrow c_p \propto \tau \quad (\text{C.16})$$

[6, 16, 40]

## Appendix D

# Derivations

As shown in section 1.5 the heat capacity at constant pressure  $c_p$  is defined as

$$c_p \equiv \left( \frac{d\langle H \rangle}{dT} \right)_p \quad (\text{D.1})$$

Calculating the differential one gets

$$c_p \equiv \left( \frac{d\langle H \rangle}{dT} \right)_p \quad (\text{D.2})$$

$$= \left( \frac{d}{dT} \right)_p \sum_i \frac{H_i \cdot e^{-H_i/RT}}{Z}, \quad \text{where } Z \equiv \sum_i e^{-H_i/RT} \quad (\text{D.3})$$

$$= \sum_i \frac{H_i^2 \cdot e^{-H_i/RT}}{RT^2 \cdot Z} - \sum_i \frac{H_i \cdot e^{-H_i/RT}}{Z} \sum_j \frac{H_j \cdot e^{-H_j/RT}}{RT^2 \cdot Z} \quad (\text{D.4})$$

$$= \frac{\langle H^2 \rangle - \langle H \rangle^2}{RT^2} \quad (\text{D.5})$$

It is seen that the heat capacity is proportional to the enthalpy fluctuations. With the same approach one can calculate the isothermal area compressibility

$$\kappa_T^A \equiv - \left( \frac{1}{\langle A \rangle} \frac{d\langle A \rangle}{d\Pi} \right) \quad (\text{D.6})$$

$$= \frac{\langle A^2 \rangle - \langle A \rangle^2}{\langle A \rangle RT} \quad (\text{D.7})$$

and the isothermal volume compressibility

$$\kappa_T^V \equiv - \left( \frac{1}{\langle V \rangle} \frac{d\langle V \rangle}{dp} \right) \quad (\text{D.8})$$

$$= \frac{\langle V^2 \rangle - \langle V \rangle^2}{\langle V \rangle RT} \quad (\text{D.9})$$

[6, 16]



## Appendix E

# Publication

The contribution to this article was the experimental work leading to the data seen in figure 1. (The experiments with menthol and AITC)

# Comparing ion conductance recordings of synthetic lipid bilayers with cell membranes containing TRP channels

Katrine R. Laub<sup>1</sup>, Katja Witschas<sup>2</sup>, Andreas Blicher<sup>1</sup>, Søren B. Madsen<sup>1</sup>, Andreas Lückhoff<sup>2</sup> and Thomas Heimburg<sup>1,\*</sup>

<sup>1</sup>Niels Bohr Institute, University of Copenhagen, Blegdamsvej 17, 2100 Copenhagen Ø, Denmark

<sup>2</sup>Institute of Physiology, Medical Faculty, RWTH Aachen University, D-52057 Aachen, Germany

**ABSTRACT** In this article we compare electrical conductance events from single channel recordings of three TRP channel proteins (TRPA1, TRPM2 and TRPM8) expressed in human embryonic kidney cells with channel events recorded on synthetic lipid membranes close to melting transitions. Ion channels from the TRP family are involved in a variety of sensory processes including thermo- and mechano-reception. Synthetic lipid membranes close to phase transitions display channel-like events that respond to stimuli related to changes in intensive thermodynamic variables such as pressure and temperature. TRP channel activity is characterized by typical patterns of current events dependent on the type of protein expressed. Synthetic lipid bilayers show a wide spectrum of electrical phenomena that are considered typical for the activity of protein ion channels. We find unitary currents, burst behavior, flickering, multistep-conductances, and spikes behavior in both preparations. Moreover, we report conductances and lifetimes for lipid channels as described for protein channels. Non-linear and asymmetric current-voltage relationships are seen in both systems. Without further knowledge of the recording conditions, no easy decision can be made whether short current traces originate from a channel protein or from a pure lipid membrane.

\*corresponding author, theimbu@nbi.dk — K. R. Laub and K. Witschas contributed equally to this work.

**Keywords:** TRP channels; TRPA1; TRPM2; TRPM8; lipid membrane pores; phase transition

**Abbreviations:** DMPC - 1,2 dimyristoyl-3-sn-phosphatidylcholine; DMPG - 1,2 dimyristoyl-3-sn-phosphatidylglycerol; AITC - allylisothiocyanate ; pdf - probability distribution function; HEK cell - human embryonic kidney cell; TRP channel - transient receptor potential channel; ADPR - adenosine diphosphate ribose

## Introduction

The cell membrane forms a diffusion barrier for hydrophilic substances, and its integrity is crucial for the viability of living organisms.

The established view is that ion channels electively regulate the flow of ions across the membrane, permitting the passage of certain ions while excluding others. In addition to their selectivity, protein ion channels have been reported to be functionally characterized by many properties such as conductance, voltage dependence, ligand activation, temperature- and mechanosensitivity. The synthetic lipid bilayer has been a model system for the biological membrane since the early days of membrane research. Biological membranes show a large compositional heterogeneity and complexity. They consist of lipid mixtures with varying amounts of unsaturation, different acyl and head groups, and they contain a multitude of imbedded or associated proteins. Lipid bilayers display chain-melting transitions. In the melting regime, the physical state of the membranes is influenced by temperature, pressure, pH, drugs including anesthetics and some neurotransmitters, and the presence of proteins (1–3).

Electrophysiological membrane models generally assume that the lipid membrane is an insulator and capacitor. This

assumption is important because a significant non-specific ion conductance of the lipid membrane itself would be inconsistent with the specific conductances required by current models of biomembranes. However, membranes are not generally insulators. Close to their chain melting temperatures, membranes become quite permeable to ions and small molecules (4). Temperature changes of only a few degrees have been reported to alter permeation rates for fluorescence markers by several orders of magnitude (5–7). More strikingly, electrophysiological transmembrane current recordings using black lipid membranes (BLMs) or patch pipettes reveal quantized conduction events that resemble those from biological membrane preparations (7–10, 10–16) (reviewed in (4)). Antonov and collaborators (9, 10) first described conduction events through membranes made of synthetic lipids eliminating all sources of current fluctuations other than those of the lipid membrane itself. Other investigations show that recordings of the conductance of synthetic membranes convincingly demonstrate its quantized nature (eg.,(4, 7, 15–17)).

The existence of lipid pores with diameters on the order of 1 nm has long been discussed in the field of electroporation (18–20). Several molecular dynamics studies have demonstrated the generation of such lipid pores by voltage (21, 22). The transient generation of lipid pores by large voltage pulses is used in clinical praxis, e.g. to transport cytostatic drugs into cancer cells or to transfect cells with DNA or RNA segments (20, 23). It seems likely that the quantized conductance events observed in synthetic membranes are a phenomenon closely related to electroporation. Nevertheless, the quantized nature of the ion currents across lipid membranes is surprising and is not really understood. It suggests that pores or defects in the lipid membrane have a well-defined size. While we believe that the explanation for fixed pore size remains an open issue, the de-

pendence of the pore formation rate on changes in temperature, pressure and other intensive thermodynamic variables is well understood. Its theory is based on the fluctuation-dissipation theorem that treats the couplings of fluctuations in enthalpy, volume, area and other extensive variables with susceptibilities such as heat capacity and compressibility (4). Thus, the occurrence of the lipid membrane channels responds to changes in temperature, pressure, voltage (4) and (for charged membranes) on pH and  $\text{Ca}^{2+}$  (24). As a consequence, they are thermosensitive, mechanoreceptive, voltage dependent and pH and  $\text{Ca}^{2+}$  sensitive. Furthermore, the fluctuation-dissipation theorem implies a connection between the magnitude of the fluctuations and the fluctuation time scale (3, 25). Fluctuations in the membrane state are especially large close to melting transitions. Therefore, the mean conductance of the membrane is larger and the channel open lifetimes are longer in the transition regime (16). This is particularly important since many biological membranes are in fact found in a state close to a melting transition, e.g., *E. coli* and *bacillus subtilis* membranes, lung surfactant (2, 26, 27), and rat central nerve membranes (unpublished data from 2011 by S. B. Madsen and N. V. Olsen, Copenhagen), suggesting that these phenomena might play a role under physiological conditions.

In this publication we compare the channel events in synthetic lipid membranes with ion channel protein conductances in biomembranes. The transient receptor potential (TRP) channel family has recently attracted considerable interest due to their involvement in sensing processes. Members of this family of ion channels have been reported to respond to environmental stimuli such as temperature, membrane tension, pH, osmolarity, pheromones, and intracellular stimuli such as  $\text{Ca}^{2+}$  and phosphatidylinositol signal transduction pathways (28). They may also be involved in detecting the taste sensations of sweet, sour and umami (33, 34).

Here, we focus on the activity of three TRP channels, namely TRPA1, TRPM2 and TRPM8. They are considered to form homotetrameric proteins with six transmembrane segments (S1-S6) in each subunit with cytosolic N- and C-termini. TRPA1 is a nociceptive channel and polymodal receptor activated by pungent or irritant chemicals such as AITC (allyl isothiocyanate) from wasabi, acrolein (in smoke), allicin and diallyl disulfide from garlic (28, 36–38). There is evidence for a cold-sensitivity of TRPA1 (34, 36). Furthermore, it is sensitive to depolarisation and to  $\text{Ca}^{2+}$  (37). Pore properties of TRPA1 vary dynamically depending on the presence of  $\text{Ca}^{2+}$  and agonist stimulation (38). The TRPM2 channel is a member of the transient receptor potential melastatin family that was first identified in cancer cells. TRPM2 currents show a linear I-V relationship indicating that this channel is not voltage-dependent. It is activated by intracellular ADP-ribose and  $\text{Ca}^{2+}$  in a synergistic manner (39), by heat, and by hydrogen peroxide, and this points to a role of the channel in oxidative stress signaling cascades (28, 40). A single channel conductance of  $\sim 62$  pS has been reported for TRPM2 (28). The closely related TRPM8 channel

is a cold receptor (41, 42) and a voltage-gated channel showing strong outward rectification. It is activated by substances that cause the sensation of cold such as menthol or menthol derivatives (e.g. WS-12). The “super-cooling” agent icilin is not structurally related to menthol activates TRPM8 in the presence of  $\text{Ca}^{2+}$  (43). TRPM8 channel activity is modulated by pH (44) and the presence of polyunsaturated fatty acids and lysophospholipids (45). A single channel conductance of  $\sim 81$  pS was reported for TRPM8 (28).

All three of these channels are selective for cations but show little selectivity for particular cations. Moreover, both TRP channels and lipid membrane channels are influenced by changes in intensive thermodynamical variables such as temperature and membrane tension (lateral pressure). Therefore, it is tempting to compare the characteristic properties of lipid and protein channel activity. In the present paper we discuss the similarities and differences of TRP channel conductance and conduction events due to synthetic lipid membrane pores. Since menthol is an agonist for human TRPM8 and TRPA1, we also study the influence of menthol on lipid phase behavior. The underlying question is whether membrane pores and protein channels are related or synergetic, and whether it is possible that they are governed by the same physical laws.

## Materials and Methods

### Synthetic membranes

**Calorimetry:** Heat capacity profiles were recorded using a VP-DSC (MicroCal, Northampton/MA, USA) with a scan rate of  $5^\circ/\text{h}$ .

**Electrophysiological recordings on synthetic lipid membranes:** We used the droplet method, whereby the planar lipid bilayer membranes is formed on the tip of a patch-clamp glass pipette that has been filled with electrolyte solution (46). The tip is in contact with the surface of a beaker filled with the same electrolyte solution. Lipids are dissolved in a hexane/ethanol mixture and are then brought into contact with the outer surface of the glass pipette. When the solution flows down the pipette, a membrane is formed spontaneously at the tip of the pipette. The solvent was allowed to evaporate for at least 30 seconds before the pipette was lowered 2–5 mm below the bath surface. The main advantage of this method is that the resulting membrane is practically solvent free.

Pipettes were pulled from 1.5 mm / 0.84 mm (outer diameter / inner diameter) borosilicate glass capillaries (#1B150F-3, World Precision Instruments, USA) with a vertical PC-10 puller from Narishige Group, Japan. A two-step pulling procedure was used, where the first pull was 8mm and the heater was set to 80% of the instrument’s maximum output. For the second pull, the heating coil was lowered 4mm and the heater setting was reduced to 45%. This produced fairly short and thick pipettes with an hourglass-like taper. For some experiments the pipette was subsequently fire polished using a Narishige MF-900 Mi-

croforge. This created pipettes that had a pipette opening in the range from 5–15  $\mu\text{m}$  in diameter. As a general rule, larger openings made it more difficult to create a stable membrane, with 20  $\mu\text{m}$  being the practical upper limit. In most experiments it was chosen to use the pipette as-is without fire polishing. These pipettes had openings of less than a 1  $\mu\text{m}$ . Unpolished pipettes were used in order to minimize the variation between experiments. The electrodes were made of high-purity, chlorinated silver wires, which were frequently re-chlorinated to avoid baseline drift and additional noise. Pipettes were always freshly prepared immediately before use. The buffers in the pipette and in the medium were identical.

Current recordings were made using an Axopatch 200B patch clamp amplifier (Axon Instruments Inc., Union City/CA, USA). The pipette and electrodes were mounted on a cooled capacitor feedback integrating headstage amplifier (Headstage CV 203BU, Axon Instruments Inc.). The headstage itself was mounted on a micro-manipulator (model SM1, Luigs and Neumann, Germany), allowing for careful and precise control of the pipette position relative to the bath surface. Lastly, the headstage and micro-manipulators were wrapped in a finely meshed metal cloth that acted as a Faraday cage. Data traces were recorded with Clampex 9.2 software (Axon Instruments) using the Whole Cell (headstage gain,  $\beta = 1$ ), voltage clamp mode. The sampling frequency was either 10kHz or 20kHz, and the signal was filtered by the patch clamp amplifier's analog 4-pole lowpass Bessel filter with the cut-off (-3dB) frequency set to 2kHz.

## Cell membranes

**Molecular biology and cell culture:** The cDNAs of human TRPM2, TRPM8 and TRPA1 were subcloned into pIRES-hrGFP-2a vectors (Stratagene, USA). Wild-type channels were stably expressed in HEK-293 cells (ATCC, USA) as described previously (35).

**Solutions:** Standard bath solution (BP1) contained 140mM NaCl, 1.2mM  $\text{MgCl}_2$ , 1.2mM  $\text{CaCl}_2$ , 5mM KCl, 10mM HEPES, pH 7.4 (NaOH). Pipette solution contained 145mM cesium glutamate, 8mM NaCl, 2mM  $\text{MgCl}_2$ , 10mM HEPES, pH 7.2 (CsOH) and the  $\text{Ca}^{2+}$  concentration was adjusted to either <10 nM (P10, 10 mM Cs-EGTA), or to 1  $\mu\text{M}$  (P10\*) as calculated with the MAXC-program (0.886mM  $\text{CaCl}_2$  and 1 mM Cs-EGTA). For the stimulation of TRPM2 currents in the inside-out configuration, ADPR (Sigma, 100 mM stock solution in distilled water) was added to the intracellular (bath) solution containing 1  $\mu\text{M}$   $\text{Ca}^{2+}$ , yielding a final concentration of 0.1 mM ADPR. Alternatively, TRPM2 currents were evoked in cell-attached configuration by application of hydrogen peroxide (Merck, 30% stock solution) to the bath solution, and after the appearance of single channel openings, a small membrane patch was excised by lifting up the pipette to reach inside-out configuration. TRPM8 currents were induced with icilin (Cayman Chemical, 10 mM stock solution in DMSO) or WS-

12 (Tocris, 30 mM stock solution in DMSO) by application to the bath (final concentrations as indicated in the experiments). For stimulation of TRPA1, allylisothiocyanate (Sigma, 30 mM stock solution in DMSO) was added directly to the bath solution. All chemicals were tested on native and vector-transfected HEK-293 cells and did not evoke single channel currents in the given range of concentrations without the presence of a TRP channel protein.

**Electrophysiology:** Single-channel recordings were routinely performed with pipettes made of borosilicate glass (outer diameter 1.8 mm / inner diameter 1.08 mm / length 75 mm, Hilgenberg, Germany). Alternatively, microelectrodes were made from borosilicate glass with slightly different specifications (outer diameter 1.5 mm / inner diameter 0.86 mm / length 100 mm, Harvard Apparatus, USA) to ensure that biophysical properties of ion channels were not dependent on the type of pipette used. Pipettes were fabricated in a two-step procedure and fire-polished with a programmable DMZ-Universal puller (Zeitz-Instrumente GmbH, Germany). Pipettes had a tip diameter in the range of 1  $\mu\text{m}$  and resistances between 5 and 7  $\text{M}\Omega$ . To reduce thermal noise, pipette tips were coated with dental wax (Moyco Industries Inc., USA). Microelectrodes were used on the day of preparation and stored in a container for the prevention of dust deposits.

Electrophysiological signals were recorded with an Axopatch 200B amplifier in combination with Digidata 1440A AD/DA converter controlled by the pClamp10 software suite (Axon CNS, USA). The CV 203 BU headstage (Axon CNS, USA) was mounted on a micro-manipulator (model SM1, Luigs and Neumann, Germany) inside a Faraday cage. Transfected cells were visually identified with an Axiovert 200 inverted microscope (Carl Zeiss MicroImaging GmbH, Germany) and a blue LED lamp (model CREE XP-E, wavelength  $\lambda = 460$  nm) serving as a light source for excitation of green fluorescence from GFP (green fluorescent protein). The Axopatch 200B amplifier was run in resistive whole-cell voltage-clamp mode ( $\beta=1$ ) to avoid contamination of traces with reset glitches due to capacitor discharge. The output gain ( $\alpha$ ) was set to  $\times 100$  when recording single-channel currents. A gap-free acquisition mode was used with a sample rate of 10 or 20 kHz and analogous filtering at 2 or 5 kHz performed with a build-in 4-pole Bessel filter (-3 db). All experiments were done at room temperature (21°C–23°C). Voltage signals were not corrected for liquid junction potentials. In order to facilitate comparison of lipid and protein traces, current and voltage signals are depicted as recorded with Clampex software from pClamp10 program suite. It is common in physiology to invert single-channel currents recorded in the cell-attached and inside-out configuration so that the inward movement of ions is represented as downward deflection. The reason for this lies in the convention that the net movement of positive ions in the direction of the outer to the inner membrane is, by definition, an inward current, but as positive ions are leaving the headstage and patch pipette this would be recorded as positive (or upward) current (47, 48). The patch-clamp com-

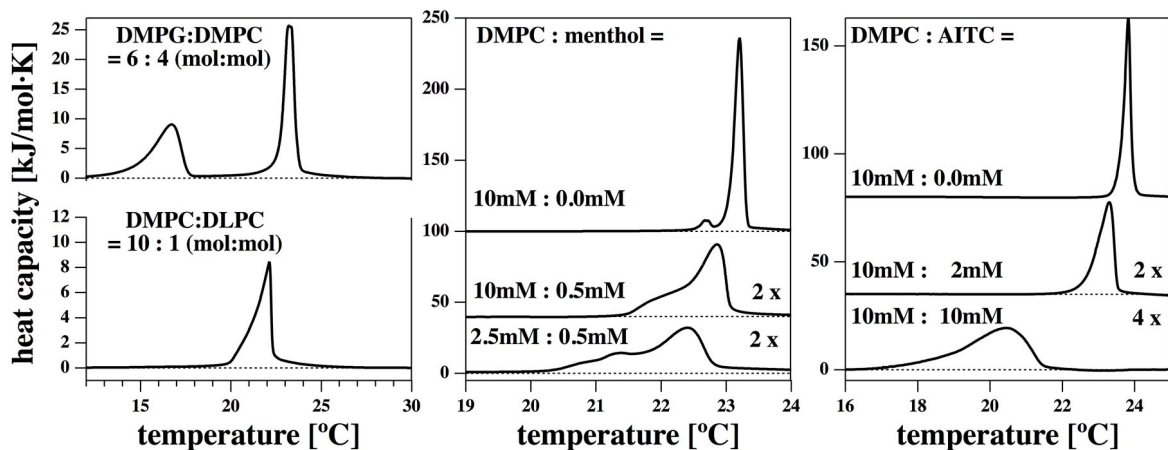


Figure 1: *Left: Heat capacity profiles of multilayered vesicles of a DMPC:DLPC=10:1 mixture in 150mM NaCl (1mM EDTA, 2mM HEPES, pH 7.4) and DMPG:DMPC=6:4 vesicles in 100 mM NaCl (1mM EDTA, 10mM HEPES, pH 7.4). The DMPC:DLPC mixture displays a pronounced maximum at 22.1 °C with wings towards higher and lower temperatures. The DMPG:DMPC mixture displays a peak at 23.2 °C and a broad pretransition peak at 16.7 °C. Center: DMPC membranes in the absence and presence of menthol (150mM KCl, 3mM EDTA, 3mM Hepes, pH 7.4). Different molar ratios are shown: 10mM DMPC in the absence of menthol (top), 10mM DMPC in the presence of 0.5mM menthol and 2.5mM DMPC in the presence of 0.5mM menthol in the buffer (before mixing). One recognizes that the presence of menthol shifts melting profiles towards lower temperatures and broadens the profiles. The bottom two traces have been amplified by a factor of 2 and baselines been shifted for better visibility. Right: 10mM DMPC membranes in the absence (top) and presence of 2mM and 10 mM AITC in the buffer (before mixing). As in the menthol experiments, the presence of AITC broadens and shifts the heat capacity profiles towards lower temperatures. The bottom two traces have been amplified by a factor of 2 and 4, respectively.*

mand voltage is positive if it increases the potential inside the micropipette. In physiology, it is common usage to report the transmembrane potential ( $V_m$ ), i.e. the potential at the inside of the cell minus the potential at the outside instead of pipette potential. In cell-attached and inside-out configuration where the pipette is connected to the outside of the membrane, a positive command voltage causes the transmembrane potential to become more negative, therefore it is hyperpolarizing (47). In the inside-out and cell-attached configuration, the transmembrane potential is inversely proportional to the command potential, in cell-attached configuration  $V_m$  is additionally shifted by the resting membrane potential of the cell (47, 48).

## Results

The results section contains data regarding the thermodynamic properties, channel-like ion conductance events, and current-voltage relationships of synthetic lipid membranes. We then compare conductance events from the synthetic membranes with biological membranes containing various transient receptor potential (TRP) ion channels.

Fig. 1 shows the heat capacity profiles of two lipid mixtures, DMPC:DLPC=10:1 and DMPG:DMPC = 6:4 in a 150 mM NaCl or KCl buffer. We have used these two mixtures for the conductance recordings that are documented below. Both

mixtures display a maximum close to room temperature where our conductance studies were performed. In the transition, the compressibility of the membrane is at maximum (26, 49). This effect results in a maximum of the membrane permeability close to the transition temperature (5, 50) and the maximum probability of finding lipid pores or lipid ion channel events (7, 16). This effect is central to our description in the following figures. Menthol is an agonist of TRP channel activity. For this reason we investigated the influence of menthol on lipid membrane phase behavior. The center panel of Fig. 1 shows the melting profile of DMPC membranes with and without menthol. The right hand panel shows the same membrane in the presence of AITC. AITC is an activator of the TRPA1 channel. It can be seen that small amounts of menthol (500  $\mu$ M) and AITC (2 mM) have a significant effect on the melting profile both with respect to peak position and width. In particular, menthol lowers the melting peak and broadens the profile significantly. The effect of both menthol and AITC is quite similar to that of a general anesthetic molecule on lipid membranes (2). The presence of both menthol and AITC should result in measurable effects on lipid membrane permeability for ions if it is measured close to the transition temperature.

Fig. 2A shows a channel recording of a DMPC:DLPC=10:1 mixture in 150 mM KCl at 50 mV at 30°C. Here and in all following experiments on synthetic membranes, the membrane was deposited on a patch pipette tip using a method described

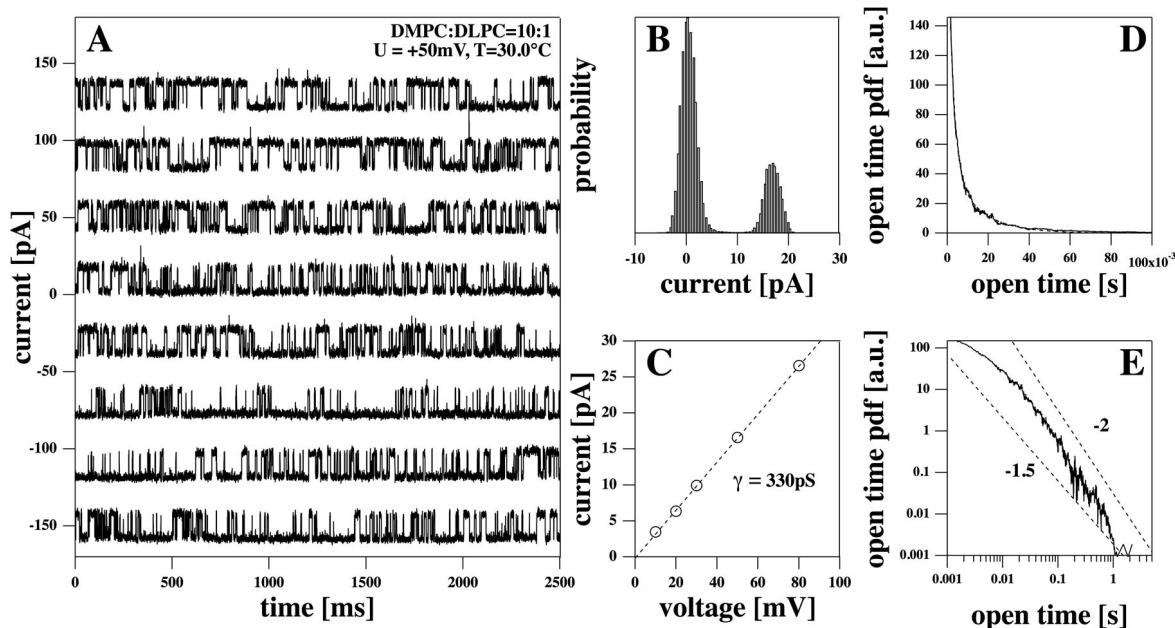


Figure 2: Patch clamp recording of a synthetic lipid membrane (DMPC:DLPC=10:1 mol:mol,  $T=30^{\circ}\text{C}$ , 150mM KCl, 1mM EDTA, 2mM HEPES, pH 7.4) at  $U=+50\text{mV}$ . Panel A: 8 representative 2.5 second segments out of a 30 minute recording. Panel B: Current histogram for the quantized steps of the left hand panel (closed channel state set to zero). Panel C: current-voltage relation for the currents of the membrane shown in the left hand panel (only positive voltages were recorded). The channel conductance is about 330pS. Panel D: Probability distribution function (pdf) for the open times of the channels in panel A. It is well fitted by an biexponential profile in the range up to 100ms open time. Panel E: The double-logarithmic representation of the data in panel D shows that for long open times the pdf is better described by a power law with a critical exponent close to -2.

by (46). This trace was stable over the complete recording time (about 30 minutes). The current histogram shows two well-defined peaks for baseline and single channel opening with an amplitude of about 18 pA at 50 mV (Fig. 2B). Also shown is the linear current-voltage relation of the single channel currents with the baseline subtracted. The single channel conductance resulted in a conductance of about 330 pS (Fig. 2C). No single-channel events were detected for negative voltages. Thus, the single-channel current-voltage relationship is only shown for positive voltages. Panels D and E show the probability distribution function (pdf) for the channel open times in linear and double-logarithmic representation. In the linear representation (Fig. 2D), it seems as if the pdf is well fitted by a bi-exponential curve with characteristic open lifetimes of 2.5 ms and 14.4 ms (the fit in the range up to 100 ms is shown as a dashed line that is hardly visible because it overlaps the pdf-profile). In the double-logarithmic representation, however, it is obvious that the bi-exponential fit underestimates the long open time probabilities, and the long open times are better described by a power law with a fractal exponent between 1.5 and 2 (Fig. 2E). Similar power-law behavior was found for the closed time pdf (data not shown).

As single channel events we consider stepwise conductance changes on top of a baseline. While the baseline current is usu-

ally believed to be related to leaks introduced by bad seals, this is not what is typically found for the synthetic membranes. We have consistently found that the background conductance reflects the thermodynamic properties of the membrane. For instance, the conductance of the overall membrane reflects the heat capacity profile (16). The conductance of single channels is strictly linear in the experiments presented here but channel open likelihoods increase with voltage (15) leading to a non-linear mean conductance. Within a certain voltage range, the current-voltage relation of the baseline is also linear. It is possible that the baseline current consists in part of unresolved conduction events that are of shorter duration than the recording resolution and the time constant of the low pass filter. In Montal-Müller type black lipid membranes, we have often found non-linear but symmetric current voltage relationships. This is to be expected for a fully symmetric bilayer. An example is given in (7, 15) for a DOPC:DPPC= 2:1 mixture (150 mM KCl, pH = 6.5 at  $T=19^{\circ}\text{C}$ ).

In experiments on patch pipettes we often find non-symmetric current-voltage profiles. In Fig. 3 the average conductance of a membrane with identical composition as in Fig. 2 (including the baseline conductance) is shown as a function of voltage. We find a nonlinear current-voltage relation with outward rectification shown here over an interval from  $-150\text{mV}$

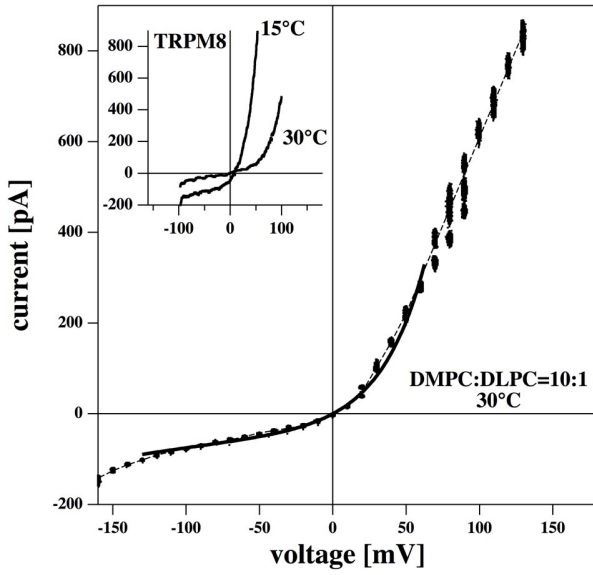


Figure 3: The current-voltage relationship of the total membrane (DMPC:DLPC=10:1 mol:mol,  $T=30^\circ\text{C}$ , 150mM NaCl, 1mM EDTA, 2mM HEPES, pH 7.4) shows an outward rectification that is probably due to asymmetries of the patch setup (e.g. induced by slight suction or by pipette shape). The dotted line is a guide to the eye. The solid line is a fit for the Eyring transition state model using a barrier position of  $\delta = 0.86$  and equal ion concentration on both sides of the membrane. The fit was from  $-130\text{mV}$  to  $70\text{mV}$ . The insert shows the outward rectified profiles of the TRPM8 channel at two temperatures (data adapted from (30)).

to  $+150\text{mV}$ . For comparison, we include an insert showing the current-voltage profiles of the TRPM8 channel at two temperatures which were adapted from (30). The I/V relationships from the synthetic membrane and the biological channels show striking similarity regarding their strong outward rectification properties. Since the TRPM8 channel is temperature sensitive, one finds different profiles at different temperatures. Because the mean conductance of lipid membranes also displays temperature dependence (16), we expect temperature sensitivity also for the current-voltage relationships. This issue has not been studied systematically here. It should be added that we always find outward rectified curves with a significant variation in magnitudes found in individual experiments. We have never seen an inward-rectified profile for any synthetic membrane. This is probably a consequence of the asymmetry of our experimental setup. We cannot exclude that conditions exist for which inward rectification indeed exists.

In the present manuscript we have exclusively used patch pipettes to monitor currents through synthetic membranes. Pipette apertures are much smaller than the holes in the teflon film of BLMs. Fig. 3 shows a conductivity profile with outward rectification (conductivity increases with increasing volt-

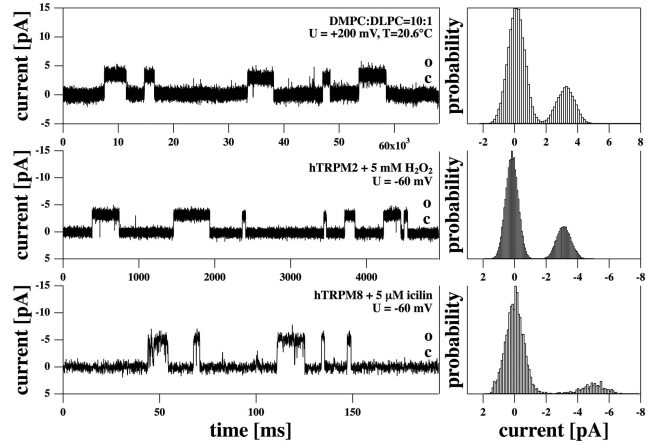


Figure 4: Single channel recordings from synthetic lipid membranes and from two TRP channels with the corresponding histograms. Top: DMPC:DLPC=10:1, 150mM KCl,  $T=20.6^\circ\text{C}$  and  $U = +200\text{mV}$  with a current of about  $3.5\text{pA}$ . Center: hTRPM2 channel activated by  $\text{H}_2\text{O}_2$  at  $U = -60\text{mV}$  (pipette voltage, inside-out configuration, pipette solution P10\*, bath solution BP1 + 5mM  $\text{H}_2\text{O}_2$ ). Bottom: hTRPM8 channel activated by  $5\ \mu\text{M}$  icilin at a pipette voltage of  $U = -60\text{mV}$  (inside-out configuration, pipette solution BP1, bath solution P10\* +  $5\ \mu\text{M}$  icilin, low pass filter  $5\text{kHz}$ ).

age) indicating that the membrane is not symmetric. One way to describe rectified current-voltage relationships is the transition state (Eyring) model (51), which assumes a free energy barrier for the ions,  $\Delta G_0$ , inside of the membrane (52). The relative position of this barrier within the membrane is given by a parameter  $\delta$ , with  $0 \leq \delta \leq 1$ . For a symmetric membrane

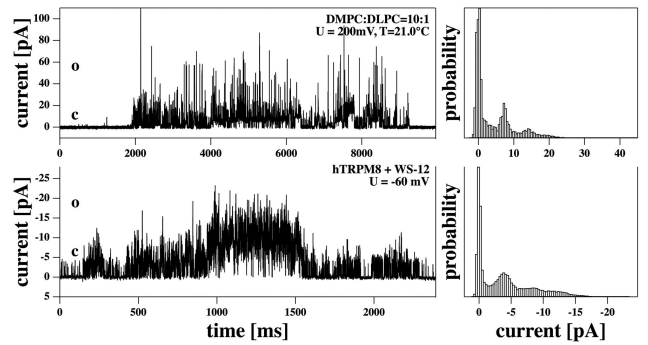


Figure 5: Conduction bursts in pure synthetic and in a cell membrane with TRP channels, and the corresponding current histograms. Top: DMPC:DLPC=10:1 (150mM KCl,  $T=20.6^\circ\text{C}$  and  $U = +200\text{mV}$ ). Bottom: Burst from hTRPM8 expressed in HEK 293 cells at a pipette potential of  $U = -60\text{mV}$  after addition of the menthol derivative WS-12. Cell-attached configuration, pipette solution P10, bath solution BP1 +  $7.5\ \mu\text{M}$  WS-12.

$\delta$  is equal to 0.5. The electrical potential is assumed to change linearly across the membrane, which means that a uniform dielectric constant within the membrane is assumed. In the presence of an applied voltage, the height of the kinetic barrier has different values, and one finds a current-voltage relationship of the following form:

$$I = zF\beta k_0 \left[ [C]_{in} \exp\left(\frac{\delta FUz}{RT}\right) - [C]_{out} \exp\left(-\frac{(1-\delta)FUz}{RT}\right) \right] \quad (1)$$

where  $z$  is the charge of the respective ion,  $F$  is Faraday's constant,  $\beta k_0$  is a rate constant reflecting the height of the barrier and the solubility of ions in the membrane.  $[C]_{in}$  and  $[C]_{out}$  are the ion concentrations inside and outside of the membrane. For equal ion concentration outside and inside ( $[C]_{in} = [C]_{out}$ ), the current  $I$  is zero at  $U = 0$ , as measured in Fig. 3. For a monovalent salt ( $z = 1$ ) eq. 1 simplifies to

$$I \propto \left[ \exp\left(\frac{\delta FU}{RT}\right) - \exp\left(-\frac{(1-\delta)FU}{RT}\right) \right] \quad (2)$$

This model describes the movement of gating particles in the Hodgkin-Huxley gate model for channel proteins (52). It has also been used to describe the voltage-sensitive conductivity of membrane patches containing TRP channels (31). If the barrier is placed at a position  $\delta = 0.5$  (the center of the membrane), the current-voltage relationship is symmetric under sign changes of the voltage. The transition state model is expected to work only if the height of the barrier is greater than the free energy of the ion in the field ( $\Delta G_0 \geq |\delta FUz|$  and  $\Delta G_0 \geq |(1-\delta)FUz|$ , see the derivation of eq. 1 in (52)), indicating that even under idealized conditions the relationship can only be used within a certain voltage regime. In Fig. 3 we show a fit of the total membrane conductance over the voltage range of  $-130$  mV to  $+70$  mV using a barrier position of  $\delta = 0.86$  that describes the conductance of the membrane reasonably well. The position of the barrier at  $\delta = 0.86$  indicates that the membrane is asymmetric. Although we cannot offer a conclusive explanation of this result, a number of possibilities present themselves. One is the application of suction in our patch experiments, which can lead to a membrane curvature that could contribute to the current-voltage asymmetry. The patch pipette itself introduces an asymmetry since it contacts only one side of the membrane. It is known that the contact of membranes with glass surfaces influences their phase behavior (53). This effect is of little relevance in the whole-cell patch-clamp configuration which was employed to record the current-voltage relationship of TRPM8 depicted in the insert of Fig. 3. In whole-cell configuration, the membrane is ruptured under the patch providing access to the intracellular space of the cell. The pipette contacts only a small area of the membrane surface while recording the current flowing over the membrane of the entire cell.

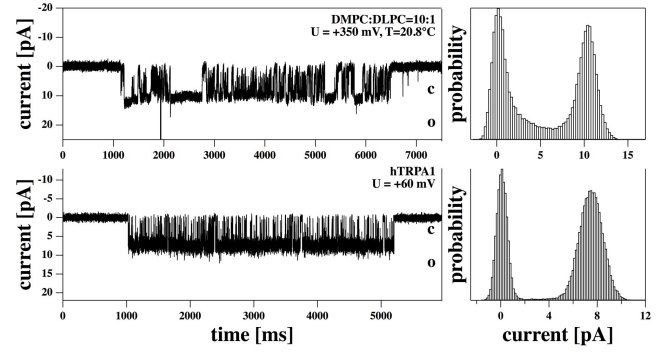


Figure 6: Flickering of a synthetic and a cell membrane containing TRP channels. Top: DMPC:DLPC=10:1 (150mM KCl,  $T=20.8^\circ\text{C}$  and  $U = +350$  mV). Bottom: hTRPA1 in HEK293 cell in cell attached configuration at a pipette potential of  $U = +60$  mV. Pipette solution BP1, bath solution P10.

### Comparison of current recordings from synthetic lipid membranes and biological preparations containing TRP channels:

The current recordings from artificial membranes showed various behaviors including single channel openings, conductance bursts, and flickering. For some samples and temperatures we found several of these phenomena in the same recordings. The occurrence of these lipid channel events differed somewhat for different pipettes and different conditions. In contrast, TRP channel activity was independent on the type of pipette used and reproducible under experimental conditions. In the following we compare some typical findings selected from artificial membranes with recordings from HEK293 cells containing TRP channels. All voltages are given as pipette potentials.

Fig. 4 (top) shows single channel events in a DMPC:DLPC=10:1 membrane with single steps of about 3.3 pA at a voltage of  $+200$  mV (corresponding to  $\sim 17$  pS) at a temperature of  $20.6^\circ\text{C}$ . This experiment shows that one finds single current events not only at 330 pS (Fig. 2 recorded at  $30^\circ\text{C}$ ) but also much smaller values depending on conditions. We compare this with the current from a HEK293 cell with over-expressed hTRPM2 channels activated by 5 mM  $\text{H}_2\text{O}_2$  at a voltage of  $-60$  mV in inside-out configuration (Fig. 4, center). We found single steps of about 3.1 pA corresponding to a conductance of 52 pS. Fig. 4 (bottom) shows the hTRPM8 channel in a HEK293 cell activated by 5  $\mu\text{M}$  icilin at a voltage of  $-60$  mV in inside-out configuration. Single-channel openings have a current amplitude of 5.1 pA corresponding to a conductance of 85 pS. Time axis scaling was adapted for the three traces to depict channel openings with a similar appearance. While the openings of TRPM2 are very long compared to TRPM8, both TRP channels show relatively short openings compared to the above trace from the synthetic membrane. Periods of repetitive channel activity separated from each other by long closures are called ‘‘bursts’’. The conductance events

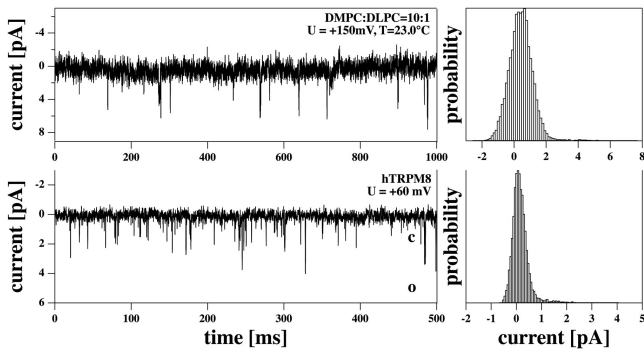


Figure 7: Spikes from synthetic membranes and from recombinantly expressed TRP channels. Top: Spikes in a recording from a DMPC:DLPC=10:1 mol:mol membrane ( $T=23^{\circ}\text{C}$ , 150mM KCl, 1mM EDTA, 2mM HEPES, pH 7.4) at  $U=+150\text{mV}$ . Bottom: Spikes from hTRPM8 in HEK293 cells in cell-attached configuration at a pipette potential of  $U = +60\text{mV}$ . Pipette solution P10, bath solution BP1.

of both synthetic membranes and biomembranes often occur in such bursts. Fig. 5 (top) shows a burst in a synthetic DMPC:DLPC=10:1 membrane recorded at 200mV and  $T=20.6^{\circ}\text{C}$ . The histogram indicates approximately evenly spaced conductance levels with an individual step size of 6.8 pA (34 pS). The total burst lasts for about 7 seconds. Fig. 5 (bottom) shows a burst of an HEK293 cell membrane containing the hTRPM8 channel activated by 7.5  $\mu\text{M}$  WS-12 at a voltage of  $-60\text{mV}$  in cell attached configuration. The bursting behavior of TRPM8 occurred for several minutes after the activator was given, only a short section is shown in Fig. 5. The histogram consists of approximately equally spaced steps of -3.5 pA (58 pS). Thus, the bursts of the synthetic membrane and the cell membrane display very similar characteristics both in the conductance of individual steps and in the appearance of the current histogram. Again, the traces by themselves appear nearly indistinguishable in both preparations.

Flickering resembles a burst with a single conductance step. Examples of this phenomenon are depicted in (Fig. 6). The top trace (Fig. 6, top) shows a flickering event from a synthetic DMPC:DLPC=10:1 membrane, the lower trace (6, bottom) shows the hTRPA1 channel in a HEK293 cell membrane recorded in cell-attached configuration. The flickering event in the artificial membrane occurred at 350 mV and  $20.8^{\circ}\text{C}$  and lasts for about 6 seconds. The step size is 10.2 pA corresponding to a single channel conductance of 23 pS. The current trace of a cell preparation expressing TRPA1 was recorded at 60 mV and displays a unitary current of 7.4 pA corresponding to a single-channel conductance of 123 pS. Except for small differences in detail, the overall appearance of the traces does not allow us to distinguish easily between the artificial membrane events from the cell preparation on the basis of the traces alone.

In Fig. 7 we show channel openings which are so brief

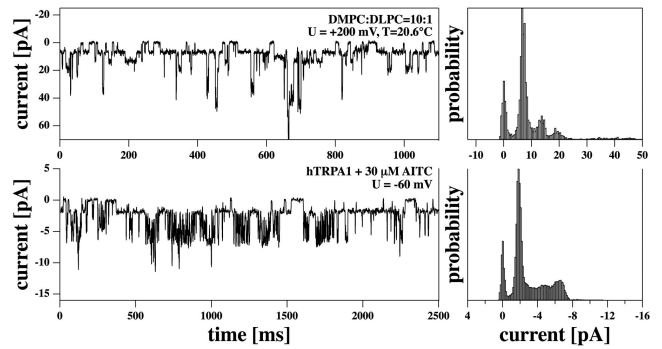


Figure 8: Multistep conductance in synthetic membranes and in a cell transfected with TRP channels. Top: DMPC:DLPC=10:1 mol:mol membrane ( $T=20.6^{\circ}\text{C}$ , 150mM KCl, 1mM EDTA, 2mM HEPES, pH 7.4) at  $U=+200\text{mV}$ . Bottom: hTRPA1 in HEK293 cells after addition of AITC in inside-out configuration at  $U = -60\text{mV}$  (pipette voltage). Bath solution P10\*, pipette solution BP1, post-recording low pass filtering with 500 Hz. In both traces the lowest conductance level has been set to zero.

that they are mostly not fully resolved, leading to a pattern of spike-like appearance with variable single-channel amplitudes truncated by low-pass filtering. The top trace is for a DMPC:DLPC=10:1 membrane recorded at 150 mV and  $23^{\circ}\text{C}$  and shows spikes with an amplitude of 4–5 pA corresponding to about 30 pS. The bottom trace is for a cell-attached recording of an HEK293 cell containing the hTRPM8 channel at  $U=60\text{mV}$ . Here, the spike has an amplitude of about 2 pA corresponding to about 33 pS. The limited time resolution of the recording system may have lead to an underestimation of the mean current related to the spikes.

Fig. 8 shows a comparison of multi-step conductances in synthetic membranes and in a biological preparation containing the hTRPA1 channel activated by 30  $\mu\text{M}$  allyl isothiocyanate (AITC). The synthetic membrane display at least four clearly distinguishable and equally spaced conductance levels with a conductance of 34 pS. The histogram of the biological preparation shows four visible steps. Since the two small peaks of the lower histogram are diffuse, two interpretations are feasible: In accordance with the upper histogram, four identical steps may be identified with a mean conductance per step of approximately 28 pS. Alternatively, this pattern of channel activity may be interpreted as long-lived openings of endogenous channels from HEK293 cells (37) or a subconductance state of TRPA1 with a small amplitude (2 pA) and overlying larger amplitudes of approximately 5 pA stemming from the main conductance state of TRPA1 with flickery openings (54). The overall appearance of the traces, the life times, and the individual conductances are once again very similar in both systems. While the appearance of the traces is different from the conduction bursts in Fig. 5, the conduction histograms display some similarities both for synthetic and cell membranes.

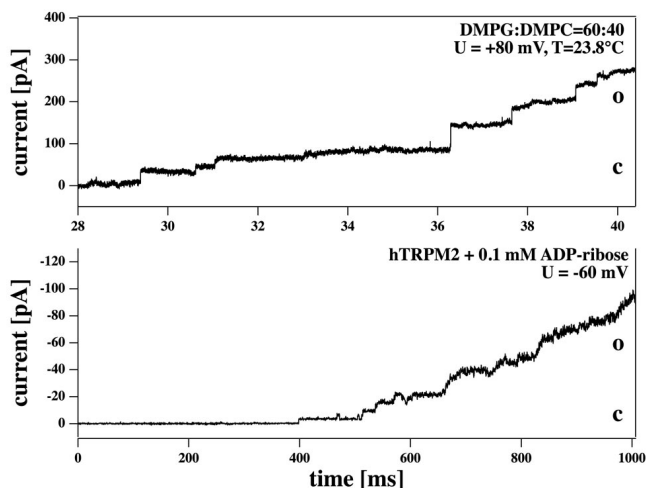


Figure 9: “Stairs” (subsequent opening of several channels) in synthetic membranes and in a biological membrane with TRP channels. Top: DMPG:DMPC=60:40 mol:mol membrane ( $T=23.8^{\circ}\text{C}$ , 50mM KCl, 1mM EDTA, 10mM HEPES, pH 7.4) at  $U=+80\text{ mV}$ . Bottom: hTRPM2 channel in HEK293 cells activated with ADP-ribose at a pipette potential of  $U=-60\text{ mV}$  in inside-out configuration. Bath solution P10\* + 0.1 mM ADP-ribose, pipette solution BP1.

In practically all synthetic lipid membrane preparations we find channel-like events under appropriate conditions. In particular, when voltage is increased the membranes eventually break at a threshold voltage, probably due to the growth of a very large pore. Below this threshold one typically finds quantized channel events. The threshold voltage is different in different preparations and depends on temperature, pipette suction, and probably on the properties of the pipette itself. Increasing the voltage to threshold values leads to rupture visible by a stepwise increase in membrane conductivity as can be seen in Fig. 9 (top) for a synthetic DMPG:DMPC=6:4 mixture. This onset of the rupture process can be reversed if the voltage is lowered. Biological preparations can also display such staircase-like behavior as shown in Fig. 9 (bottom) for the TRPM2 channel activated by 0.1mM ADP-ribose in the presence of  $1\ \mu\text{M}\ \text{Ca}^{2+}$ . In contrast to membrane rupture, which is mostly an irreversible process, activation of TRPM2 by ADPR is reversible as is obvious from the current going downstairs in a stepwise fashion until finally the baseline is reached (not shown).

## Discussion

In this paper we have compared conductance traces from biological (HEK293) cells over-expressing TRP channels with recordings from synthetic lipid bilayers. We have demonstrated that suitable adjustments of temperature and voltage (or mem-

brane tension) can always lead to conductance traces in synthetic membranes that are indistinguishable from recordings of biological preparations containing particular proteins. The experimental conditions are not necessarily the same but are comparable to those used in biomembrane experiments. This similarity is sufficiently pronounced that an inspection of short traces may fail to identify whether recordings are from synthetic membranes or from cells.

Protein ion channel activity in patch clamp experiments was characterized by typical and repetitive current events which were visually distinctive among different members of the TRP channel family. Those fingerprint openings from TRP channels with typical conductance and lifetime were absent under control conditions in patches of native HEK293 cells or of vector-transfected cells. In many experiments on pure lipid bilayers, strikingly similar traces were observed, although synthetic membranes did not exhibit the fingerprint-like behavior of channels with their highly reproducible and predictable reactions. Lipid membranes displayed various responses and the conditions for any specific response could not be controlled exactly. We selected several types of events found in sections of current recordings from artificial membranes for comparison with representative traces of TRP channels pointing phenomenologically at their striking similarities. We found similar single-channel events, multistep conductance, conduction bursts, flickering, conduction spikes and staircase behavior in synthetic membranes and in HEK293 cells containing three different TRP channels. Conductances and current histograms as well as lifetime distributions are all similar. Further, we found asymmetric non-linear current-voltage relationships in synthetic membranes that could be described by an Eyring-type kinetic barrier model that has also been used to describe the current-voltage relationship of TRP channels (31). The question arises whether, in spite of their similarity, channel events in the lipid membrane and protein channels can be considered as completely independent. Some findings in the literature suggest that these similarities are not merely accidental and point at a common origin of the conduction events in the two systems. Seeger et al. (55) found that both the mean conductance and the open lifetimes of the KcsA potassium channel exactly follow the heat capacity profile of the membrane into which the protein is reconstituted. The protein shows precisely the behavior expected for its host lipid membrane, indicating that lipid membrane properties dominate the experimental characteristics of the system. It was suggested that physical properties of the lipid bilayer influence ion channel activity via a fine-tuning of protein conformation, but it was also pointed out that the lipid membrane itself displays a similar behavior (55). It was also found that the mean conductance is proportional to the protein concentration. Further, conduction events could still be blocked by tetraethyl ammonium (TEA), which is a KcsA blocker. Thus, the conduction events are clearly correlated with the presence of the proteins. A similar correlation of channel activity with lipid membrane phase behavior was found for the sarcoplasmic reticulum cal-

cium channel (56), where the highest conduction activity and the longest open times were found close to the phase boundaries of the host lipid matrix. These findings suggest a strong correlation and possibly mutual modulation of the lipid properties with protein channel activity.

While the importance of protein channels and receptors is widely accepted, the finding of quantized conductance events in synthetic membranes is striking but little known (e.g., (7–10, 14–16)). Such events occur more frequently close to the melting transition of the lipid membranes. Mean conductances and lifetimes are in agreement with the fluctuation-dissipation theorem that defines the coupling between the amplitude of area fluctuations and the lifetime of the fluctuations (4). The mean open and closed lifetimes of a lipid membrane channel is closely related to the fluctuation lifetime (16). The consequences for lipid membranes can be summarized in the following manner: In the vicinity of the lipid melting transition, area fluctuations and the likelihood of finding pores (or channels) are maximal. Simultaneously, the fluctuation relaxation time is at maximum as is the mean lifetime of open channels. Different phenomenological behavior as shown in Figs. 4-9 probably reflects the properties of different points in the phase diagram of the lipid mixtures.

Pores in lipid membranes have been discussed for more than 25 years (5, 19, 21, 22, 50). Elastic theory suggests the existence of stable pores of a diameter of approximately 1 nm. This is close to the suggested size of aqueous pores in ion channel proteins. The experimentally measured pores, i.e., channel events in synthetic membranes, have a diameter similar to that suggested by theory. In Blicher et al. (7) aqueous pores of 0.7 nm diameter were described, close to the theoretical value and close to the aqueous pore sizes suggested for protein channels.

In our synthetic membrane experiments we typically observe coherent trends. For instance, it is possible to induce channel events in lipid membranes if one increases the voltage above some threshold value. This threshold probably varies with temperature. The same is true for increasing pipette suction. Further, channel events are more likely in the melting regime. However, the details of these phenomena varied from experiment to experiment. We believe that this is partially due to strong influences of the patch pipette on the phase behavior of lipid membranes. It is known that the contact of membranes with glass or mica can shift the lipid melting transition by as much as to 5 degrees towards higher temperatures (53). For this reason, the melting behavior of our synthetic membrane patches may be influenced by the patch pipette and vary as a function of the exact surface features of the pipette perimeter. Further, typical domain sizes of lipid mixtures in the transition regime can be several micrometers large (57). With pipette diameters on the order of  $1\mu\text{m}$  (smaller than some domains) one may therefore observe considerable variation in the relative amounts of fluid and gel domains in different experiments. We have found more reproducible patterns in the larger mem-

brane patches in BLM experiments or in macroscopic permeation events that do not involve interfaces (7, 15). One of the most obvious differences of lipid membrane channels and biological protein preparations is that in the latter case the conductances seem to be more reproducible and stable. Thus, cells transfected with particular channel proteins display characteristic electrical properties whereas lipid membranes do not exhibit such fingerprint-like features.

In Fig. 2E we show that the open time pdf displays power law behavior. The same was found to be true for the closed time pdf (data not shown). Recently we have demonstrated that this applies for other synthetic membranes as well (17). Power law behavior implies that very long closed times occur with a much higher frequency than in stochastic Markovian kinetics. It leads to the possibility of long silent periods between burst of activity. For protein channels this fractal kinetics has been long discussed (58–61) as an alternative to multi-state Markovian kinetics (62). In this context it is interesting to note that power law behavior is also a natural consequence of critical behavior of membranes close to transitions (63). Fig. 5 shows that the bursts from TRPM8 in HEK293 cells display very similar phenomenological behavior compared to synthetic membranes close to phase transitions both in respect to channel amplitudes, lifetimes and conduction histograms. This is also true for flickering activity as shown in Fig. 6. Obviously, the temporal patterns of both classes of events obey similar kinetics.

Channels in synthetic lipid membranes can be influenced by drugs if these drugs affect the melting behavior of the membrane. For instance, anesthetics lower and broaden the melting transition of membranes (2) and thereby have been shown to be able to “block” lipid membrane channel events without binding to macromolecular receptors (7). Many other drugs affect the melting behavior and permeability of lipid membranes, e.g., the pesticide lindane (6) or the neurotransmitter serotonin (3). We have also shown that the anesthetic octanol and serotonin can influence the fluctuation lifetimes of lipid membranes and thereby probably the lipid membrane channel lifetimes. This implies that the response of channels to drugs is not necessarily the consequence of specific binding of the drugs to a receptor. This result could rather be a more general consequence of thermodynamic changes in the surrounding lipid matrix. Here we have shown that menthol, an agonist of human TRPM8 and TRPA1 channels, and AITC, an agonist of the TRPA1 channel are also able to influence the state of the lipid membrane (Fig. 1). In particular, both menthol and AITC lower and broaden the cooperative melting events of membranes in a manner very similar to general anesthetics. This means that menthol and AITC partition in the lipid membrane and are much more soluble in the fluid phase than in the gel phase. In fact, menthol has been compared to general anesthetics (e.g., propofol) (64). Interestingly, no specific binding site of menthol is known for TRP channels, in contrast to AITC in the case of TRPA1. For human TRPM8, the amino acids implied in menthol sensitivity are conserved in menthol-insensitive

TRPM2 (65, 66). This would be in agreement with the idea that the effects of menthol on TRP channels are related to its influence on the host lipid matrix. Above the melting transition, menthol should act as an antagonist of lipid channel formation (because the transition is shifted away from experimental temperature), and below the transition as an agonist (because the transition is shifted towards experimental temperature). Precisely this effect has been observed for general anesthetics such as octanol (7). Interestingly, menthol was reported to have a bimodal action on mouse TRPA1 (67). At high concentrations of menthol an inhibitory effect was found while low concentrations lead to channel activation. In contrast, human TRPA1 is exclusively activated by menthol (68). The authors of this study note that there is no direct evidence that menthol specifically binds to TRPA1, instead the possibility of indirect effects of menthol was considered, e.g. involving modifications of the lipid bilayer. Since effects of menthol on the physical properties of model membranes are better characterized than its binding to TRP channels, it may be speculated that these effects are governed by interaction at the membrane interface.

The same may apply for the sensitivity to temperature, a hallmark of this family of thermosensitive channels. We have shown that many biological membranes display transitions slightly below body temperature, including *E. coli* membranes, bacillus subtilis membranes (2, 27), bovine lung surfactant (26, 27) and the membranes from the central nerve of rat brains (S. B. Madsen and N. V. Olsen, recent unpublished results). Further, we have shown that channel conductance in synthetic lipid membranes displays a strong temperature dependence close to the melting transition of the membranes (7, 16). Transition in biomembranes are found about 10 degrees below physiological temperature (27) and display a half width of order 10 degrees, corresponding to a van't Hoff enthalpy  $\Delta H$  of about 300 kJ/mol and an entropy  $\Delta S$  of about 1000 J/mol K. Similar values have been found for the temperature activation of TRP channels. Talavera et al. reported activation enthalpies on the order of 200 kJ/mol for TRPM4, TRPM5, TRPM8 and TRPV1 channels (33). Further, they report  $\Delta S \approx 500$  J/mol K for several TRP channels. While the origin of the very large  $\Delta H$  and  $\Delta S$  for the TRP channels remains mysterious, the order of magnitude is just in the range of the melting transition of the biological membrane. For this reason, it has been speculated in the past if the temperature dependence of TRP channels may originate from transitions in the surrounding membrane (33).

## Conclusion

In the present study, we have explored the possibility that lipid bilayers, in addition to their role as electrical insulators and solvents for membrane proteins, provide relevant ion permeabilities as well as changes of permeabilities, by themselves and without the presence of channel-forming proteins. Indeed, lipid membranes exhibited non-linear and asymmetric current-

voltage profiles in pipette experiments. We document a wide spectrum of electrical phenomena in synthetic membranes such as bursts, spikes, flickering and multi-step openings that are normally considered typical for the activity of protein ion channels. Furthermore, we show the similarity of current events from lipid bilayers with single-channel recordings of TRP channels. Thus, electrical properties of lipid bilayers may contribute to membrane excitability generated by protein ion channels. On the other hand, electrical properties of pure lipid bilayers also display clear differences as compared to those of cell membranes containing channel proteins, such as the different regulation by specific ligands. Importantly, the observed electrical phenomena in synthetic membranes lack stability that would warrant reproducible responses in the presence of slightly changing conditions. This is illustrated by the problems to obtain strictly reproducible electrical events with tip-dipping using glass pipettes on pure lipid bilayers, in contrast to the single-channel recordings with similar pipettes on cell membranes. The response of lipid membranes to electrical stimuli demonstrated in this study may broaden our view how ion channels in biological membranes are regulated and how channel proteins and their lipid matrix may cooperate in signal transduction in excitable cells.

**Acknowledgments:** We thank Prof. Andrew D. Jackson for a careful reading of the manuscript and valuable comments.

## References

1. Heimburg, T., 2007. Thermal biophysics of membranes. Wiley VCH, Berlin, Germany.
2. Heimburg, T., and A. D. Jackson. 2007. The thermodynamics of general anesthesia. *Biophys. J.* 92:3159–3165.
3. Seeger, H. M., M. L. Gudmundsson, and T. Heimburg. 2007. How anesthetics, neurotransmitters, and antibiotics influence the relaxation processes in lipid membranes. *J. Phys. Chem. B* 111:13858–13866.
4. Heimburg, T. 2010. Lipid ion channels. *Biophys. Chem.* 150:2–22.
5. Papahadjopoulos, D., K. Jacobson, S. Nir, and T. Isac. 1973. Phase transitions in phospholipid vesicles. fluorescence polarization and permeability measurements concerning the effect of temperature and cholesterol. *Biochim. Biophys. Acta* 311:330–340.
6. Sabra, M. C., K. Jørgensen, and O. G. Mouritsen. 1996. Lindane suppresses the lipid-bilayer permeability in the main transition region. *Biochim. Biophys. Acta* 1282:85–92.
7. Blicher, A., K. Wodzinska, M. Fidorra, M. Winterhalter, and T. Heimburg. 2009. The temperature dependence of lipid membrane permeability, its quantized nature, and the influence of anesthetics. *Biophys. J.* 96:4581–4591.
8. Yafuso, M., S. J. Kennedy, and A. R. Freeman. 1974. Spontaneous conductance changes, multilevel conductance states and negative differential resistance in oxidized cholesterol black lipid membranes. *J. Membr. Biol.* 17:201–212.
9. Antonov, V. F., V. V. Petrov, A. A. Molnar, D. A. Predvoditelev, and A. S. Ivanov. 1980. The appearance of single-ion channels in unmodified lipid

- bilayer membranes at the phase transition temperature. *Nature* 283:585–586.
10. Antonov, V. F., E. V. Shevchenko, E. T. Kozhomkulov, A. A. Molnar, and E. Y. Smirnova. 1985. Capacitive and ionic currents in BLM from phosphatidic acid in  $\text{Ca}^{2+}$ -induced phase transition. *Biochem. Biophys. Research Comm.* 133:1098–1103.
  11. Kaufmann, K., and I. Silman. 1983. Proton-induced ion channels through lipid bilayer membranes. *Naturwissenschaften* 70:147–149.
  12. Kaufmann, K., and I. Silman. 1983. The induction by protons of ion channels through lipid bilayer membranes. *Biophys. Chem.* 18:89–99.
  13. Gögelein, H., and H. Koepsell. 1984. Channels in planar bilayers made from commercially available lipids. *Pflügers Arch.* 401:433–434.
  14. Antonov, V. F., A. A. Anosov, V. P. Norik, and E. Y. Smirnova. 2005. Soft perforation of planar bilayer lipid membranes of dipalmitoylphosphatidylcholine at the temperature of the phase transition from the liquid crystalline to gel state. *Eur. Biophys. J.* 34:155–162.
  15. Wodzinska, K., A. Blicher, and T. Heimburg. 2009. The thermodynamics of lipid ion channel formation in the absence and presence of anesthetics. *blm experiments and simulations. Soft Matter* 5:3319–3330.
  16. Wunderlich, B., C. Leirer, A. Idzko, U. F. Keyser, V. Myles, T. Heimburg, and M. Schneider. 2009. Phase state dependent current fluctuations in pure lipid membranes. *Biophys. J.* 96:4592–4597.
  17. Gallaher, J., K. Wodzinska, T. Heimburg, and M. Bier. 2010. Ion-channel-like behavior in lipid bilayer membranes at the melting transition. *Phys. Rev. E* 81:061925.
  18. Winterhalter, M., and W. Helfrich. 1987. Effect of voltage on pores in membranes. *Phys. Rev. A* 36:5874–5876.
  19. Glaser, R. W., S. L. Leikin, L. V. Chernomordik, V. F. Pastushenko, and A. I. Sokirko. 1988. Reversible breakdown of lipid bilayers: Formation and evolution of pores. *Biochim. Biophys. Acta* 940:275–287.
  20. Neumann, E., S. Kakorin, and K. Tønsing. 1999. Fundamentals of electroporative delivery of drugs and genes. *Bioelectrochem. Bioenerg.* 48:3–16.
  21. Tieleman, D. P., H. Leontiadou, A. E. Mark, and S. J. Marrink. 2003. Simulation of pore formation in lipid bilayers by mechanical stress and electric fields. *J. Am. Chem. Soc.* 125:6382–6383.
  22. Böckmann, R., R. de Groot, S. Kakorin, E. Neumann, and H. Grubmüller. 2008. Kinetics, statistics, and energetics of lipid membrane electroporation studied by molecular dynamics simulations. *Biophys. J.* 95:1837–1850.
  23. Gehl, J. 2003. Electroporation: theory and methods, perspectives for drug delivery, gene therapy and research. *Acta Physiol. Scand.* 177:437–447.
  24. Träuble, H., M. Teubner, P. Woolley, and H. Eibl. 1976. Electrostatic interactions at charged lipid membranes. i. effects of pH and univalent cations on membrane structure. *Biophys. Chem.* 4:319–342.
  25. Grabitz, P., V. P. Ivanova, and T. Heimburg. 2002. Relaxation kinetics of lipid membranes and its relation to the heat capacity. *Biophys. J.* 82:299–309.
  26. Ebel, H., P. Grabitz, and T. Heimburg. 2001. Enthalpy and volume changes in lipid membranes. i. the proportionality of heat and volume changes in the lipid melting transition and its implication for the elastic constants. *J. Phys. Chem. B* 105:7353–7360.
  27. Heimburg, T., and A. D. Jackson. 2005. On soliton propagation in biomembranes and nerves. *Proc. Natl. Acad. Sci. USA* 102:9790–9795.
  28. Wu, L.-J., T.-B. Sweet, and D. E. Clapham. 2010. International union of basic and clinical pharmacology. LXXVI. Current progress in the mammalian TRP ion channel family. *Pharmacol. Rev.* 62:381–404.
  29. Clapham, D. E., L. W. Runnels, and C. Strübing. 2001. The TRP ion channel family. *Nat. Rev. Neurosci.* 2:387–396.
  30. Voets, T., G. Droogmans, U. Wissenbach, A. Janssens, V. Flockerzi, and B. Nilius. 2004. The principle of temperature-dependent gating in cold- and heat-sensitive TRP channels. *Nature* 430:748–754.
  31. Nilius, B., K. Talavera, G. Owsianik, J. Prenen, G. Droogmans, and T. Voets. 2005. Gating of TRP channels: a voltage connection? *J. Physiol.* 567:35–44.
  32. Voets, T., K. Talavera, G. Owsianik, and B. Nilius. 2005. Sensing with TRP channels. *Nat. Chem. Biol.* 1:85–92.
  33. Talavera, K., K. Yasumatsu, T. Voets, G. Droogmans, N. Shigemura, Y. Nishiyama, R. F. Margolskee, and B. Nilius. 2005. Heat activation of TRPM5 underlies thermal sensitivity of sweet taste. *Nature* 438:1022–1025.
  34. Venkatchalam, K., and C. Montell. 2007. TRP channels. *Annu. Rev. Biochem.* 76:387–417.
  35. Kühn, F. J. P., K. Witschas, C. Kühn, and A. Lückhoff. 2010. Contribution of the S5-pore-S6 domain to the gating characteristics of the cation channels TRPM2 and TRPM8. *J. Biol. Chem.* 285:26806–26814.
  36. del Camino, D., S. Murphy, M. Heiry, L. B. Barrett, T. J. Earley, C. A. Cook, M. J. Petrus, M. Zhao, M. D’Amours, N. Deering, G. J. Brenner, M. Costigan, N. J. Hayward, J. A. Chong, C. M. Fanger, C. J. Woolf, A. Patapoutian, and M. M. Moran. 2010. TRPA1 contributes to cold hypersensitivity. *J. Neurosci.* 30:15165–15174.
  37. Doerner, J. F., G. Gisselmann, H. Hatt, and C. H. Wetzel. 2007. Transient receptor potential channel a1 is directly gated by calcium ions. *J. Biol. Chem.* 282:13180–13189.
  38. Banke, T. G., S. R. Chaplan, and A. D. Wickenden. 2010. Dynamic changes in the TRPA1 selectivity filter lead to progressive but reversible pore dilation. *Am. J. Physiol. Cell Physiol.* 298:C1457–C1468, 2010. 298:C1457–C1468.
  39. Csanady, L., and B. Töröcsik. 2009. Four  $\text{Ca}^{2+}$  ions activate TRPM2 channels by binding in deep crevices near the pore but intracellularly of the gate. *J. Gen. Physiol.* 133:189–203.
  40. Bari, M. R., S. Akbar, M. Eweida, F. J. P. Kühn, A. J. Gustafsson, A. Lückhoff, and M. S. Islam. 2009.  $\text{H}_2\text{O}_2$ -induced  $\text{Ca}^{2+}$  influx and its inhibition by N-(p-aminocinnamoyl) anthranilic acid in the beta-cells: involvement of TRPM2 channels. *J. Cell Mol. Med.* 13:3260–3267.
  41. McKemy, D. D., W. M. Neuhäusser, and D. Julius. 2002. Identification of a cold receptor reveals a general role for TRP channels in thermosensation. *Nature* 416:52–58.
  42. Peier, A. M., A. Moqrich, A. C. Hergarden, A. J. Reeve, D. A. Andersson, G. M. Story, T. J. Earley, I. Dragoni, P. McIntyre, S. Bevan, and A. Patapoutian. 2002. A trp channel that senses cold stimuli and menthol. *Cell* 108:705–715.
  43. Chuang, H.-H., W. M. Neuhäusser, and D. Julius. 2004. The supercooling agent icilin reveals a mechanism of coincidence detection by a temperature-sensitive TRP channel. *Neuron* 43:859–869.
  44. Andersson, D. A., H. W. N. Chase, and S. Bevan. 2004. Trpm8 activation by menthol, icilin, and cold is differentially modulated by intracellular pH. *J. Neurosci.* 24:5364–5369.

45. Andersson, D. A., M. Nash, and S. Bevan. 2007. Modulation of the cold-activated channel *trpm8* by lysophospholipids and polyunsaturated fatty acids. *J. Neurosci.* 27:3347–3355.
46. Hanke, W., C. Methfessel, U. Wilmsen, and G. Boheim. 1984. Ion channel reconstruction into lipid bilayer membranes on glass patch pipettes. *Bioelectrochem. Bioenerg.* 12:329–339.
47. Maertz, W. E., editor, 2008. *The Axon Guide, A Guide to Electrophysiology & Biophysics Laboratory Techniques 2500-0102 Rev. C.* MDS Analytical Technologies, 3rd edition.
48. Wyllie, D. J. A., 2007. Single-channel recording. In *Patch-Clamp analysis: Advanced techniques* (Walz, W., editor). Humana Press, New Jersey, 69–119.
49. Heimburg, T. 1998. Mechanical aspects of membrane thermodynamics. Estimation of the mechanical properties of lipid membranes close to the chain melting transition from calorimetry. *Biochim. Biophys. Acta* 1415:147–162.
50. Nagle, J. F., and H. L. Scott. 1978. Lateral compressibility of lipid mono- and bilayers. Theory of membrane permeability. *Biochim. Biophys. Acta* 513:236–243.
51. Tsien, R. W., and D. Noble. 1969. A transition state theory approach to the kinetics of conductance changes in excitable membranes. *J. Membr. Biol.* 1:248–273.
52. Johnston, D., and S. M. S. Wu, 1995. *Cellular Neurophysiology.* MIT Press, Boston.
53. Yang, J., and J. Appleyard. 2000. The main phase transition of mica-supported phosphatidylcholine membranes. *J. Phys. Chem. B* 104:8097–8100.
54. Nagata, K., A. Duggan, G. Kumar, and J. García-Añoveros. 2005. Nociceptor and hair cell transducer properties of TRPA1, a channel for pain and hearing. *J. Neurosci.* 25:4052–4061.
55. Seeger, H. M., A. Alessandrini, and P. Facci. 2010. KcsA redistribution upon lipid domain formation in supported lipid bilayers and its functional implications. *Biophys. J.* 98:371a.
56. Cannon, B., M. Hermansson, S. Györke, P. Somerharju, and J. A. Virtanen. 2003. Regulation of calcium channel activity by lipid domain formation in planar lipid bilayers. *Biophys. J.* 85:933–942.
57. Korlach, J., J., P. Schwille, W. W. Webb, and G. W. Feigensohn. 1999. Characterization of lipid bilayer phases by confocal microscopy and fluorescence correlation spectroscopy. *Proc. Natl. Acad. Sci. USA* 96:8461–8466.
58. Liebovitch, L. S., J. Fischbarg, J. P. Koniarek, I. Todorova, and M. Wang. 1987. Fractal model of ion-channel kinetics. *Biochim. Biophys. Acta* 896:173–180.
59. Liebovitch, L. S. L., J. Fischbarg, and J. P. Koniarek. 1987. Ion channel kinetics: a model based on fractal scaling rather than multistate Markov processes. *Math. Biosci.* 84:37–68.
60. Liebovitch, L. S. 1989. Analysis of fractal ion channel gating kinetics: kinetic rates, energy levels, and activation energies. *Math. Biosci.* 93:97–115.
61. Liebovitch, L., D. Scheurle, M. Rusek, and M. Zochowski. 2001. Fractal methods to analyze ion channel kinetics. *Methods* 24:359–375.
62. Millhauser, G. L., E. E. Salpeter, and R. E. Oswald. 1988. Diffusion models of ion-channel gating and the origin of power-law distributions from single-channel recording. *Proc. Natl. Acad. Sci. USA* 85:1503–1507.
63. Nielsen, L. K., T. Bjørnholm, and O. G. Mouritsen. 2000. Critical phenomena - fluctuations caught in the act. *Nature* 404:352.
64. Watt, E. E., B. A. Betts, F. O. Kotey, D. J. Humbert, T. N. Griffith, E. W. Kelly, K. C. Veneskey, N. Gill, K. C. Rowan, A. Jenkins, and A. C. Hall. 2008. Menthol shares general anesthetic activity and sites of action on the gaba(a) receptor with the intravenous agent, propofol. *Eur. J. Pharmacol.* 590:120–126.
65. Bandell, M., A. E. Dubin, M. J. Petrus, A. Orth, J. Mathur, S. W. Hwang, and A. Patapoutian. 2006. High-throughput random mutagenesis screen reveals *trpm8* residues specifically required for activation by menthol. *Nature Neurosci.* 9:493–500.
66. Voets, T., G. Owsianik, A. Janssens, K. Talavera, and B. Nilius. 2007. *Trpm8* voltage sensor mutants reveal a mechanism for integrating thermal and chemical stimuli. *Nature Chem. Biol.* 3:174–182.
67. Karashima, Y., N. Damann, J. Prenen, K. Talavera, A. Segal, T. Voets, and B. Nilius. 2007. Bimodal action of menthol on the transient receptor potential channel *trpa1*. *J. Neurosci.* 27:9874–9884.
68. Xiao, B., A. E. Dubin, B. Bursulaya, V. Viswanath, T. J. Jegla, and A. Patapoutian. 2008. Identification of transmembrane domain 5 as a critical molecular determinant of menthol sensitivity in mammalian *trpa1* channels. *J. Neurosci.* 28:9640–9651.

# Bibliography

- [1] Sir James George Frazer. *The golden bough: a study in magic and religion, Volume 1, Part 1*. Forgotten Books, 1935.
- [2] Michael Frampton. *Embodiments of Will*. Michael Frampton, 2008.
- [3] Sidney Ochs. *a History of nerve function: From Animal spirit to molecular mechanisms*. Number 1. Cambridge University Press, 1 edition, November 2004.
- [4] Gilbert L Ling. *In search of the physical basic of life*. plenum press, New York and London, 1 edition, 1984.
- [5] [Http://en.wikipedia.org/wiki/Cell\\_\(biology\)](http://en.wikipedia.org/wiki/Cell_(biology)). 10.23-2011.
- [6] Thomas Heimburg. *Thermal biophysics of membranes*. Wiley-VCH, 1st editio edition, 2007.
- [7] S J Singer and G L Nicolson. The fluid mosaic model of the structure of cell membranes. *Science (New York, N.Y.)*, 175(23):720–31, February 1972.
- [8] O G Mouritsen and M Bloom. Mattress model of lipid-protein interactions in membranes. *Biophysical journal*, 46(2):141–53, August 1984.
- [9] [Http://en.wikipedia.org/wiki/File:Cell\\_membrane\\_detailed\\_diagram\\_4.svg](http://en.wikipedia.org/wiki/File:Cell_membrane_detailed_diagram_4.svg). 3. Nov 2011.
- [10] Andreas Blicher. Permeability studies of lipid vesicles by Fluorescence Correlation Spectroscopy and Monte Carlo simulations. Master's thesis, University of Copenhagen, 2007.
- [11] Gerrit van Meer, Dennis R Voelker, and Gerald W Feigenson. Membrane lipids: where they are and how they behave. *Nature reviews. Molecular cell biology*, 9(2):112–24, February 2008.
- [12] [Http://www.avantilipids.com/](http://www.avantilipids.com/). 3. Nov 2011.
- [13] Thomas Heimburg and Andrew D Jackson. The thermodynamics of general anesthesia. *Biophysical journal*, 92(9):3159–65, May 2007.

- [14] Thomas Heimburg and Andrew D Jackson. On the action potential as a propagating density pulse and the role of anesthetics. *Biophysical Reviews and Letters*, 2(1):13, 2006.
- [15] H Ebel, P Grabitz, and T Heimburg. Enthalpy and Volume Changes in Lipid Membranes. I. The Proportionality of Heat and Volume Changes in the Lipid Melting Transition and Its Implication for the Elastic Constants. *The Journal of Physical Chemistry B*, 105(30):7353–7360, 2001.
- [16] Thomas Heimburg. Review : Lipid Ion Channels. *Biophysics*.
- [17] [Http://en.wikipedia.org/wiki/Nervous\\_system](http://en.wikipedia.org/wiki/Nervous_system). 10.23-2011.
- [18] A.L. Hodgkin and A.F. Huxley. A Quantitative description of membrane current and its application to conduction and excitation in nerve. *Physiol*, 117:500–544, 1952.
- [19] [Http://upload.wikimedia.org/wikipedia/commons/c/cc/Action\\_potential\\_vert.png](http://upload.wikimedia.org/wikipedia/commons/c/cc/Action_potential_vert.png). 3. Nov 2011.
- [20] I. Tasaki and K. Iwasa. Pages 172-176. *Biochemical and Biophysical Research Communications*, 101(1):172–176, 1981.
- [21] J M Ritchie and R D Keynes. The production and absorption of heat associated with electrical activity in nerve and electric organ. *Quarterly Reviews of Biophysics*, 18(4):451–476, 1985.
- [22] K. Iwasa and I. Tasaki. Mechanical changes in squid giant axons associated with production of action potentials. *Biochemical and biophysical research communications*, 95(3):1328–1331, 1980.
- [23] Thomas Heimburg and Andrew D Jackson. On soliton propagation in biomembranes and nerves. *Proceedings of the National Academy of Sciences of the United States of America*, 102(28):9790–5, July 2005.
- [24] Ichiji Tasaki, Kiyoshi Kusano, and Paul M. Byrne. Rapid mechanical and thermal changes in the garfish olfactory nerve associated with a propagated impulse. *Biophysical journal*, 55(June):1033–1040, 1989.
- [25] T Heimburg. Mechanical aspects of membrane thermodynamics. Estimation of the mechanical properties of lipid membranes close to the chain melting transition from calorimetry. *Biochimica et biophysica acta*, 1415(1):147–62, December 1998.
- [26] B Lautrup, A D Jackson, T Heimburg, and A L Hodgkin. The stability of solitons in biomembranes and nerves. 2008.
- [27] R Fettiplace and D A Haydon. Water permeability of lipid membranes. *Physiological Reviews*, 60(2):510–550, 1980.

- [28] Bertil (University of Washington) Hille. *Ionic Channels of Excitable Membranes*. Edition, s edition, 1992.
- [29] Terry Kenakin. Principles: receptor theory in pharmacology. *Trends in Pharmacological Sciences*, 25(4):186–192, 2004.
- [30] H P Rang. The receptor concept: pharmacology’s big idea. *British journal of pharmacology*, 147(S1):S9–S16, 2006.
- [31] Long-Jun Wu, Tara-Beth Sweet, and David E Clapham. International Union of Basic and Clinical Pharmacology. LXXVI. Current progress in the mammalian TRP ion channel family. *Pharmacological Reviews*, 62(3):381–404, 2010.
- [32] E Neher and B Sakmann. Single-channel currents recorded from membrane of denervated frog muscle fibres. *Nature*, 260(5554):799–802, 1976.
- [33] Nobelprize.org. "Physiology or Medicine 1991 - press release" 11 OTC 2011.
- [34] [Http://en.wikipedia.org/wiki/Patch\\_clamp](http://en.wikipedia.org/wiki/Patch_clamp). 2. nov 2011.
- [35] Md. Shahidul Islam. Transient Receptor Potential Channels. *Advances in Experimental Medicine and biology*, 704, 2011.
- [36] I. Scott Ramsey, Markus Delling, and David E. Clapham. AN INTRODUCTION TO TRP CHANNELS. *Annu. Rev. Physiol.*, 68:619–47, 2006.
- [37] M Yafuso, S J Kennedy, and A R Freeman. Spontaneous conductance changes, multilevel conductance states and negative differential resistance in oxidized cholesterol black lipid membranes. *The Journal of membrane biology*, 17(3):201–212, 1974.
- [38] Konrad Kaufmann, Wolfgang Hanke, and A. Corcia. Ion channel fluctuations in pure lipid bilayer membranes: control by voltage. [http://www.membranes.nbi.dk/Kaufmann/pdf/1989\\_Kaufmann\\_book3\\_ed.pdf](http://www.membranes.nbi.dk/Kaufmann/pdf/1989_Kaufmann_book3_ed.pdf), 1983.
- [39] Heiko M Seeger, Laura Aldrovandi, Andrea Alessandrini, and Paolo Facci. Changes in single K(+) channel behavior induced by a lipid phase transition. *Biophysical journal*, 99(11):3675–83, December 2010.
- [40] Peter Grabitz, Vesselka P Ivanova, and Thomas Heimburg. Relaxation kinetics of lipid membranes and its relation to the heat capacity. *Biophysical journal*, 82(1 Pt 1):299–309, January 2002.
- [41] Keith J. Laidler. *The World of Physical Chemistry*. 1993.

- [42] P.L. Privalov, D.R. Monaselisze, G.M. Mrevlishvili, and V.A. Magaldadze. No Title. *Sov. Phys. JETP*, 47:2073, 1964.
- [43] PL Privalov and VV Plotnikov. Three generations of scanning microcalorimeters for liquids. *Thermochimica acta*, 139:257–277, 1989.
- [44] V P Ivanova and T Heimburg. Histogram method to obtain heat capacities in lipid monolayers, curved bilayers, and membranes containing peptides. *Physical Review E - Statistical, Nonlinear and Soft Matter Physics*, 63(4 Pt 1):041914, 2001.
- [45] T. Narahashi, J. W. Moore, and W. R. Scott. Tetrodotoxin Blockage of Sodium Conductance Increase in Lobster Giant Axons. *The Journal of General Physiology*, 47(5):965–974, May 1964.
- [46] Wouter Everaerts, Maarten Gees, Yeranddy a Alpizar, Ricard Farre, Cindy Leten, Aurelia Apetrei, Ilse Dewachter, Fred van Leuven, Rudi Vennekens, Dirk De Ridder, Bernd Nilius, Thomas Voets, and Karel Talavera. The capsaicin receptor TRPV1 is a crucial mediator of the noxious effects of mustard oil. *Current biology : CB*, 21(4):316–21, February 2011.
- [47] [Http://en.wikipedia.org/wiki/Allyl\\_isothiocyanate](http://en.wikipedia.org/wiki/Allyl_isothiocyanate). 2. Nov 2011.
- [48] [Http://en.wikipedia.org/wiki/Menthol](http://en.wikipedia.org/wiki/Menthol). 2. Nov 2011.
- [49] David D McKemy, Werner M Neuhausser, and David Julius. Identification of a cold receptor reveals a general role for TRP channels in thermosensation. *Nature*, 416(6876):52–58, 2002.
- [50] Peter L Privalov. Cold denaturation of proteins. *Biochemistry and Molecular Biology*, 281-307(4. vol 25):310–323, 1990.
- [51] MicroCalorimeter. VP-DSC MicroCalorimeter User Manual. *System*.
- [52] Roland Winter, Dahabada Lopes, Stefan Grudzielanek, and Karsten Vogtt. Towards an Understanding of the Temperature/ Pressure Configurational and Free-Energy Landscape of Biomolecules. *Journal of Non-Equilibrium Thermodynamics*, 32(1):41–97, February 2007.
- [53] Unpublished - Email correspondence November 2011 - between Thomas Heimburg and Roland Winter.
- [54] [Http://www.microcal.com/products/Software-accessories/pressure-perturbation-calorimetry.asp](http://www.microcal.com/products/Software-accessories/pressure-perturbation-calorimetry.asp). Nov. 6 th. - 2011.
- [55] Diana M Bautista, Jan Siemens, Joshua M Glazer, Pamela R Tsuruda, Allan I Basbaum, Cheryl L Stucky, Sven-Eric Jordt, and David Julius.

The menthol receptor TRPM8 is the principal detector of environmental cold. *Nature*, 448(7150):204–8, July 2007.

- [56] Raymond W. Colburn, Mary Lou Lubin, Dennis J. Stone, Yan Wang, Danielle Lawrence, Michael R. D’Andrea, Michael R. Brandt, Yi Liu, Christopher M. Flores, and Ning Qin. Attenuated Cold Sensitivity in TRPM8 Null Mice. *Neuron*, 54(3):379–386, May 2007.

